UNIVERSITY OF CALIFORNIA
SANTA CRUZ

RIVERS AS RECORDS OF LAND USE HISTORY, CLIMATE, AND LITHOLOGY

A dissertation submitted in partial satisfaction
of the requirements for the degree of

DOCTOR OF PHILOSOPHY

in

EARTH & PLANETARY SCIENCES

by

William Alan Longhurst Chapman

June 2024

The Dissertation of William A. L. Chapman is approved:

_____
Professor Noah Finnegan, chair

_____
Professor Andrew Fisher

_____
Amy East, Ph.D.

_____
Peter Biehl
Vice Provost and Dean of Graduate Studies

Table of Contents

List of Figures

Chapter 1

Chapter 2

Chapter 3

List of Tables

Abstract

Rivers as records of land use history, climate, and lithology

William A. L. Chapman

Rivers are dynamic features of Earth's surface that contain information about both past and present landscape processes. Shifts in the balances of sediment and flow in a watershed are often reflected in the character of the riverbed, channel geometry, or patterns of sediment transport, making rivers an invaluable tool for investigating changes in the overall sediment transport regime. Through three related studies, this work explores the various ways in which rivers not only respond to changing watershed conditions, but also reflect the broader climatic and lithologic character of a landscape.

This dissertation begins with a case study of the San Lorenzo River in California, in which the causes and timing of river floodplain abandonment are investigated through a combination of field measurements of channel geometry, theoretical estimates of channel depth, and radiocarbon dating of charcoal. Results suggest that significant channel incision can be attributed to historical practices associated with clear-cut logging, underscoring the long-lasting legacy of land use on landscapes and river networks.

Broader relationships between sediment transport, river characteristics, and environmental factors are explored in the following two studies. Chapter 2 uses an aridity index in tandem with suspended sediment rating curves for 71 rivers across the

United States to establish a compelling relationship between climate and sediment transport efficiency, and explores the influence of vegetation density and flow variability on sediment supply and riverbed grain size sorting. Chapter 3 follows up on these results by directly examining the link between suspended sediment rating curves and the organization of the riverbed. This study strengthens the interpretations made in Chapter 2 by confirming the likely significance of riverbed grain size and armoring on sediment transport efficiency across climates.

By pairing a case study with both novel and far-reaching geomorphic analysis, this research contributes to a deeper understanding of the mechanisms governing fluvial sediment transport and river form. The specific findings and new applications of old methods provide helpful resources to researchers and policymakers seeking to mitigate the effects of climate change and environmental degradation on river ecosystems and adjacent communities.

Acknowledgments

There are countless people who supported me during my doctoral program and the writing of my dissertation. I would first like to thank my advisor, Noah Finnegan, for sparking my interest in geomorphology, for guiding my scientific pursuits with expert advice and enthusiasm, and for reassuring me whenever I needed it. Thank you to my committee members, Andy Fisher and Amy East, who provided invaluable insight that greatly improved this work, and always did so with kindness and encouragement.

I would also like to thank the many people in the Earth & Planetary Sciences department that helped create a wonderful community both academically and personally. Moreover, to my friends in Santa Cruz and elsewhere: thank you for all the warmth and laughter over the years to help balance out the rigor of a graduate degree. A special thanks as well to my labmate, Colleen Murphy, for fieldwork help, reliably great feedback on scientific and aesthetic questions, and many fun times as well. Finally, I am deeply grateful for all the support from my family, who were my foundation through this entire journey: my partner, Nathan; Mom; Dad; Maddy; and Ethan. I would not have made it here without your support.

Published material

The text of this dissertation includes two reprints of previously published works. These publications, comprising the first two chapters of this document, are as follows:

Chapman, W. A. L., Finnegan, N. J., Pfeiffer, A. M., & La Selle, S. (2022). River floodplain abandonment and channel deepening coincide with the onset of clear-cut logging in a coastal California redwood forest. *Earth Surface Processes and Landforms, 47*(4), 994–1012. https://doi.org/10.1002/esp.5299

Chapman, W. A. L., & Finnegan, N. J. (2024). The signature of climate in fluvial suspended sediment records. *Journal of Geophysical Research: Earth Surface, 129*(1), e2023JF007429. https://doi.org/10.1029/2023JF007429

Introduction

Rivers, like many features of Earth's surface, carry information about active processes shaping the landscape. In their seemingly simple role of moving water and sediment from hillslopes to the ocean, these dynamic, self-regulating systems evolve to transport the sediment that is available to them, which is ultimately a function of the many different geologic, hydrologic, biologic, or climatic forces present in a watershed. The morphology and behavior of rivers thus reflect a balance between the supply of sediment, including the volume and sizes of grains, and the capacity of the river to transport that sediment—that is, the flow of water through river systems. This complex relationship between a river's form and surroundings is in fact an important asset for better understanding Earth's surface: to learn more about a landscape, we can turn to the rivers and streams that cross it.

Notably, rivers also record when the conditions in a watershed change, either through natural or anthropogenic means. These disturbances in the sediment transport regime—either through shifts in the sediment supply or transport capacity of a river—will often alter river morphology in significant ways. For example, large increases in the total sediment influx to a river can occur following wildfires, timber harvesting, or road construction, leading to major aggradation and widening of river channels (Brown & Krygier, 1971; Neary et al., 2005; Roberts & Church, 1986; Sankey et al., 2017; Shakesby & Doerr, 2006). On the transport side, increases in precipitation or the straightening of channels by humans can lead to significant incision in river channels (Simon & Rinaldi, 2006; Slater et al., 2019). Given that particular changes

in a watershed will affect both sediment supply and transport capacity in different ways, it is not often clear what the net effect on the river channel will be; if clear-cutting a forest increases runoff to streams, but also increases short-term sediment supply, will the river incise or aggrade? To answer these types of specific and complex questions that relate rivers, land use, climate, and other variables, numerous studies are required at both the case-study and synoptic level.

There are a number of river features we can examine to better understand processes occurring on the landscape or within the channel, as well as many methods and theories for predicting river behavior. Researchers directly measure physical parameters such as grain size and channel depth, for example, as well as the concentration of sediment across a variety of stream discharges. These can be compared to predictions of channel geometry based on sediment mobility or bankfull flow depth (i.e., Parker, 1978; Wolman & Miller, 1960) for an estimate of channel change over time. The behavior of sediment transport in a river can also be investigated statistically through regressions between suspended sediment concentration and discharge, also known as suspended sediment rating curves (e.g., Asselman, 2000; Syvitski et al., 2000; Walling, 1977). Metrics and theories such as these provide powerful tools for understanding the interplay between landscape and river processes, and have multiple applications such as habitat restoration, natural hazard assessment, and sustainable development.

For many of these analytical methods, however, much is still unknown. For example, is it possible to see the impact of climate or land use on widely employed

methods of sediment transport, or to find links between various distinct parameters like riverbed grain size and suspended sediment concentration? This body of work aims to test the use of these long-established geomorphologic methods across different scales, explore novel applications of those methods, and identify fundamental relationships between river attributes in an effort to further our understanding of fluvial response to changing land use and climate.

Chapter 1 incorporates multiple geomorphologic methods into a case study of the San Lorenzo River along the central coast of California, where the exceptional depth of the channel prevents regular inundation of the most-recent floodplain surface, but the magnitude and causes of incision are unknown. Suspended sediment records, continuous stream discharge measurements, and a model of bedload sediment transport are used to estimate the total depth of incision, which is corroborated by measurements of hanging tributaries above the mainstem San Lorenzo River. This incision estimate is paired with radiocarbon dating of detrital charcoal found in floodplain sediments, which suggests active floodplain deposition at least until the last few hundred years. Discussion of possible drivers of incision follows; based on the style of incision, timing, and other nearby studies of river incision, clear-cut logging of coastal redwoods during the late 19th and early 20th centuries is the most likely culprit. While other forces such as climate and tectonics have the potential to produce river incision by altering the balance of sediment supply and transport capacity, these are ultimately ruled out in favor of an anthropogenic explanation.

Chapter 2 widens the scope considerably by considering an important question about the role of climate in sediment transport behavior: Do rivers in arid locations transport sediment more efficiently than those in more humid climates, and if so, what drives this relationship? This study centers on the suspended sediment rating curve as a metric of sediment mobility and transport efficiency, and quantifies rating curve behavior for 71 stream gauge stations across the United States using the power law coefficient and exponent. Results reveal a significant relationship between overall aridity and rating curve shape, and suggest that rivers in arid regions transport considerably more sediment at low to moderate flow rates than their temperate counterparts. Possible explanations include climate-driven differences in vegetation density and flow variability, which influence the magnitude and frequency of sediment delivery to river channels and grain size sorting of the riverbed.

While the interpretations in Chapter 2 rely on indirect evidence to associate rating curves with the riverbed, Chapter 3 directly explores this relationship by pairing suspended sediment rating curves with field measurements of riverbed grain sizes and grain sorting. Twelve stream gauge stations were selected and split into two primary groups based on contrasting rating curve behavior, and surface and subsurface grain sizes were measured at each station. Results reveal a strong correlation between the riverbed and the suspended sediment rating curve parameters examined in Chapter 2; sites with steeper rating curves generally had coarser surface grains and a larger difference between surface and subsurface grain diameters, indicating a greater degree of grain size sorting. This supports the hypothesis posited

in Chapter 2 that climate-based differences in sediment transport efficiency are related to the character of the bedload. Additional analyses explore the relative contributions of climate and lithology to the overall sediment transport regime; both are found to strongly influence riverbed structure and suspended sediment rating curve behavior.

Together, these three chapters provide new perspectives on the relationships between sediment transport, river form, natural and anthropogenic processes, and geomorphic analysis. The findings of this research contribute to a greater understanding of how rivers reflect the complex balance of forces in a watershed, and grant researchers and policymakers additional tools to investigate and mitigate the impacts of human activity and climate change on communities and ecosystems.

Chapter 1

River floodplain abandonment and channel deepening coincide with the onset of clear-cut logging in a coastal California redwood forest

William A. L. Chapman, Noah J. Finnegan, Allison M. Pfeiffer, & SeanPaul La Selle

1.1 Abstract

Changes in both land use and climate can alter the balance of transport capacity and sediment supply in rivers. Hence, the primary driver of recent incision or aggradation in alluvial channels is often unclear. The San Lorenzo River on the central coast of California is one location where both climate and land use—specifically, clear-cut forestry of coast redwoods—could explain recent vertical incision and floodplain abandonment. At our field site on the San Lorenzo, we estimate the magnitude of recent incision using both the ratio of bankfull to critical Shields numbers ($\tau^*_{bf}/\ \tau^*_c$) and the geomorphically effective discharge, calculated from historical gauge data. The Shields number ratio suggests that the normalized bankfull stress of the San Lorenzo River is in the upper 1-2% of West Coast rivers, and the effective discharge corresponds to flow depths ~2-4 m below current bankfull conditions. Radiocarbon ages from detrital charcoal in floodplain sediment reveal active floodplain deposition during the 1600s and possibly into the 1800s, constraining the timing of incision to the last few centuries. Multiple hanging tributaries above the mainstem San Lorenzo River, along with patterns in vegetation on terrace surfaces, corroborate our estimates of the magnitude and timing of incision. Taken together, our findings suggest that floodplain abandonment in this reach was

mainly due to methods employed during logging that increased shear stress on the channel bed and reduced sediment storage capacity. We suggest that direct channel modifications to river channels can counterbalance increases in sediment delivery due to clear-cutting, resulting in channel incision rather than aggradation. Today, a young, lower surface appears to be forming adjacent to the San Lorenzo River, which we interpret as an incipient floodplain that is in equilibrium with modern sediment supply and transport capacity.

1.2 Introduction

Alluvial river channels, by definition, adjust to move the coarse sediment supplied to them (Parker et al., 2007), thereby directly linking channel aggradation and erosion to changes in sediment mass balance (Exner, 1925). For this reason, vertical incision or aggradation in alluvial rivers can be interpreted as a consequence of disequilibrium between transport capacity and sediment supply (e.g., Wickert & Schildgen, 2019). Because transport capacity is controlled in part by runoff, and sediment supply is governed by catchment erosion rates, studies of river incision or aggradation provide a means of assessing the integrated impacts of land use and climate on watersheds.

Vertical incision in alluvial river channels has been attributed to various natural mechanisms, and commonly to climate change in particular. Throughout western North America, for instance, many alluvial river channels incised vertically at various points during the Quaternary Period, interpreted as evidence of decreased

sediment supply relative to transport capacity. In some studies, incision was associated with greater flood magnitudes and increased runoff from snowmelt in the late Pleistocene (Dethier, 2001; Hanson et al., 2006). However, there have also been several documented increases in erosion rates—and therefore sediment supply—in the late Pleistocene and early Holocene that likely led to aggradation and bedrock terrace planation in transport-limited settings (Fuller et al., 2009; Marshall et al., 2015; Personius et al., 1993), thus setting the stage for channel incision throughout the Holocene as erosion rates decreased toward present-day levels. In British Columbia, for example, rivers are presently eroding through valley fill and remobilizing sediment deposited during the Last Glacial Maximum, demonstrating that Pleistocene climate change still influences the present-day balance of sediment supply to transport capacity (Church & Slaymaker, 1989). Unrelated to the glacial-interglacial cycle, more recent variations in the late Holocene climate may have influenced river incision via changes in sediment supply; for example, in some parts of the western United States, modest fluctuations in temperature drove changes in fire frequency (Pierce et al., 2004), which can alter the delivery of sediment to alluvial river channels (Jackson and Roering, 2009; Shakesby and Doerr, 2006; Swanson, 1981). Cycles of incision and aggradation have also been documented throughout the Holocene in semi-arid and arid climates of North America (Pierce et al., 2011; Townsend et al., 2019).

It also has long been recognized that anthropogenic land use changes disrupt the balance of sediment supply and river transport capacity in alluvial channels (e.g.,

Belmont et al., 2011; Gilbert, 1917; Walter & Merritts, 2008). A review of 20th century river channel changes at 25 locations around the world shows that, on average, alluvial channels have narrowed by ~50% and incised by ~1 m over the latter half of the century, frequently leading to formation of anthropogenic river terraces (Downs & Piégay, 2019). Causes of 20th century incision include reductions in sediment supply due to damming, increases in runoff from land-use or land-cover changes, removal of in-channel wood deposits, channel modification during logging operations, gravel mining from riverbeds, and planned reforestation (Liébault and Piégay, 2002; Napolitano, 1998; Rinaldi, 2003; Rinaldi and Simon, 1998).

At a practical level, river incision changes flood hydraulics (e.g., Wyżga et al., 2016), alters planform morphology (e.g., Stecca et al., 2019), and severs the connection between channels and their floodplains, thereby eliminating critical habitat for aquatic species (Jeffres et al., 2008; Quinn & Peterson, 1996). For example, salmon and trout populations have dramatically decreased on the West Coast of North America due to human-driven degradation of river channel habitat (Katz et al., 2013; Weitkamp et al., 1995). For these reasons, incised river reaches are a common focus of river restoration efforts (e.g., Harvey & Watson, 1986; Rosgen, 1997). A challenge of river restoration and management of incised reaches, however, is disentangling the influence of anthropogenic changes to the balance of sediment supply and transport capacity, which may be possible to mitigate (Harvey & Watson, 1986), and the impact of, for instance, climate change, which may not. Gibling (2018) concluded that anthropogenic river effects are much more common than has been

recognized in the literature, and should be considered as a matter of course in interpreting late Pleistocene and Holocene changes in river morphology.

In this contribution we examine an alluvial reach of the San Lorenzo River, the principal coastal drainage of the Santa Cruz Mountains in the central California Coast Ranges, where the relative importance of climate change, anthropogenic land use, and other factors as drivers of incision is unclear (Fig. 1.1). Like much of coastal California, the San Lorenzo River watershed was intensively logged throughout the late 19th and early 20th centuries, with 95 sawmills in operation between 1842 and 1975 (Rood, 1975) (Fig. 1.2). In California, harvesting of coast redwood forests was particularly widespread; between the mid-1800s and 1960, all but 5% of the coast between Big Sur on the central coast and the Oregon border had been cleared of original forest cover (Lowell, 1990). This is relevant to incision by way of a nearby example in the Santa Cruz Mountains, where

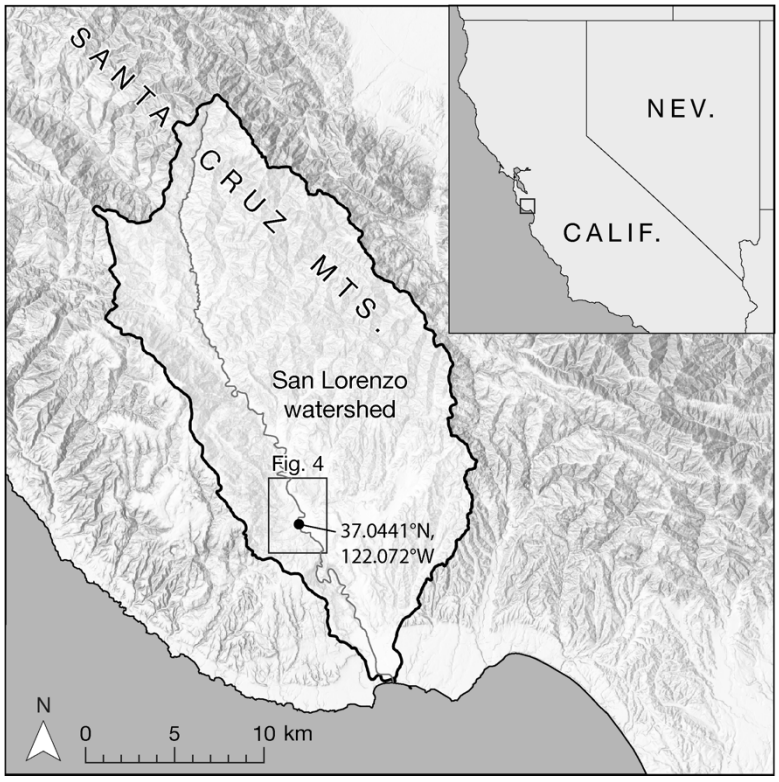

Figure 1.1. Location of the San Lorenzo River watershed in California, USA. The rectangle within the watershed boundary shows the extent of Figure 1.4. Coordinates indicate location of the USGS Big Trees gauge (#11160500). Hillshade basemap from Esri (2020).

significant channel downcutting has been tied to practices employed during clear-cut logging in the mid-1800s through early 1900s. Channel degradation in the Pescadero-Butano Creek watershed coincided with the construction of in-channel skid roads with logs pulled by work animals or steam-powered engines, as well as the seasonal use of "splash dams"—temporary dams that, when removed, release floods capable of moving large numbers of harvested logs downstream (BalanceGeo, 2015).

Beyond the Santa Cruz Mountains, splash-damming and the requisite clearing of logjams from channels have also been invoked as drivers of incision in both bedrock and alluvial rivers on the West Coast of North America (Collins et al., 2016; Napolitano, 1998; Schanz et al., 2019). Specifically, dam-release floods bearing huge numbers of logs can scour channel bottoms, due to elevated shear stresses of abnormally large peak flows and the direct, physical abrasion by logs (Napolitano, 1998). The clearing of natural wood from rivers prior to log

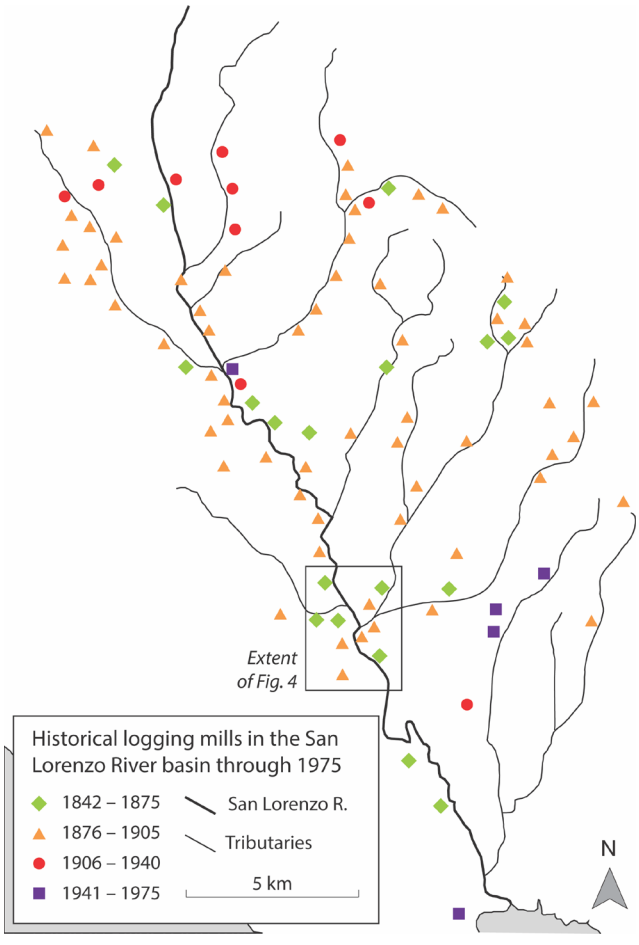

Figure 1.2. Locations of sawmills operating within the San Lorenzo River watershed between 1842 and 1975. Adapted from Rood (1975).

drives is also significant; logjams provide significant sediment storage capacity in rivers by effectively reducing local shear stresses, causing sediment to accrete around the jam (Brummer et al., 2006). This effect is so significant, in fact, that aggradation due to logjams can produce forced alluvial reaches in steep mountain streams that would otherwise be bedrock channels (Montgomery et al., 1996; Montgomery et al., 2003). Thus, removal of in-channel wood may lead to a loss of alluvial cover and potentially erosion into the underlying bedrock.

Logging practices are also associated with changes to the balance of transport capacity and sediment supply in river catchments. Deforestation can increase runoff to streams, thereby increasing transport capacity (Andréassian, 2004); for instance, in one study in the Pacific Northwest, loss of interception following clear-cutting of Douglas fir forests led to increases in peak stormflow by up to ~40% (Moore & Wondzell, 2005), and similar observations have been documented in redwood forests, where annual runoff increased by 20-30% after clear-cutting (Reid & Lewis, 2009). However, clear-cut logging is more often associated with increased sediment supply to channels, resulting in aggradation, channel widening, and downstream-propagating waves of sediment (e.g., Brown & Krygier, 1971; Kondolf et al., 2002; Madej & Ozaki, 1996; Roberts & Church, 1986), while the establishment of vegetation near rivers can decrease sediment supply to channels, leading to incision and narrowing (Liébault and Piégay, 2002). On a similar note, Safeeq et al. (2019) showed that while increases in streamflow following timber harvest in a study watershed produced higher overall sediment transport, sediment supply to channels increased by over an

order of magnitude. In summary, it is unlikely that elevated runoff alone is sufficient for channel incision, and more often than not, rivers will tend to aggrade in response to logging unless counteracted by factors like direct channel modification, logjam removal, or large dam-release floods.

As noted above, however, river channels throughout the western US have incised into alluvial deposits (and sometimes into underlying bedrock) in many locations during the Quaternary (e.g., Dethier, 2001; Fuller et al., 2009; Schildgen et al., 2002), a period marked by significant changes in precipitation, temperature, and fire frequency (Adam and West, 1983; Pierce et al., 2004). Thus, although logging and land use changes likely had some impact on the San Lorenzo River channel, it is also plausible that channel incision is linked to recent climate history through changes to river sediment transport capacity relative to supply.

With this context in mind, we seek to answer two questions. First, how much has the San Lorenzo River incised below its floodplain, and is the present-day channel geometry representative of the sediment supply and transport capacity? Second, when did significant vertical incision occur, and does this timing reveal the likely cause of incision—land use changes, climate, or other factors? Answering these questions furthers our knowledge of what the San Lorenzo River channel was like in the past, which is crucial for addressing the ecological impacts of historical incision and future restoration.

1.3 Geologic and geomorphic setting

The San Lorenzo River is located in Santa Cruz County, on the central coast of California (Fig. 1.1). With headwaters about 700 m above sea level in the Santa Cruz Mountains, the river flows for nearly 50 km before reaching its outlet into Monterey Bay. For the majority of this distance, the San Lorenzo is a bedrock river, traveling primarily through Paleogene and early Neogene sedimentary rocks, and occasionally through Cretaceous quartz diorite and Paleozoic-to-Mesozoic schist (Fig. 1.3). These rocks are broadly representative of the ~360 km^2 San Lorenzo watershed as a whole, with the addition of other intrusive igneous rocks and occasional older marbles. Faults in the immediate vicinity of the San Lorenzo River are minor or inactive; the Ben Lomond Fault, which generally follows much of the river trace, last ruptured 85 ka with just 3 cm of offset (Stanley and McCaffrey, 1983), and the Zayante Fault has been inactive in this watershed since the Miocene or Pliocene at the latest (Clark, 1981).

In addition to the bedrock reaches of the San Lorenzo River, there are two primary alluvial segments as well: one at the mouth of the river in the city of Santa Cruz, and one ~10 km upstream. The former is typical of a coastal river near its outlet, but the other alluvial section is located upstream of a region of diorite. In the Santa Cruz Mountains, exhumation of the relatively resistant diorite is typically associated with local geomorphic evidence for landscape disequilibrium indicating that rock uplift rates are larger than erosion rates where the diorite is present (Anderson, 1990; Gudmundsdottir et al., 2013). For this reason, we interpret the

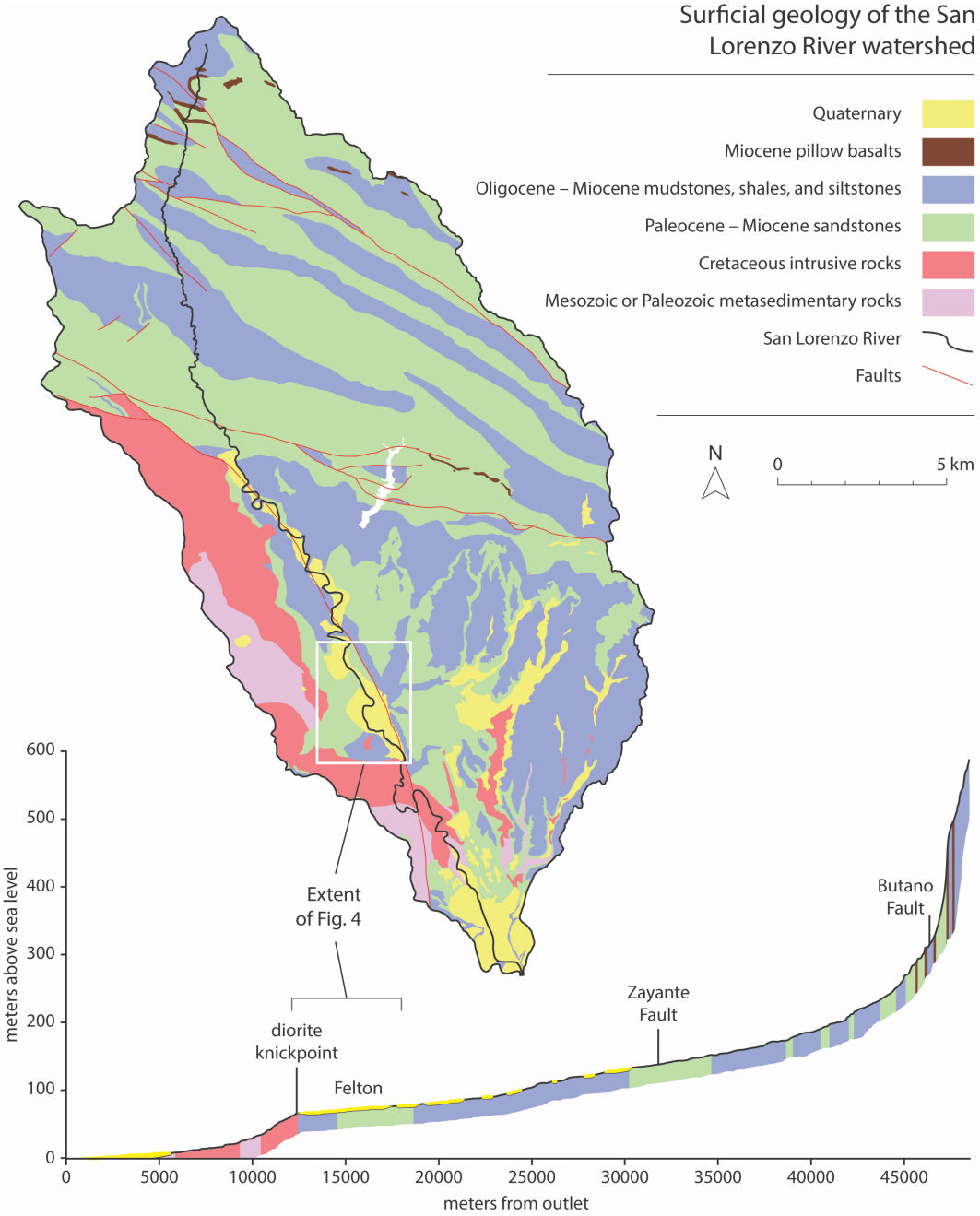

Figure 1.3. Geologic map of the San Lorenzo River watershed, and long profile of the San Lorenzo with surficial geology shown. Particularly noteworthy is the presence of Quaternary alluvium immediately upstream of quartz diorite, wherein the San Lorenzo is an alluvial river. The extent of Figure 1.4 is also shown along the San Lorenzo profile.

alluvial section upstream of the diorite as evidence that the diorite has prevented upstream propagation of relative base level into the upper San Lorenzo catchment (Forte et al., 2016), an interpretation that is supported by the large knickpoint associated with the exhumed diorite along the San Lorenzo River (Fig. 1.3). Alluvial deposition is extensive upstream of the knickpoint, where a broad valley contains multiple distinct fluvial terraces capped by Quaternary alluvium (Fig. 1.4). Thickness of alluvium on older terraces is typically on the order of centimeters or meters, such that when a terrace directly abuts the San Lorenzo River channel, the underlying sandstone or mudstone bedrock is exposed.

The extensive flat surface immediately adjacent to the San Lorenzo River in this valley, presumed to be the most recent floodplain, comprises alluvial sediments ranging in size from silts to medium sands. The thickness of alluvium here is at least several meters; we observe no bedrock below these floodplain deposits in our study area. Where the San Lorenzo River meets this surface, the banks are cohesive and vegetated. Consistently throughout the valley, this floodplain surface is over five meters above the base of the San Lorenzo River channel (Fig. 1.4). This observation raises multiple questions: Is the surface indeed an active floodplain? Is channel geometry in equilibrium with the present-day hydrology and sediment load? Finally, was there was a recent period of incision to which the channel has not yet adjusted?

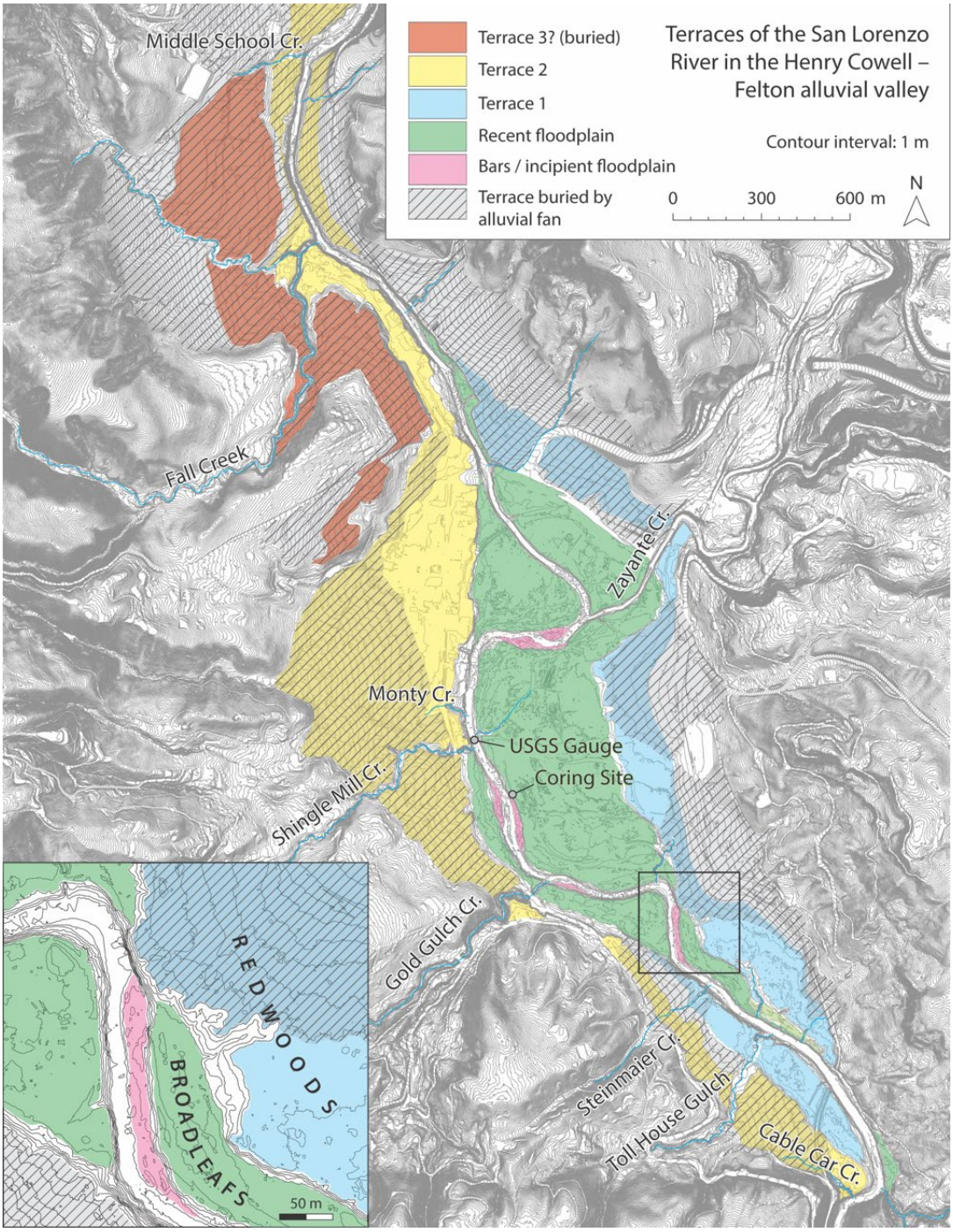

Figure 1.4. Fluvial terraces in the Henry Cowell and Felton valley. Terrace estimates based on elevation, and shaded where they appear to be covered by alluvial fan deposits. Incipient floodplains or major bars are shown in pink. Also depicted are major and minor tributaries to the San Lorenzo, USGS gauge station, and the coring site used in this study. Inset: closer view of a flight of terraces adjacent to the river, with the dominant tree type labeled.

In some reaches of the alluvial valley, there also appear to be young, narrow surfaces roughly 1-2 m above the channel bottom, wedged between the channel and the presumed floodplain surface (Fig. 1.4). These low surfaces are flat, are often populated by young trees, and sometimes have levees. They are only present in a few locations, however, and it is more common that the aforementioned higher surface abuts the river channel directly.

At the USGS Big Trees gauge (#11160500) in Henry Cowell State Park (U.S. Geological Survey, 2020), the San Lorenzo River has a drainage area of 275 km^2. This reach of the river is primarily a pool-riffle channel with a slope of ~0.2%, and top and bottom channel widths of 20 and 38 m, respectively. The banks are dominated by white alder with scattered California bay and small shrubs; coast redwoods occasionally populate the edges of the channel farther downstream, typically on higher terraces.

1.4 Part I: Testing the equilibrium conditions of the San Lorenzo River

1.4.1 Methods

Shields number analysis

The equilibrium condition of the San Lorenzo River channel with regard to present-day sediment supply and hydrology is testable using the Shields number, τ^*, which quantifies non-dimensional shear stress on a riverbed. Parker (1978) incorporated the Shields number into his bankfull threshold channel model for gravel-bedded rivers. According to this model, a river evolves and self-regulates such that its

banks are stable and the shear stress acting on the river bottom is just high enough to move the bed material when the river is at bankfull flow. The critical Shields number (τ_c^*), or the non-dimensional bed surface shear stress at which sediment begins to move, is generally between 0.03 and 0.08 (Buffington & Montgomery, 1997), and the Shields number in a channel at equilibrium and bankfull conditions (τ_{bf}^*) often just exceeds this value. Notably, the critical Shields number varies systematically with channel slope (Lamb et al., 2008), so when comparing τ_{bf}^* of different rivers in varied environments, it is often useful to normalize by τ_c^*. Moreover, Pfeiffer et al. (2017) showed that there is wide regional variation in the ratio of bankfull to critical Shields numbers, which they attribute to a greater sediment supply and hence systematically finer bed surface in these rivers (Buffington & Montgomery, 1999). Thus, rivers in tectonically active regions—such as the West Coast of North America—are expected to have much higher τ_{bf}^*/τ_c^* than elsewhere on the continent.

With this in mind, we assess whether the San Lorenzo River is a bankfull threshold channel by comparing slope-dependent estimates of the critical Shields number with the bankfull Shields number and to those of other rivers, and whether the river is anomalous with regard to τ_{bf}^*/τ_c^*. In theory, if a river has an unusually high τ_{bf}^*/τ_c^*, particularly when compared to similar rivers in comparable tectonic settings, that may indicate that bankfull conditions are deeper than expected "threshold" conditions given channel geometry, sediment supply, and transport capacity; conversely, if τ_{bf}^*/τ_c^* is very low, the channel could be shallower than anticipated. Regarding the critical Shields number, multiple studies exist for

empirically estimating τ_c^* for gravel-bedded rivers using channel slope. Three such approximations from Mueller et al. (2005) and Lamb et al. (2008) are used here:

$$\tau_c^* \approx \tau_r^* = 2.18S + 0.021 \quad \text{(general formula)} \quad \text{(Mueller et al., 2005)} \quad (1.1)$$

$$\tau_c^* \approx \tau_r^* = 8.60S + 0.016 \quad \text{(for } H_{bf} / D_{50} > 20\text{)} \quad \text{(Mueller et al., 2005)} \quad (1.2)$$

$$\tau_c^* = 0.15S^{0.25} \quad \text{(Lamb et al., 2008)} \quad (1.3)$$

where S is the slope, D_{50} is the median grain size, and H_{bf} is the bankfull depth. Note that, in place of τ_c^*, Mueller et al. (2005) use the "reference" Shields number, τ_r^*, which is defined using a dimensionless transport parameter to approximate the initiation of sediment mobilization. For our purposes, we treat τ_c^* and τ_r^* as equivalent.

The bankfull Shields number can be calculated via:

$$\tau_{bf}^* = \frac{R_{bf}S}{\left(\frac{\rho_s}{\rho_w} - 1\right)D_{50}}, \quad (1.4)$$

where R_{bf} is the hydraulic radius at bankfull depth, and ρ_s and ρ_w represent the densities of sediment and water, respectively.

We used 2-ft resolution, NAD digital elevation data from airborne LiDAR (Quantum Spatial, 2020) to calculate the average slope of the San Lorenzo River in a ~2 km reach centered on the Big Trees gauge, with which we estimated τ_c^* and τ_{bf}^*.

To determine the hydraulic radius, we used an auto level and stadia rod to survey a cross section of the San Lorenzo River channel at the USGS Big Trees gauge and at a second location 200 m downstream of the gauge. We used the left bank of the channel at the USGS gauge location for our estimate of the bankfull channel depth, as the right bank is from a higher, older terrace (Fig. 1.4). Wolman Pebble Counts were used to measure 478 pebble diameters on point bars at two locations within 1 km of the second survey site in October 2018. Finally, we assume a density of 2.65 g/cm^3 for the bedload, which is reasonable given the high proportion of silicic rocks in the area (Fig. 1.3).

To put our estimate of τ_{bf}^*/τ_c^* for the San Lorenzo in context, we first examine 72 reaches of single-thread alluvial rivers of varying climate types and size from Parker et al. (2007). More recently, Pfeiffer et al. (2017) assessed bankfull Shields numbers of over 300 North American rivers, which they grouped into three broad geographic regions. We recalculate τ_{bf}^*/τ_c^* for both datasets using Equation 1.3 and Equation 1.4. Although we use three different equations to calculate τ_c^* for the San Lorenzo River, only that of Lamb et al. (2008) is used for these comparative datasets.

Effective discharge and magnitude-frequency tradeoff

Another metric for evaluating the equilibrium of an alluvial river channel involves the geomorphic concept of magnitude-frequency tradeoffs described by Wolman and Miller (1960). Central to this concept is a balance between the capacity of a flood to transport sediment and the probability of that particular flood. That is,

large storm events have enormous potential to move sediment, but occur infrequently, and the converse is true for small storm events. Therefore, over time, there is a specific flood magnitude that transports the most sediment. In natural settings, it is commonly observed that this specific storm magnitude fills the channel to its floodplain, such that the depth of this "effective discharge" aligns with the depth corresponding to bankfull discharge (e.g., Emmett & Wolman, 2001). This is perhaps unsurprising, as the event transporting the most sediment over time should have the greatest effect on the geometry of a stable alluvial river channel. Below, we use this concept to evaluate whether the geometry of the San Lorenzo River channel is consistent with historical hydrology and estimates of both bedload and suspended sediment flux.

We used 15-minute discharge measurements from the USGS Big Trees gauge in Henry Cowell Redwoods State Park to characterize the likelihood of flood events on the San Lorenzo River. This dataset ranges from October 1987, when these particular measurements first began, to the present. We log-transformed the full discharge series and used a Gaussian kernel density estimation to evaluate the probability density of the data. After discretizing the distribution into 10,000 equidistant intervals in log space, we calculated the integral of the probability density between each set of adjacent bounds, thus estimating the probability of events within each range of log-discharges. We then restored the log-transformed discharge intervals back to linear space.

We also estimated the bedload and suspended sediment flux transported by different flood magnitudes. We used 142 historical measurements of discharge and suspended sediment concentration at the Big Trees gauge from 1972 to 1993 (U.S. Geological Survey, 2020). Notably, suspended sediment levels throughout this period were significantly higher than most years due to a combination of widespread road construction in the watershed and a particularly large winter storm in 1982 (East et al., 2018). However, this is the most complete dataset at this location, so we proceed here with the caveat that we may overestimate the suspended sediment effective discharge.

Typically, rating curves between discharge and suspended sediment concentration follow a log-normal relationship, such that a linear regression of log-transformed data appropriately captures their behavior (Walling, 1977; Wolman & Miller, 1960). This relationship at the Big Trees gauge, also shown in Figure 1.5, is:

$$SS\ concentration = 12.7 \times Q^{1.14} \quad (1.5)$$

We applied this rating curve to each discretized interval in the larger discharge-probability dataset, using the mean discharge of each interval to approximate the suspended sediment concentration for that range of discharge values. We then multiplied each concentration by the mean discharge to calculate the suspended sediment flux (m^3/s) at every interval.

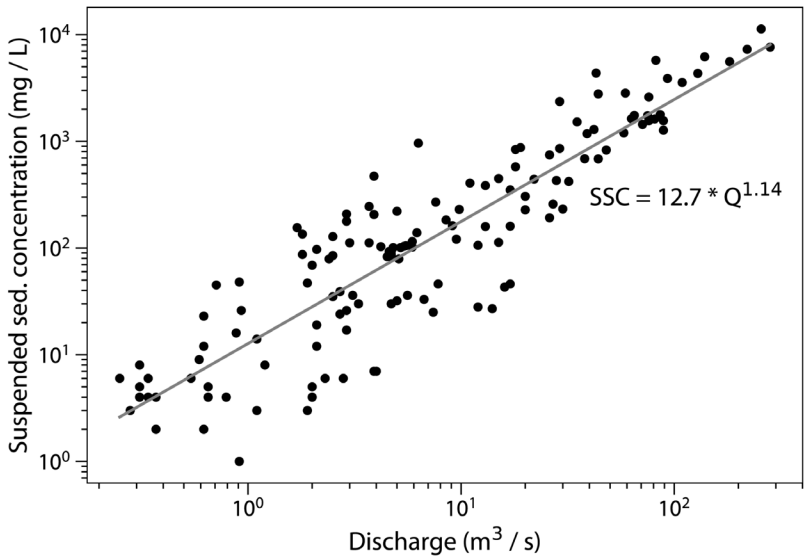

Figure 1.5. Rating curve between discharge and 142 suspended sediment concentration measurements at the Big Trees USGS gauge in Henry Cowell State Park, collected between 1972 and 1993. Log-log-linear fit between variables and associated equation are also displayed.

Next, given our lack of direct bedload measurements, we turned to the bedload transport model of Recking (2013) for sand- and gravel-bedded rivers, allowing us to approximate bedload flux for each discharge interval using the grain size distribution, river slope, width, and flow depth. Two noteworthy decisions were made when implementing this model.

First, we use a Gaussian kernel density estimation of the sampled grain sizes and a cumulative density function to approximate a complete probability distribution of grain size as a continuous variable. The D_{50} and D_{84} were drawn from this distribution, rather than from the original pebble count, though ultimately the original and modeled values varied by less than 1 mm.

Second, we modeled flow depth by estimating the stage of the mean discharge within each interval and comparing that to the average stage of the submerged channel bottom. This was accomplished by first making a visual fit between stage, which was available for some but not all events in the USGS database, and discharge,

which was available for all events. We used the visual fit to estimate stage at every discharge interval. For each representative discharge, the estimated stage was compared to the channel profile to determine which segments of the channel were submerged. We summed the individual widths of these submerged segments to estimate the total width of the flow event, and then calculated an average bed elevation that was subtracted from the stage of the event to obtain an average flow depth. Notably, for floods that do not fully submerge the channel bottom, estimates of average channel depth are likely less accurate and more influenced by irregularities in the bed and the precision of our cross-sectional survey. However, these low-flow events are far below the effective discharge, and thus relatively unimportant to our calculations.

After following the outlined procedure from Recking (2013) while applying these two modifications, we calculated the bedload flux (m^3/s) at the mean discharge for every interval in the larger dataset.

The probability of each range of discharges was then multiplied by the representative bedload and suspended sediment flux (m^3/s) for each interval, producing the *probability-adjusted sediment flux.* This parameter represents the tradeoff between the magnitude and frequency of hydrologic events discussed above. The discharge at which this is maximized is the effective discharge.

The probability-adjusted suspended sediment flux was also calculated for the 142 direct measurements of suspended sediment at the Big Trees gauge. First, each suspended sediment concentration was multiplied by discharge to produce the

suspended sediment flux. Next, each event in this dataset was assigned a probability based on the corresponding discharge interval from the larger discharge-probability distribution calculated above. Finally, the probability was multiplied by the suspended sediment flux. This allowed us to compare the larger empirically determined dataset to the original measured data from which they were derived.

1.4.2 Results

Shields number analysis

We solved for the critical and bankfull Shields number by entering appropriate values for the San Lorenzo River into Equations 1.1–1.4. Slope, D_{50}, and bankfull depth at the USGS gauge were 0.204%, 2.5 cm, and 5.61 m, respectively. Based on the formulas from Mueller et al. (2005) (Eq. 1 and 2) and Lamb et al. (2008) (Eq. 1.3), estimates of the critical Shields number were 0.025, 0.034, and 0.032, with a mean value of 0.030. We calculated a bankfull Shields number of ~0.20. Thus, the bankfull Shields number greatly exceeds the critical Shields number, with τ_{bf}^*/τ_c^* ranging from 5.8 to 7.7 for this reach of the San Lorenzo River.

Across the 72 reaches in Parker et al. (2007), the median τ_{bf}^*/τ_c^* was 1.2, and the maximum was 3.4. Among all rivers from Pfeiffer et al. (2017), median τ_{bf}^*/τ_c^* was also ~1.2. Importantly, however, the authors noted significant regional variation in this ratio, with rivers on the West Coast of North America having a median and upper quartile τ_{bf}^*/τ_c^* of ~2.4 and 3.6, respectively, likely due to the effect that a higher sediment supply has on the surface sorting of grains.

Effective discharge and magnitude-frequency analysis

Our probability-weighted sediment flux results illustrate the magnitude-frequency tradeoff described by Wolman & Miller: the number of events of a given size decreases steeply at high discharges (Fig. 1.6A), yet this is accompanied by a dramatic increase in both bedload and suspended sediment flux at higher discharges

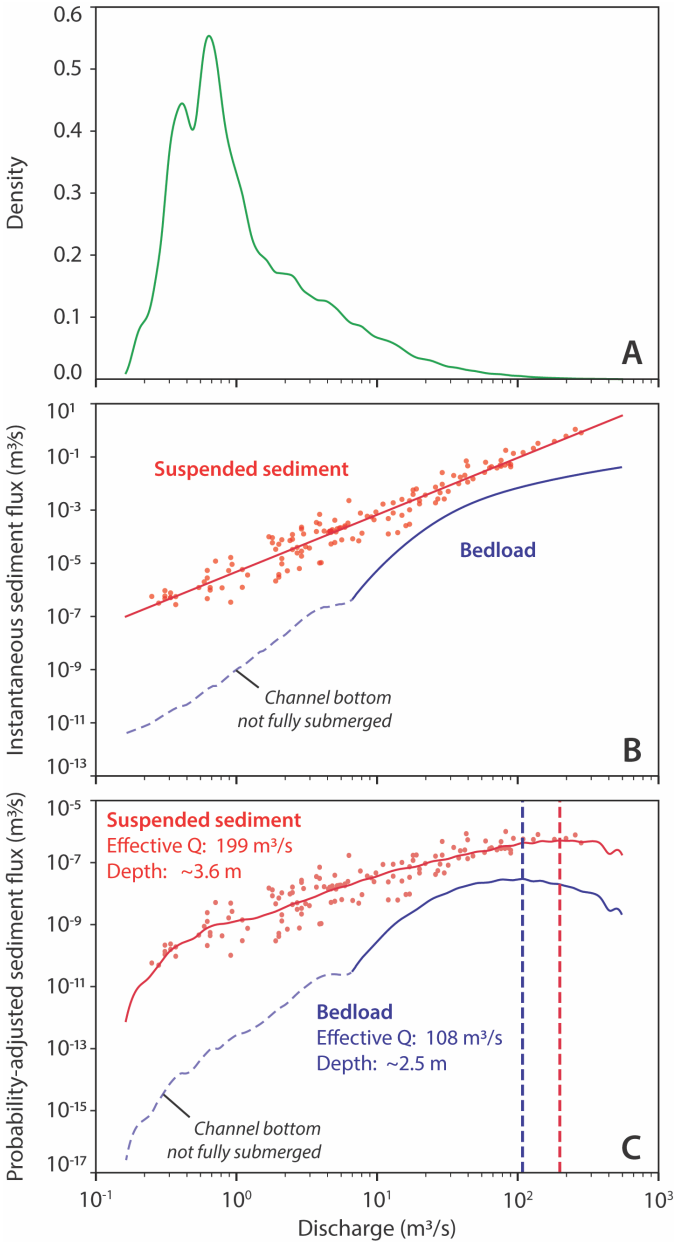

Figure 1.6. Results of effective discharge analysis for bedload and suspended sediment at the Big Trees USGS gauge. **A:** Probability density of discharge evaluated using a kernel density estimation, discretized into 10,000 equal intervals in log space. **B:** Suspended sediment (red) and bedload (blue) flux estimated with an empirical suspended sediment rating curve and a bedload transport model. 142 discrete suspended sediment measurements used in determining the rating curve are also plotted. Low discharges that do not fully submerge the channel bottom in our model are unreliable, and thus dashed in lighter blue. **C:** Probability-adjusted suspended sediment (red) and bedload (blue) flux vs. discharge, with corresponding effective discharges depicted as vertical dashed lines. Effective discharge values and associated depth estimates are also shown.

(Fig. 1.6B). The product of the probability and sediment flux—the probability-adjusted sediment flux—represents the overall ability of any individual event to transport sediment over time (Fig. 1.6C). The probability-adjusted bedload curve peaks at Q = 108 m^3/s, while the suspended sediment curve peaks at Q = 199 m^3/s. The probability-adjusted sediment flux of the 142 discrete events is also plotted as points over the smooth suspended sediment curve for reference.

The discharge at which the probability-adjusted flux is maximized represents an estimate of the effective discharge on the San Lorenzo River. The peak of the probability-adjusted bedload flux occurs at a slightly lower discharge than that of the probability-adjusted suspended sediment flux, but the two values are fairly comparable, suggesting agreement within ~1 m of flow depth between the bedload and suspended sediment models. Moreover, this difference is not unexpected, given that the we likely overestimated the suspended sediment concentration for a given discharge due to the timeframe of our suspended sediment data—a period of elevated sediment supply to rivers due to widespread road construction and major storms (East et al., 2018)—resulting in a steeper suspended sediment flux curve.

1.4.3 Discussion of San Lorenzo River equilibrium conditions: Estimating vertical incision

The ratio of bankfull Shields number to critical Shields number on the San Lorenzo River is considerably higher than many other natural rivers. Our estimate of 5.8-7.7 is greater than that for any river in the dataset from Parker et al. (2007) and

ranks in the upper 1-2% of rivers in the dataset compiled by Pfeiffer et al. (2017). Given that the bankfull Shields number increases with sediment supply, perhaps this is initially unsurprising for a tectonically active region; however, even within the North American West Coast subset characterized by higher sediment supply and $\tau_{bf}^{*}/\tau_{c}^{*}$ ratios, the San Lorenzo River has a ratio greater than 92-96% of rivers. Moreover, if any rivers in this sample population are also vertically incised, the large Shields number ratio of the San Lorenzo River is all the more significant. These findings strongly imply that the channel has neither adjusted to a bankfull threshold equilibrium (as in Parker et al., 2007) nor a high sediment supply equilibrium (as in Pfeiffer et al., 2017).

There have been only three events since 1987—February 1998, February 2017, and January 2023—that exceeded bankfull height at the USGS gauge, and neither flooded widely within the study area. The scarcity of floodplain-inundating events in our records suggests that the disequilibrium is primarily attributable to excess bankfull height due to channel incision. By converting bankfull Shields numbers to flow depth, we can quantify the magnitude of incision on the San Lorenzo River. Given the tendency for the bankfull Shields number of West Coast rivers in general to significantly exceed the critical Shields number, it is unsurprising that this is also true for the San Lorenzo River, and thus unhelpful to use the disparity between τ_{bf}^{*} and τ_{c}^{*} alone as a proxy for documented incision. Instead, we can establish an *expected* bankfull Shields number from the larger dataset of West Coast rivers, which can then be translated into an expected channel depth.

We take 2.4, the median τ^*_{bf}/τ^*_c of the North American West Coast subset of rivers from Pfeiffer et al. (2017), as the typical ratio of bankfull Shields number to critical Shields number for a channel with high sediment supply in a tectonically active region. We multiply this by our calculated range of τ^*_c for the San Lorenzo River to determine the representative expected bankfull Shields number in this reach: τ^*_{bf} = 0.062-0.081. Using our measured values for slope, grain size, and grain density, a channel depth of 1.4-1.9 m is required to meet this expected bankfull Shields number—3.7-4.2 m less than the observed bankfull depth of 5.6 m (Fig. 1.7). Of course, this comparison is simplistic given the wide variety in climate and sediment supply among West Coast rivers. Even so, for additional context, the 75th percentile of the West Coast dataset has τ^*_{bf}/τ^*_c = 3.6, corresponding to a depth of 2.2-3.1 m on the

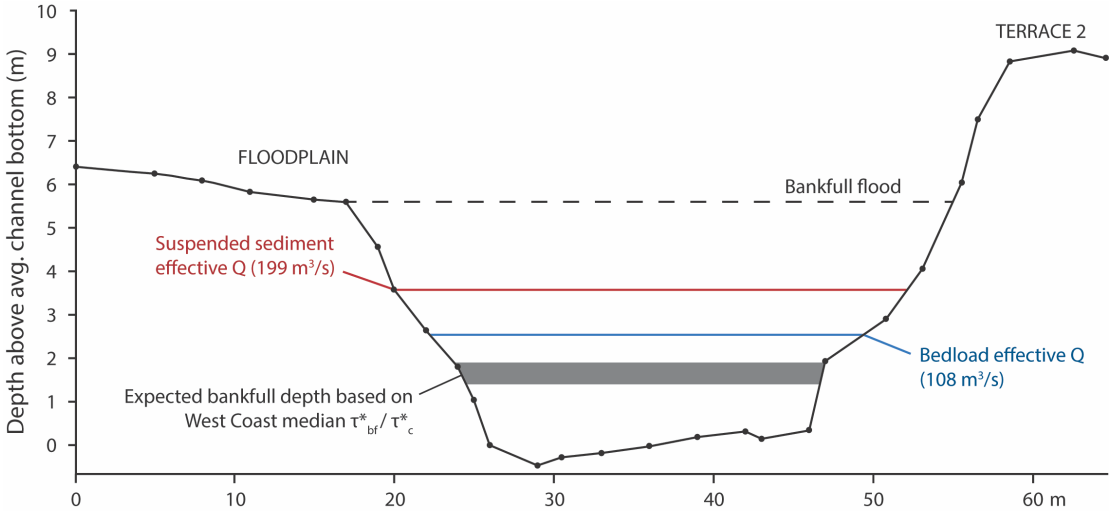

Figure 1.7. Cross section of the San Lorenzo River at the USGS gauge. Bankfull flood is shown as a dotted line. Estimated depths of flows corresponding to the bedload and suspended sediment effective discharges and the estimated bankfull depth based on West Coast bankfull-to-critical Shields number ratios are also shown. Expected bankfull depth from Shields numbers is derived from the West Coast median τ^*_{bf}/τ^*_c of 2.4. Observed bankfull conditions are based on the left bank, as the right side of the channel is part of a higher terrace (Fig. 1.4).

San Lorenzo River—still over two meters short of the observed depth. This reinforces our hypothesis that the San Lorenzo channel is deeper than anticipated by a meaningful degree.

Based on historical discharge vs. stage measurements at the Big Trees gauge, we can also compare our approximations of effective discharge to channel depths, which then can be measured against the true depth of the channel. The effective discharge estimate from bedload data corresponds to a depth of 2.5 m, and we estimate a depth of 3.6 m from the suspended sediment data (likely an upper limit given that the period of data collection was one of elevated sediment supply). Based on traditional interpretations of the effective discharge, the floodplain surface (5.6 m above the average channel bottom) is roughly 2.0-3.1 m higher than where we would expect it to be based on hydrology and sediment load (Fig. 1.7). This range of expected bankfull depths is higher than the range predicted using the median Shields numbers ratio from West Coast rivers, but the two are relatively consistent. We note that Emmett & Wolman (2001) showed that for five channels, the effective discharge with respect to bedload is quite close to the bankfull discharge, providing further support of this metric as an index of incision.

Taken together, estimates of the bankfull Shields number and the effective discharge suggest a channel that is ~2-4 m deeper than expected for a river at equilibrium with the current sediment supply and transport capacity. We interpret this excess depth as vertical incision to which the channel has not yet adjusted. In the following section, we address the timing and potential triggers of this incision.

1.5 Part II: Radiocarbon dating of alluvial sediments

1.5.1 Methods

According to our analysis of the Big Trees gauge record, only two storms have exceeded the bankfull depth at the gauge location since 1987. Moreover, our field observations following the February 7, 2017 flood, the 6th largest on record since 1937, revealed no fine sediment deposition outside of the channel within the study site. Hence, due to the considerable degree of incision discussed in the previous section, there appears to be little if any significant deposition of sediment on the now-abandoned, historical San Lorenzo floodplain. For this reason, dating material within floodplain sediments should provide an estimate of how recently the floodplain was still active. Fortunately, San Lorenzo alluvial sediment is rich in detrital charcoal, which we exploit to illuminate the history of floodplain abandonment.

We focused our charcoal sampling 200 m downstream of the USGS Big Trees gauge, where there is an easily defined historical floodplain and natural levee. Between the levee and the present-day river is a 5-m erosional scarp dropping down to a lower surface immediately adjacent to the San Lorenzo River (Fig. 1.8).

In the field, we extracted a ~2.5 m sediment core from the floodplain approximately 3 m behind the scarp. We used an aluminum irrigation pipe with a 76.2 mm outer diameter and 1.3 mm wall thickness, attached to a concrete vibrator powered by a modified four-stroke engine. Coring depth was limited by the sediment coarseness and compaction; the dense silts and fine sands prevented us from coring more than 2.5 m below the surface.

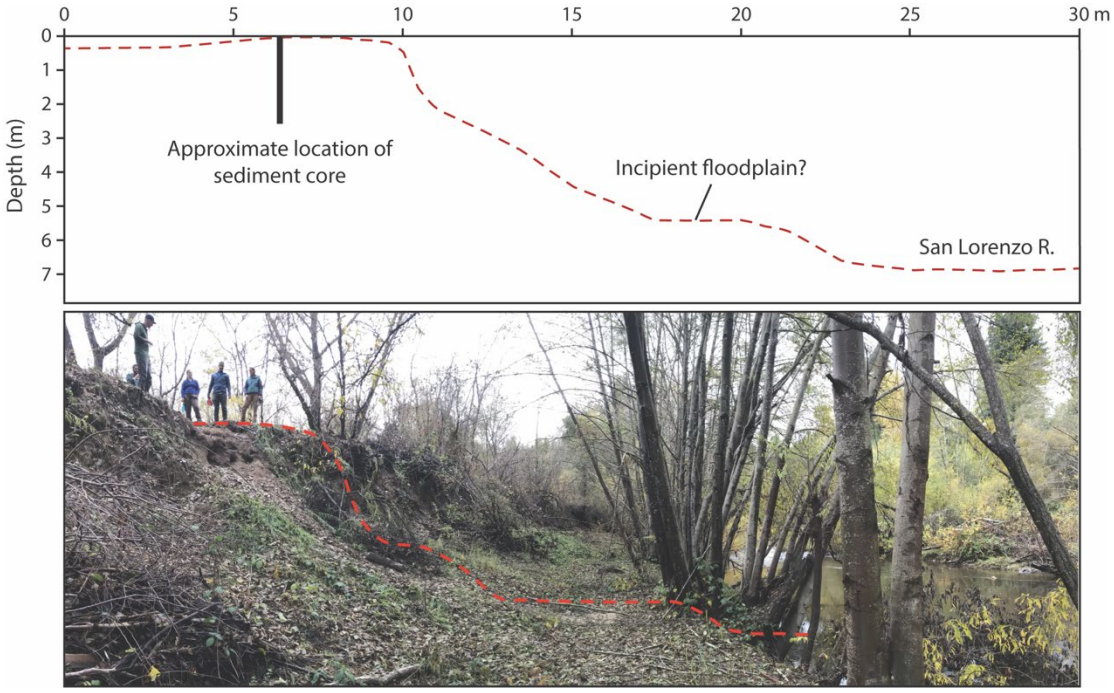

Figure 1.8. Cross section and photo of coring site, with the upper, abandoned floodplain on the left, San Lorenzo River on the right, and lower surface (possible incipient floodplain) in center. The red dashed line superimposed on the photo is approximately perpendicular to the river channel, and roughly follows the trace of the cross section above. This site is about 200 m downstream of the USGS gauge location (Fig. 1.4).

Although deeper coring was not possible with our equipment, we accessed lower strata using the erosional scarp. After clearing away the exposed surface material of the scarp, we obtained two bags of sediment from ~185 cm and ~330 cm below the floodplain surface. While the structure of these lower sediments could not be preserved, the samples yielded enough material for additional radiometric dating of detrital charcoal.

The sediment core was brought to the USGS Pacific Coastal and Marine Science Center core facility, where it was split in half. Its internal structure was imaged with a Geotek Rotating X-Ray CT scanner (Nasr et al., 2021). We extracted pieces of detrital charcoal based on the availability of high-quality detrital charcoal in

visibly undisturbed layers, rather than in regular intervals (Fig. S1.1). Priority was placed on large, angular charcoal pieces to minimize the risk of dating older, reworked material, which is more likely to have been repeatedly broken down and redeposited (Blong and Gillespie, 1978). However, if large, singular pieces were not available at a desired interval, multiple smaller but still angular pieces were extracted within a 1-2 cm stratigraphic range until meeting the mass of 5 mg necessary for radiometric dating. For the two bagged sediment samples from the erosional scarp (UFP-185 and UFP-330), we extracted all available charcoal for a bulk radiocarbon measurement.

Nine charcoal samples and one piece of plant material from the floodplain were submitted to AMS facilities for cleaning and radiometric ^{14}C dating. Of those samples, seven were from the sediment core and analyzed at the WM Keck Carbon Cycle AMS at University of California Irvine, and two samples were from the erosional scarp and processed by Beta Analytic. The radiocarbon dates were calibrated and plotted using the OxCal 4.4 software per the IntCal20 Northern Hemisphere calibration curve (Bronk Ramsey, 2009, 2017, 2020; Reimer et al., 2020).

We were also interested in determining the reservoir age of charcoal in present-day river sediment. We collected sediment from an active bar 150 m downstream of our coring site; the bar was composed of fine to medium sands that closely resembled the floodplain sediments in size. Four charcoal samples were extracted from the sediment and submitted to UC Irvine for cleaning and analysis.

Finally, we extracted wood cores from trees to approximate the age of the lower surface between the San Lorenzo River and the floodplain at our sediment coring site (Fig. 1.8). In April 2019, we used a 5-mm diameter manual borer to extract wood cores from 13 white alder trees populating the edge of the river, selecting only the largest (and presumably oldest) trees available. We then counted annual rings to obtain approximate ages of the trees.

1.5.2 Results

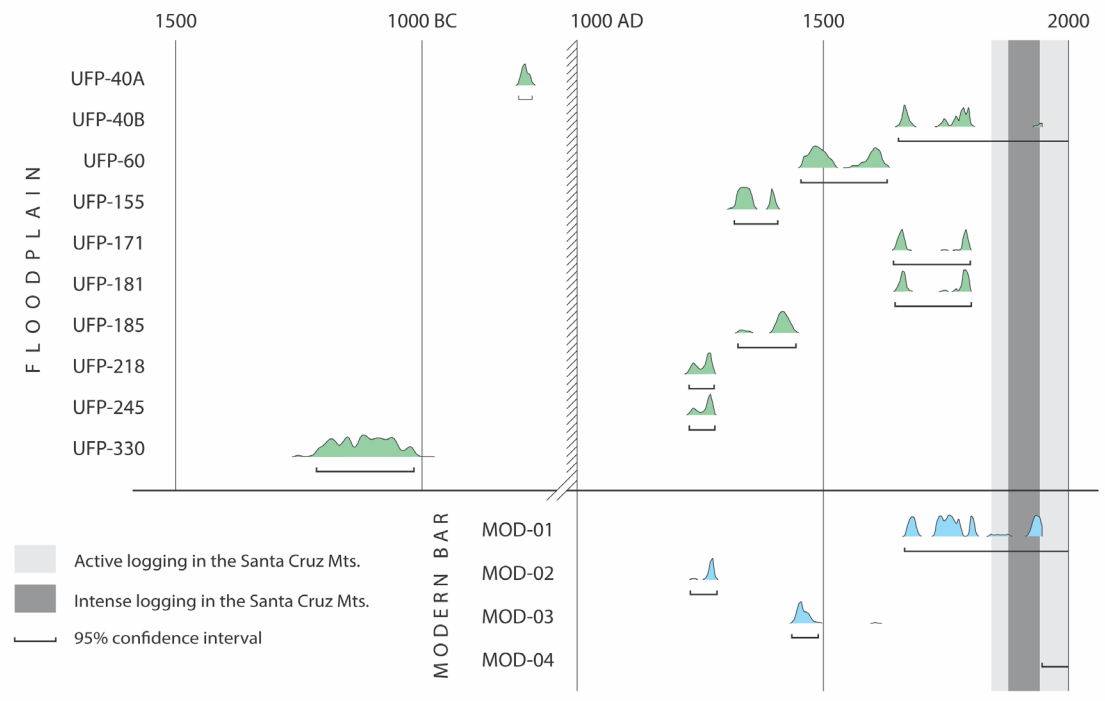

Figure 1.9. Calibrated radiocarbon ages of samples gathered from floodplain (green, top) and modern bar sediments (blue, bottom). Sample numbers for floodplain sediments (UFP) correspond with depths in centimeters. Full age ranges and their associated 95% confidence intervals are shown as kernel density distributions and black lines, respectively. Logging activity began in 1842, with the most intensive forestry practices involving splash-damming and removal of natural logjams in operation primarily between 1876 and 1940.

Calibrated radiocarbon ages from the ten floodplain samples are plotted as kernel density estimations with 95% confidence intervals, ordered by depth relative to the coring surface (Fig. 1.9) and recorded in Table 1.1. Assuming the greatest possible error, charcoal dates range from 150 BP to 3168 BP (calibrated years before 1950), with all but two of the nine dates clustering on the younger end between 150 BP (1800 AD) and 790 BP (1160 AD). There is a 90.5% likelihood that the plant material

Sample	Depth (cm)	Material	Calibrated years BP		% confidence
			from	to	
UFP-47A	47	charcoal	2753	2726	95.4
UFP-47B	47	plant	298	267	30.3
			214	195	10.1
			190	147	50.1
			15	-	4.9
UFP-67	67	charcoal	495	426	57.9
			379	320	37.6
UFP-155	155	charcoal	632	591	72.9
			562	544	22.5
UFP-171	171	charcoal	307	280	55.1
			171	151	40.3
UFP-181	181	charcoal	305	275	43.3
			208	200	1.7
			186	150	50.5
UFP-185	185	charcoal	624	601	7.9
			556	506	87.5
UFP-218	218	charcoal	724	673	95.4
UFP-235	235	charcoal	723	671	95.4
UFP-330	330	charcoal	3163	2965	95.4
MOD-1	10	charcoal	285	256	17.8
			225	166	43.9
			156	138	10.3
			111	107	0.4
			78	74	0.4
			35	–	22.5
MOD-2	10	charcoal	721	706	6.2
			694	666	89.2
MOD-3	10	charcoal	515	460	95.4
MOD-4	10	charcoal	modern		–

Table 1.1. List of ^{14}C radiocarbon dates from charcoal and plant samples. Stratigraphic depth is listed in centimeters. UFP samples were taken from floodplain sediments in the core and erosional scarp, while MOD samples were from a modern bar in the river. Additional information available in Table S1.1.

at 40 cm depth (UFP-40B) dates to 147-298 BP (1652-1803 AD), with a ~5% likelihood that it is modern. For some of the younger radiocarbon dates, fluctuations in the atmospheric calibration curve over the past 300 years prevented more precise calibration. Assuming the two oldest dates are outliers, there appears to be a slight increase in age with depth, but this is speculative. There was no immediately apparent structure to the sediment core (Figure S1.1). Despite a lack of obvious stratigraphic relationships, the broad conclusion is that all samples are late Holocene to modern in age.

While we attempted to select the largest and most angular charcoal pieces, the resulting ages strongly suggest that some reworked detrital material was sampled. Moreover, coast redwood trees abundant in the Santa Cruz Mountains can live for over 500 years in a mature forest, and a ^{14}C age of charcoal from a redwood could represent any age within the tree's lifespan. Therefore, it is likely that both redeposition and the wide range of possible ages for trees contributed to the scatter in our radiocarbon results.

The four samples from modern river sediments range from 721 calibrated years before present to modern. The 95% confidence intervals on two of the four samples extended to the present. Ages of alder trees on the surface below our coring site had a median age of 16 years, and maximum of 19 years. Thus, the trees began growing by the year 2000 or later.

1.5.3 Discussion of radiocarbon ages: When did the channel incise?

While the ages of detrital charcoal are variable, they significantly clarify the history of channel incision in this reach of the San Lorenzo River. Given the possibility of redeposited material and centuries-old trees, each sample provides a maximum age for when the floodplain was still active. As such, the youngest dates are the most likely to represent the age of the sediments in which the samples were deposited, and to provide maximum age estimates of floodplain deposition. This interpretation is corroborated by the ages of material in the recent bar deposits. Although the oldest date is hundreds of years old, one sample is modern (MOD-4) and the 95% confidence interval on another extends to the present (MOD-1). Given there is active deposition today, it is reasonable to interpret the oldest ages as redeposited material or from ancient trees, and only examine the youngest as representative of the true age of the deposit (a radiocarbon age of zero). Thus, placing emphasis on the youngest ages in a given sediment deposit is appropriate.

With this in mind, the youngest radiocarbon dates from the San Lorenzo River floodplain imply that it was active up until at least the 17th century and possibly into the 19th century, and roughly 2-4 m of channel incision discussed above occurred sometime thereafter.

1.6 Part III: Additional evidence of incision in tributaries and vegetation

Other features in our study area also support our proposed timeline and magnitude of incision. One independent check on whether a river has recently

incised—and if so, by how much—is to examine its tributaries. While larger tributaries of alluvial rivers often experience a wave of incision propagating upstream from the confluence with an incising river (e.g., Germanoski & Ritter, 1988; Musselman, 2011), this is not always the case for smaller streams. For instance, if a tributary lacks the sediment transport capacity to respond quickly to incision of the main river, its mouth will hang above the river channel, in much the same way that bedrock channels lacking erosive potential can form hanging tributaries in bedrock canyons (e.g., Crosby et al., 2007; Wobus et al., 2006). Therefore, the height of a tributary hanging above the edge of the river channel is another proxy for depth of incision. This reasoning has been used to quantify anthropogenic channel incision at nearby Pescadero Creek, where many tributaries are perched 2-4 m above the mainstem river (BalanceGeo, 2015).

Our estimates of both the magnitude and timing of incision on the San Lorenzo River are supported by multiple small, hanging tributaries. We note four such tributaries in our study area: Middle School Creek, Monty Creek, Steinmaier Creek, and Cable Car Creek (Fig. 1.4). All but Monty Creek are bedrock tributaries where they meet the San Lorenzo River. The tributaries are quite small, with drainage areas smaller than 0.5 km^2; larger tributaries in the area with watersheds greater than 1 km^2 (such as Shingle Mill Creek, Gold Gulch Creek, and Toll House Creek) appear to have fully adjusted to incision of the San Lorenzo, as there was neither a major elevation difference at the confluence nor an upstream knickpoint.

Figure 1.10. Other evidence of incision on the San Lorenzo River, including hanging tributaries (**A-D**) and exposed redwood tree roots near Steinmaier Creek (**E**). Dashed white lines in tributary photos show a cross-sectional transect of the channel at the tributary lip, while blue dashed lines show the approximate route of the tributary from the hanging lip to the San Lorenzo River. Tributary names: **A**. Middle School Creek; **B.** Monty Creek; **C.** Steinmaier Creek; **D.** Cable Car Creek.

Each of the four hanging tributaries had a distinct "lip" above a vertical drop (Fig. 1.10, A-D). All but one had a steep slope or steps leading from the bottom of the vertical drop to the San Lorenzo River. Tributary profiles are concave upstream of the vertical drop, and the lips occur at elevations similar to or just below that of the recent floodplain surface. These observations indicate the steep mouths of hanging

tributaries are expressions of recent incision, and not simply the edges of older terraces.

We measured the total vertical distance from the tributary lip to the edge of the riverbed directly adjacent to the tributary. These heights, recorded in Table 1.2, are between one and four meters. Three of the heights are greater than 2.5 m, which is consistent with our estimates of San Lorenzo River incision depth (~2-4 m). The fourth tributary, Cable Car Creek, hangs just 1.1 m above the channel. However, it is also within 50 m of the mapped quartz diorite bedrock contact, where the channel abruptly transitions from gravel-bedded to bedrock (Fig. 1.3), so vertical incision of the mainstem San Lorenzo may be dampened near the highly resistant rock. With this in mind, the tributaries corroborate our results from the previous two sections. Vegetation patterns along the river offer additional evidence for incision of the magnitude estimated above. First, downstream of the outlet of Steinmaier Creek, there is a redwood tree overhanging the San Lorenzo River (Fig. 1.10E). Presumably, the top of the tree roots—approximately 4 m above the channel thalweg—represents where the bank was once located. Since then, the bank has eroded and been undercut, exposing the deep roots of the tree. While undercutting does not necessarily signify downcutting of the channel, it is noteworthy that the tree is on a slight inner bend of the river, where lateral incision would not

Tributary	**Minimum incision recorded (m)**
Middle School Creek	3.5
Monty Creek	2.7
Steinmaier Creek	3.0
Cable Car Creek	1.1

Table 1.2. Estimates of incision recorded by hanging tributaries to the San Lorenzo River, based on vertical distance between tributary lips and the edge of the river channel.

typically occur without destabilization of the bank by other means (i.e., vertical incision). While we could not obtain an accurate age of the tree, its diameter suggests an age on the order of 10^2 years, implying geologically recent incision.

Second, the dominant vegetation on different terraces also offers evidence for incision in the last couple hundred years. There is a clear divide in tree species between two surfaces in Henry Cowell State Park (Fig. 1.4, inset). Floodplain tree species (primarily white alders, California sycamores, and California bays) dominate the recent floodplain immediately adjacent to the current channel, while old- and second-growth redwood trees are located on Terrace 1, the next surface up. Notably, we have very few records of inundation of the recent floodplain surface, which is approximately 5-7 m above the San Lorenzo River; yet, if neither surface is presently connected to the river, and there is no apparent lithologic explanation, what explains the stark difference in vegetation? Perhaps this signals two distinct histories of the terraces, with the lower, broadleaf-dominated surface being subject to more recent alluvial activity and sedimentation prior to incision of the San Lorenzo. That said, it is unclear why young redwoods have not yet appeared on the lower terrace, given that the surface has been effectively abandoned for at least a few decades. Nonetheless, the division in vegetative character is profound, and likely represents different histories related to relatively recent abandonment of the lower terrace. The patterns of vegetation thus support the findings of the previous two sections.

1.7 Discussion: Triggers of incision on the San Lorenzo River

While there are multiple potential drivers of incision in rivers on the West Coast of North America, our results strongly favor anthropogenic land use change as the likely impetus for floodplain abandonment on the San Lorenzo River. We address various possible processes below.

Tectonics has often been cited as a driver of incision on rivers (e.g., Pazzaglia, 2013; Yanites et al., 2010), but we rule this out on the basis of no significant and recent fault offset on the San Lorenzo River since the Pleistocene (Clark, 1981; Stanley and McCaffrey, 1983). Fluvial terraces can sometimes be formed autogenically via meander migration (Limaye and Lamb, 2016), but there is little evidence this occurred recently on the San Lorenzo River, given the river has entrenched into its floodplain and both banks are quite steep in our study area.

We also consider climate, which is a commonly cited driver of river incision and terrace formation. If incision and subsequent floodplain abandonment occurred in response to glacial-interglacial climate fluctuations, we would not expect any detrital charcoal in floodplain deposits to be late Holocene in age; we therefore can safely eliminate this as a possible cause of incision. Recent climate variability over the last millennium has been invoked as an explanation of incision in river systems in arid and semi-arid regions of the western United States (Pierce et al., 2011; Townsend et al., 2019); however, coast redwood forests are characterized by relatively low to moderate disturbances (Lorimer et al., 2009), in part due to a high resilience to fire as well as the cool temperate setting in which redwoods live. The San Lorenzo River

watershed is thus less susceptible to the high-frequency fluctuations in land cover discussed in these studies of more arid locations. Hence, we focus on recent anthropogenic land use changes as the main trigger of river incision in our study area.

There are a number of ways humans can alter a catchment in a manner that would lead to river incision, but the most likely culprit is extensive clear-cutting during the 19th and 20th centuries. As discussed in the introduction, there are clear links between timber harvesting and changes to river channels, and there was widespread logging in the San Lorenzo watershed between the 1840s and mid-1900s (BalanceGeo, 2015; Kondolf et al., 2002; Napolitano, 1998; Rood, 1975). In fact, the onset of logging in the watershed follows our youngest ^{14}C date by 42 to 197 years, based on the 95% confidence interval (Fig. 1.9). In other words, the floodplain may still have been active in 1803 AD, and we have no evidence of active floodplain deposition after the first sawmill was established in 1842 AD (108 BP by radiocarbon convention). We acknowledge that this is a strictly temporal link, but it is hard to attribute this magnitude of incision to any other process given that in the last few centuries logging was likely the most significant change in the land use patterns of the San Lorenzo watershed.

If timber harvesting is indeed the principal driver of river incision in this reach, it may be somewhat counterintuitive that we observe incision in response to clear-cut logging, a disturbance often linked to large increases in sediment supply and subsequent aggradation in many locations through its influence on hillslope erosion rates (e.g., Brown & Krygier, 1971; Madej & Ozaki, 1996; Roberts & Church, 1986;

Safeeq et al., 2019; Swanson & Dyrness, 1975). For example, Kondolf et al. (2002) observed on two rivers that reforestation was the likely cause of channel narrowing and incision, while deforestation led to channel widening, aggradation, and ultimately a transition to a braided stream system. Additionally, Lyons & Beschta (1983) showed aggradation in river channels was due to landslides triggered by clear-cut logging in the Oregon Coast Range. Although a modest increase in runoff often accompanies clear-cutting (Moore & Wondzell, 2005; Reid & Lewis, 2009), that does not seem sufficient to overcome the increased sediment supply from logging and to cause channel incision.

Still, there is a striking temporal coincidence between the timing of San Lorenzo floodplain abandonment and a period of intense clear-cut logging in the watershed, suggesting that other processes related to logging led to the meters of incision we see today. In a nearby watershed in the Santa Cruz Mountains, similar conclusions have been made: following a period of intensive logging and conversion of land into agricultural fields, some reaches of the Pescadero-Butano Creek system were incised by 5 m, with in-channel log skidding, trampling by work animals, and operation of splash dams all cited as possible sources of channel degradation (BalanceGeo, 2015). Moreover, splash-damming and removal of logjams are argued to be causes of incision in other heavily logged watersheds (Collins et al., 2016; Napolitano, 1998; Schanz et al., 2019). Large, dam-release floods exert enormous shear stresses on channels and the logs physically abrade channel bottoms, stripping away alluvium or even eroding underlying bedrock. Furthermore, as described earlier,

removal of wood from channels—in preparation for splash-damming or otherwise—leads to reduced sediment storage, channel simplification, and increased shear stresses on channels (Brummer et al., 2006; Collins et al., 2012). It is also possible that in clear-cut watersheds, lack of trees on the floodplain could prevent reestablishment of logjams in the river for a considerable amount of time, potentially prolonging the period of incision. These factors, summarized in Figure 1.11, have all been tied to incision on the order of meters in West Coast rivers.

While we do not have unequivocal evidence of the aforementioned practices in the San Lorenzo watershed, there is reason to suspect they were in use. First, reports from the nearby Pescadero-Butano Creek watershed show that splash-damming, in-channel log skidding, and removal of riparian vegetation and in-channel

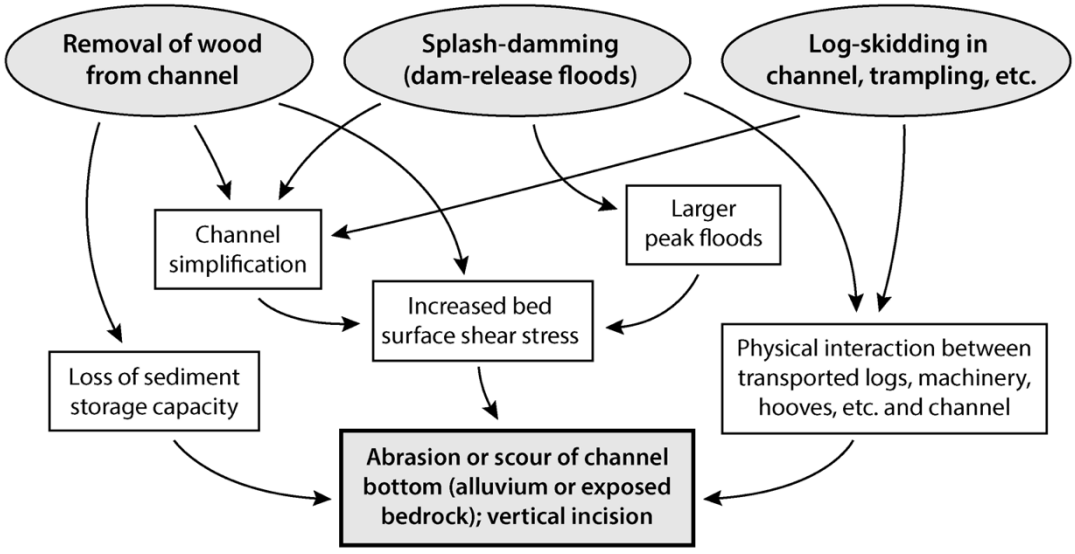

Figure 1.11. Conceptual diagram linking a few possible logging practices to vertical incision through various physical processes. Some or all of these techniques may have been used in the San Lorenzo River (all were present in nearby Pescadero-Butano Creek watershed). Further incision may be promoted by feedbacks between some of these processes, but such feedbacks are omitted from this diagram for visual simplicity.

wood occurred in the Santa Cruz Mountains. Moreover, dozens of lumber mills were operational in the San Lorenzo watershed in the late 19th century, closely aligning with the most pronounced period of timber harvesting activities in the Pescadero-Butano watershed from 1860 to 1890, giving credence to the comparison between the two locations in terms of which practices were employed (BalanceGeo, 2015; Rood, 1975). Finally, based on the large size of old-growth redwood trees relative to the width and depth of the San Lorenzo River, we expect that recruitment of trees from the floodplain and major accumulations of wood in the channel once played an important role in setting channel morphology (Abbe & Montgomery, 2003). However, the present-day San Lorenzo River channel clearly lacks old-growth logjams, and even second-growth logjams are infrequent in this alluvial reach of the river, indicating that wood must have been cleared from channels. With these observations in mind, it is reasonable to conclude that at least some logging practices associated with channel incision in other watersheds were likely used in the San Lorenzo watershed as well.

It follows that whatever logging techniques directly affected the San Lorenzo River channel—possibly splash-damming, log skidding, and the removal of large woody debris from the river channel—were more consequential in altering channel geometry than any changes in sediment supply or runoff. That is, even if deforestation in the Santa Cruz Mountains increased sediment supply to rivers, that additional sediment load could have been counteracted by, for example, the highly erosive peak flows of splash-damming, direct scour of the channel bottom by transported logs, loss

of large woody debris that previously stored sediment and reduced shear stresses in the channel, or some combination of these or additional factors. This ultimately resulted in the incised channel we see today. Furthermore, the tributaries discussed earlier strongly support this particular interpretation. Hanging tributaries indicate that incision began along the San Lorenzo River and propagated outward, rather than affecting the entire watershed broadly, as we would expect with catchment-scale changes to hydrology and sediment supply. This is consistent with our understanding of the processes ancillary to clear-cutting during this period, which probably occurred along the mainstem river more than in tributaries. Thus, although the relationships between sediment supply, transport capacity, incision, aggradation, clear-cutting, and associated logging practices are difficult to disentangle, we can point to the evidence of incision on the San Lorenzo River and link it to recent timber harvesting with relatively high confidence.

Another way to reconcile our findings with observations of aggradation in other clear-cut watersheds relates to specific locations along the river profile. While we suspect there was a larger proportional increase in overall transport capacity relative to sediment supply in Henry Cowell State Park in particular, this may not be the case in other reaches. Indeed, this would not be surprising given results from nearby rivers; although much of Pescadero Creek is thought to have cut down by 5 m since the mid-19th century, its lagoon and marsh complexes—natural sediment sinks—have aggraded considerably during the same period, with the areal extent of historically tidal reaches of the river shrinking by 50% (BalanceGeo, 2015). If

Pescadero Creek is an analogue for the San Lorenzo River, we can imagine simultaneous incision in upstream reaches and aggradation in shallower, downstream reaches of the river, which would be consistent with our study. However, due to extensive engineering of the channel of the San Lorenzo River where it enters the ocean in Santa Cruz, California, it is difficult to test this hypothesis directly.

As a final question about aggradation in this reach, it is worth considering a situation in which the incision we observe, rather than being the initial response to a disruption, is actually a return to equilibrium channel conditions after a major episode of aggradation. It is noteworthy that between 60 cm and 245 cm depth in our stratigraphic section, ^{14}C ages vary by between 176 and 403 years, suggesting relatively rapid aggradation. Of course, we acknowledge that our dates are open-ended—only representing maximum ages of deposition—so this rate is far from reliable; nevertheless, we should address the hypothetical scenario of rapid initial aggradation with subsequent incision, as has been observed, for example, following a period of commercial logging and road-building in Redwood Creek, California (Madej & Ozaki, 1996), or hydraulic mining in the Sierra Nevada foothills (James, 2013). In short, while there may very well have been an initial pulse of aggradation in the river channel in response to logging in the watershed, a larger-scale event like this seems unlikely based on our field observations. Most importantly, bedrock is exposed at the mouths of three hanging tributaries (Middle School Creek, Steinmaier Creek, and Cable Car Creek), suggesting that the San Lorenzo River incised through Quaternary alluvium and into the underlying bedrock in these locations. If incision

occurred simply as a readjustment following large-scale aggradation, it is unlikely that the river would have cut into bedrock at all, and furthermore, meters of alluvium—not bedrock—would now be exposed in the vertical faces of hanging tributaries. Thus, there is little to no field evidence for any appreciable aggradation preceding the inferred incision event. Incidentally, this is another argument against a climate-based explanation for incision; most examples of late Holocene changes in fire frequency, storm intensity, or other climate processes involve cycles of aggradation and incision (Hsieh and Knuepfer, 2001; Pierce et al., 2011). The lack of significant aggradation at this site further confirms our conclusions regarding land use as the trigger for vertical incision.

To bring together our data, field observations, interpretations, and prior studies on rivers in clear-cut landscapes, we propose a conceptual model for how a river responds to logging. All else being equal, clear-cutting large portions of a river catchment is expected to cause river aggradation due to decreased hillslope and soil stability, and thus increased sediment delivery to the channel. However, in the cases we have examined in which logging is associated with vertical incision, the authors attributed incision to the removal of wood from river channels, splash dams, and direct changes to the river channel (BalanceGeo, 2015; Collins et al., 2016; Napolitano, 1998; Schanz et al., 2019). These findings suggest that local factors that directly affect the channel and its margins are ultimately more important than catchment-scale processes like increased runoff or elevated erosion. In summary, we posit that in small and mid-sized rivers with forested catchments, local processes

directly affecting the river channel—woody debris removal, channel simplification, and splash-damming, for example—can cause channels to incise vertically despite any increases in sediment delivery following clear-cutting that would otherwise cause aggradation.

It is worthwhile to consider how long it will take the San Lorenzo River channel to adjust to the pulse of incision. In some rivers, incision has continued long after the end of splash-damming; the Teanaway River in Washington State, for example, still lacks logjams that were removed when the region was intensively logged, preventing sediment retention and encouraging incision even today (Schanz et al., 2019). Indeed, formation of logjams can cause aggradation and widening of channels, create erosion-resistant locations, and sometimes even lead to island formation (Collins et al., 2012), which could stabilize channels or perhaps even undo past incision. Unlike the Teanaway River, the San Lorenzo River appears to have maintained a roughly stable or gradually aggrading channel bed elevation at the Big Trees USGS gauge over the past few decades (Fig. 1.12), and occasional second-growth logjams can be found throughout the alluvial reach of the river. Given that the jams are not particularly common, however, it seems unlikely that current channel stability has come entirely from in-channel wood, but recent logjams may still play some stabilizing role. Ultimately, we do not have a clear limit on when channel incision stopped or when logjams reappeared on the river, but Rood (1975) noted that large-scale clear-cutting was mostly phased out by 1941 in favor of selective logging governed by forest management legislation. Moreover, the concrete foundation of the

bridge at the USGS gauge in Henry Cowell State Park was built in the early 1930s, and there is no evidence the riverbed was ever lower than the bridge foundation. The channel probably stopped incising before the 1940s, allowing over 80 years for a new equilibrium channel geometry to develop. In most locations, based on the height of the floodplain above the channel bottom, the San Lorenzo has not yet adjusted to over 2 m of incision. Thus, it will probably take decades to hundreds of years more to fully adjust to a new channel geometry consistent with the present hydrology and sediment supply of the river. Furthermore, this timeline will likely vary depending on river management strategies, especially given the potential influence of logjams—whether they are removed, left alone, or perhaps even introduced to rivers—on channel evolution.

In a few locations along the river, however, adjustment of the channel to modern conditions appears to be underway. At our coring site downstream of the

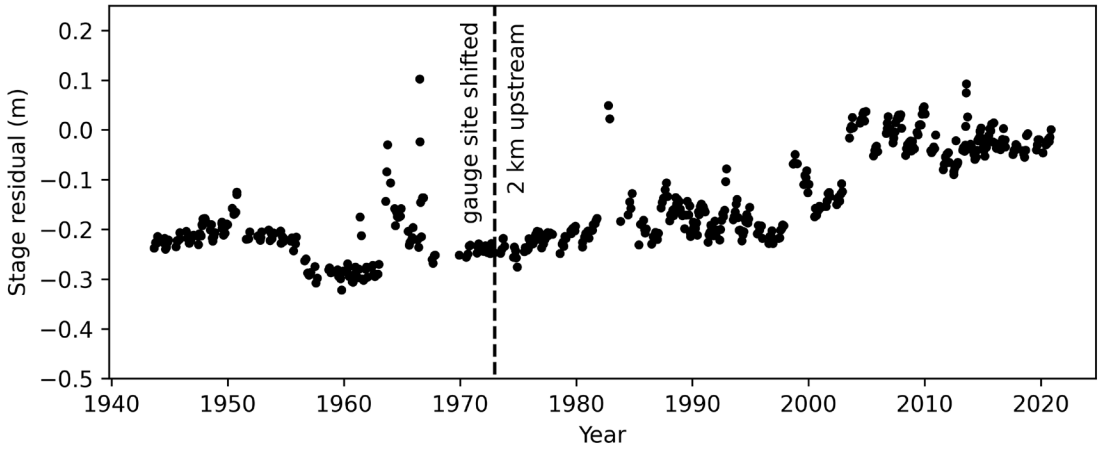

Figure 1.12. Stage residuals at the USGS Big Trees gauge on the San Lorenzo River. These values represent the historical elevation of the riverbed relative to the present. There has been a modest increase in the river stage for a given discharge (likely the result of riverbed aggradation) over the last several decades, following the end of log drives in the 1940s. See supplementary information for stage residual methodology.

gauge location, there is a 5-10 m wide surface below the inactive floodplain adjacent to the river channel, approximately 1.4 m above the channel bottom (Fig. 8). This surface could represent an incipient floodplain forming at a height accordant with present-day hydrology and sediment load in the San Lorenzo River. In fact, if we calculate a hypothetical bankfull Shields number using 1.4 m as the depth, we obtain 0.057, which is 1.7-2.3 times the estimated critical Shields numbers at this site. This is well within the range of expected $\tau_{bf}^{*}/\tau_{c}^{*}$ for North American West Coast rivers, which had a median Shields number ratio of 2.4.

The ages of white alder trees that have colonized the edge of the lower floodplain may also shed light on present-day floodplain activity. Tree rings from 13 of the oldest alders measured in April 2019 gave a median age of 16 years with the oldest trees being 19 years old, suggesting one or multiple colonization events between 2000 and 2003, and either an absence or a complete reworking of the lower floodplain shortly before the trees were established. Notably, the largest flood on record occurred in February 1998, so it is possible that this event is largely responsible for the creation or reworking of the incipient floodplain. Therefore, the lower surface is probably a dynamic and active part of the alluvial channel.

Similar surfaces 1-2 m above the channel bottom appear sporadically throughout this alluvial reach of the San Lorenzo River, suggesting that a new surface is forming at a consistent height throughout the area (Fig. 1.4). If these surfaces represent segments of a new floodplain, it is reasonable to expect them to expand—both along the river and outward as the abandoned floodplain is eroded—to form a

continuous, singular, active floodplain for the San Lorenzo River consistent with its current hydrology and sediment load.

1.8 Conclusions

Here we investigate the causes for ~2-4 m of apparent recent vertical incision along an alluvial section of the San Lorenzo River in the Santa Cruz Mountains, California. Evidence for this incision comes primarily from an analysis of channel morphology, the ratio of bankfull to critical Shields numbers of the river, and the effective discharge based on hydrologic records, suspended sediment concentrations, and a model of bedload transport. Radiocarbon ages from detrital charcoal in fluvial deposits constrain the timing of this incision to within the last few hundred years, before which there was active sedimentation on the floodplain surface. Given this recent date and the large-scale logging operations in the Santa Cruz Mountains in the late 19th and early 20th centuries, we associate incision with this widespread change in land use. While we are uncertain of the specific logging techniques implemented in the San Lorenzo watershed during this period, the removal of logjams, splash-damming, and physical damage to channels during timber harvest have been linked to vertical incision in multiple West Coast streams—including elsewhere in the Santa Cruz Mountains—through increases in bed surface shear stress, loss of sediment storage capacity, and direct scour of the channel bottom. These or similar processes seem more likely to have driven incision than catchment-scale changes in sediment supply or transport capacity, given the evidence of mainstem incision of the San

Lorenzo River prior to tributary response. More broadly, we suggest that while clear-cutting in a given catchment typically leads to aggradation of the river channel, direct alteration of the channel itself through logging-related techniques can instead cause a river to incise vertically. This framework may be useful for river restoration efforts, which require a complete understanding of the processes governing channel geometry. Despite the historical disruption on the San Lorenzo, reversion to an "equilibrium channel" is likely underway, as evidenced by multiple surfaces throughout the alluvial reach of the river near Henry Cowell State Park that have a bankfull to critical Shields number ratio consistent with other West Coast rivers in North America, signaling that the legacy effects of logging on rivers can fade over decadal to centennial timescales.

1.9 Supplementary information

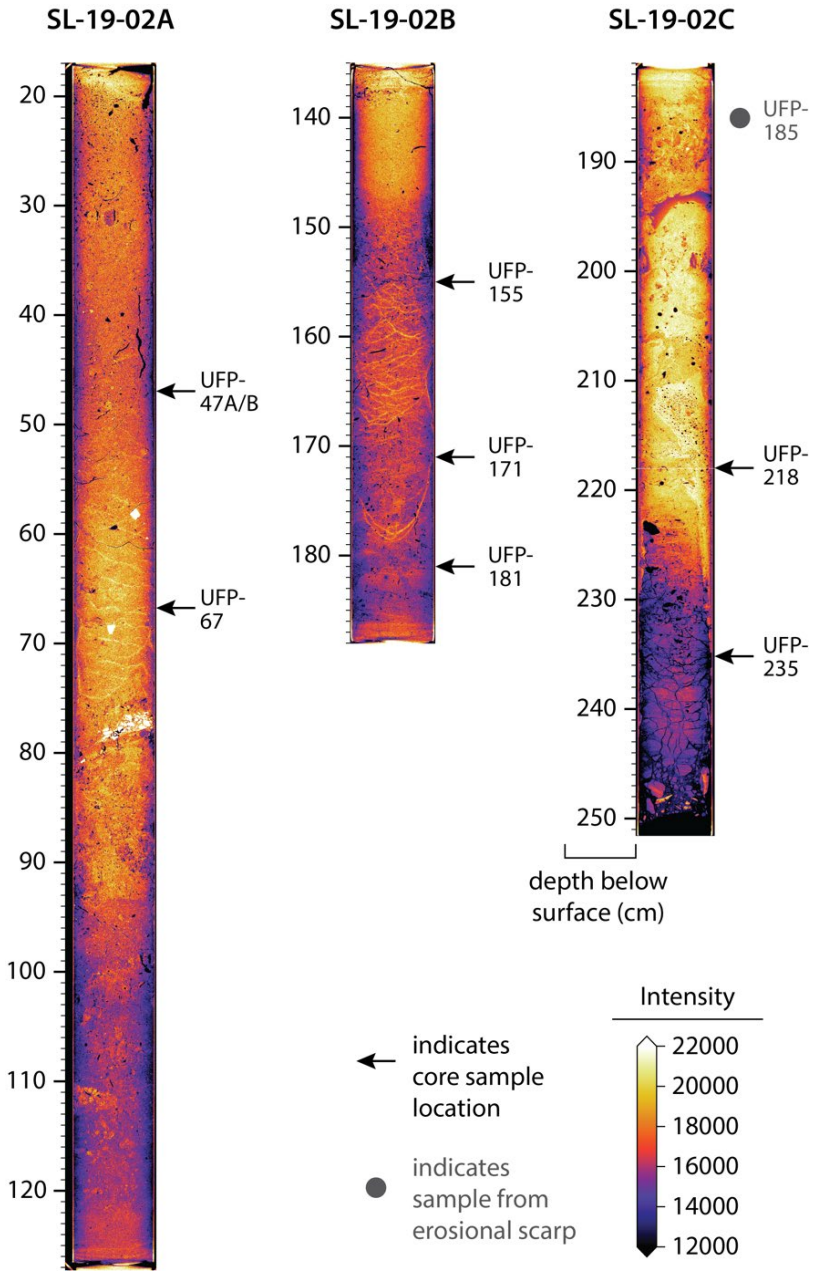

Figure S1.1. CT scans of SL-19-02 sediment core from the recently abandoned San Lorenzo floodplain. Higher intensity (brighter colors) generally represents denser materials. Depth below floodplain surface (not corrected for compaction) is shown on the left side of each core section, and sample intervals for radiocarbon dating are on the right. Additional charcoal was sampled from the erosional scarp 185 and 330 cm below the floodplain surface.

Sample	Depth (cm)	Material	$\delta^{14}C$ (‰)	±	^{14}C age (BP)	±	Calibrated years BP		% confidence
							from	to	
UFP-47A	47	charcoal	-276.3	1.3	2595	15	2753	2726	95.4
UFP-47B	47	plant	-25.2	1.6	205	15	298	267	30.3
							214	195	10.1
							190	147	50.1
							15	-	4.9
UFP-67	67	charcoal	-45.1	2.0	370	20	495	426	57.9
							379	320	37.6
UFP-155	155	charcoal	-70.4	1.5	585	15	632	591	72.9
							562	544	22.5
UFP-171	171	charcoal	-28.5	1.6	230	15	307	280	55.1
							171	151	40.3
UFP-181	181	charcoal	-27.1	1.8	220	15	305	275	43.3
							208	200	1.7
							186	150	50.5
UFP-185	185	charcoal	-62.68	3.5	520	30	624	601	7.9
							556	506	87.5
UFP-218	218	charcoal	-92.1	1.5	775	15	724	673	95.4
UFP-235	235	charcoal	-91.2	1.4	770	15	723	671	95.4
UFP-330	330	charcoal	-305.6	2.6	2920	30	3163	2965	95.4
MOD-1	10	charcoal	-20.5	1.5	165	15	285	256	17.8
							225	166	43.9
							156	138	10.3
							111	107	0.4
							78	74	0.4
							35	-	22.5
MOD-2	10	charcoal	-89.7	1.4	755	15	721	706	6.2
							694	666	89.2
MOD-3	10	charcoal	-50.8	1.8	420	20	515	460	95.4
MOD-4	10	charcoal	11.2	1.9	modern	-	-	-	-

Table S1.1. Complete results from radiocarbon analysis of detrital charcoal and plant material in floodplain sediments. UFP samples were extracted from the recent floodplain, and MOD samples were taken from modern river sediments. $\delta^{14}C$ and ^{14}C age were calibrated using OxCal 4.4 and the IntCal20 Northern Hemisphere calibration curve (Bronk Ramsey, 2009, 2017, 2020; Reimer et al., 2020).

Supplementary Text S1.1

Stage residual analysis

Maintenance of USGS stream gauges involves frequent updates to the stage-discharge rating curve to account for changes in channel geometry. Because many stream gauges have been in place for decades, these paired measurements of discharge and stage, or height of the water surface above an arbitrary datum, serve as a valuable record of channel change through time.

Stage-rating curve residuals (hereafter "stage residuals") measure the difference between a paired measurement of stage and discharge made in the field, and the stage predicted for that discharge based on the rating curve (Figure S1.2). If the stage residual increases through time, we can infer that the channel experienced some combination of 1) an increase in channel bed elevation, 2) a decrease in channel width, or 3) an increase in hydraulic roughness. USGS stream gauges are intentionally located along stable reaches lacking in brush (Juracek et al., 2009), and changes in hydraulic roughness such as the growth or loss of in-channel vegetation tend to be seasonal. Thus, changes in stage residual are commonly assumed to reflect changes in channel bed elevation (e.g., Pfeiffer et al., 2019; Anderson and Konrad, 2019; O'Connor et al., 2009; Weatherly and Jakob, 2014).

We calculate stage residuals for the San Lorenzo River at Big Trees (USGS gauge #11160500) using the method described by Pfeiffer et al. (2019). In short, we calculate the stage residual using the most recent rating curve, and exclude

measurements made in the lower half of the discharges in the record. The stage residuals shown in Figure 11 are not smoothed. Gauge #11160500 was moved 2 km upstream in October 1972, at which point a new datum was established. Both the old and new gauge sites fall within the study reach (Figure 4). In Figure 11, we have rectified the two stage residual records, making the assumption that no change in stage residual occurred between the measurement immediately preceding and following the datum shift (as in Pfeiffer et al., 2019).

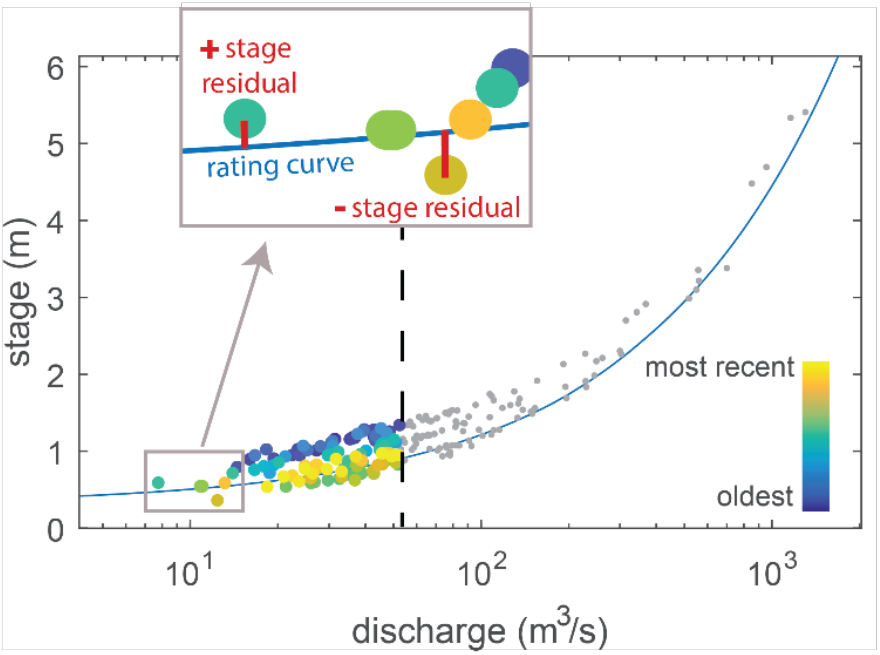

Figure S1.2 (from Pfeiffer et al., 2019). Example showing the method for calculating stage residuals from USGS field discharge data and a rating curve. Field measurements of discharge and associated stage are shown as points, with the lower-discharge data (which we use in this analysis) colored by date of measurement according to the color bar shown in the lower right of the figure. Stage residuals are calculated as the difference between the field measurement of discharge and the discharge predicted for that stage based on the rating curve.

Chapter 2

The signature of climate in fluvial suspended sediment records

William A. L. Chapman & Noah J. Finnegan

2.1 Abstract

Arid regions are often characterized by exceptionally high rates of fluvial sediment transport, but the processes responsible for this apparent connection between climate and sediment transport remain unclear. We examined decades of continuous flow records and suspended sediment concentrations from 71 rivers across the United States by comparing the suspended sediment rating curve behavior, quantified using power law coefficients and exponents, to an aridity index. Results indicate that higher aridity correlates with both greater overall suspended sediment concentration and lower sensitivity of concentration to changes in discharge, demonstrating that rivers in arid locations on average have greater suspended sediment transport efficiency across most discharges, and achieve high transport rates at a relatively lower discharge than rivers in temperate climates. Furthermore, based on additional analyses of the Normalized Difference Vegetation Index (NDVI), specific suspended sediment yield, and a hydrograph flashiness index, we attribute the relationships between sediment transport and climate primarily to differences in vegetation density, precipitation, and runoff, variables that all influence both sediment supply and riverbed grain sorting. Finally, we note that the observed contrasts in sediment transport behavior likely represent climate-driven differences in the

magnitude and frequency of sediment supply rather than annual suspended sediment load, which does not depend significantly on climate. This study highlights a critical connection between multiple interrelated climatic factors and sediment transport, an important finding for future hazard mitigation in a changing climate with rapidly shifting vegetation patterns and hydrology.

2.2 Introduction

Alluvial river morphology depends largely on the magnitude, frequency, and intensity of sediment transport. Given that both river morphology and sediment transport—and thus river channel behavior—vary widely across climates (Slater & Singer, 2013), understanding the connection between hydroclimatology and fluvial sediment transport is fundamental to predicting how alluvial rivers evolve in response to shifting climatic conditions.

One noteworthy difference between rivers relates to sediment transport efficiency, or the sediment flux at a given discharge or stream power. Specifically, there is evidence that rivers in arid locations transport greater volumes of sediment at a given flow rate than rivers in temperate locations. For instance, case studies of flashy, frequently dry streams in desert climates often document exceptionally high sediment transport rates (e.g., Stark et al., 2021; Wilcox et al., 2016). In ephemeral rivers in Israel, both bedload sediment transport rates and suspended sediment concentrations can be orders magnitude higher than in perennial rivers in more humid climates, though sediment transport typically occurs during large but infrequent flash

floods (Cohen & Laronne, 2005; Laronne & Reid, 1993; Reid & Laronne, 1995). On a larger scale, Ludwig & Probst (1996) showed in a study of 60 world rivers that rivers in dry climates had higher mean annual total suspended sediment than rivers in temperate climates for a given specific runoff. Thus, although wetter regions have much greater total precipitation and streamflow than dry regions, this does not necessarily translate into greater rates of sediment transport, as has also been demonstrated using erosion rates across a large climate gradient along the Andes (Carretier et al., 2013; 2018).

Notably, the relationship between sediment transport efficiency and climate is distinct from that between annual sediment yield and climate, a topic of considerable scrutiny over several decades. Early work by Fournier (1949) and Langbein & Schumm (1958) explored the connection between sediment yield and precipitation, putting forth distinct models for how climate affects sediment yield through its influence on runoff and vegetation cover. However, additional work over the following years suggests that there is no clear universal control of climate on sediment yields (Jansson, 1988; Milliman & Farnsworth, 2011; Syvitski & Milliman, 2007; Walling & Webb, 1983). The lack of an obvious signal between these two variables makes the aforementioned observations of high sediment transport efficiency in arid locations all the more noteworthy. That is, if the *total* amount of sediment rivers transport annually does not strongly depend on climate, then the magnitude and frequency of sediment transport may instead explain differences in observed sediment transport rates across climates.

Past work may reveal potential links between sediment transport efficiency and climate through the shape of the suspended sediment rating curve. Syvitski et al. (2000), in an effort to predict rating curve behavior from numerous variables, found covariance between rating curves, mean discharge, flow variability, precipitation, and temperature, among other factors. Although it featured few sites from arid climates, their study suggests a connection between climatic variables and the behavior of sediment transport beyond overall sediment yield. For example, there is indeed a clear correlation between climate and runoff variability, an important determinant of erosion on landscapes and sediment transport in river channels (Rossi et al., 2016). Vegetative cover is also intimately related to climate, which affects both runoff and soil erosion, and thus the total contribution of sediment to fluvial systems, as well as the magnitude and frequency of events that supply sediment to channels (e.g., Gyssels et al., 2005; Loch, 2000; Noble, 1965; Puigdefábregas, 2005). While some of the variables investigated by Syvitski et al. (2000) may themselves not directly have a strong impact on suspended sediment transport (such as temperature or latitude), they may reflect the combined effect of multiple climatic factors that could reasonably cause differences in the efficiency of sediment transport across climate types. However, a high-level, detailed analysis of sediment transport behavior across a much larger range of climates is necessary to make such connections.

To uncover the potential links between climate and sediment transport efficiency, here we present an investigation of continental-scale patterns in direct suspended sediment measurements, and explore possible mechanisms responsible for

the observed trends. While there are many local catchment variables that influence rates of sediment transport in individual rivers—land cover, dominant lithology, vegetation type, or slope, for example—examining overall patterns across dozens of rivers may cut through the noise to reveal fundamental relationships between climate and sediment transport.

This work is highly relevant to risk management, particularly with respect to flood hazards and infrastructure damage. Sediment supply and transport efficiency are directly related to variability in riverbed elevation and flood conveyance (Pfeiffer et al., 2019), which are particularly high in arid settings (Slater et al., 2019; Slater & Singer, 2013). This volatility in channel geometry leads to major erosion and sediment deposition problems near channels (e.g., Merritt & Wohl, 2003; Wilcox et al., 2016). Thus, understanding the processes driving high rates of sediment transport will help assess which rivers pose the greatest danger to nearby development, particularly in the face of shifting climatic and hydrologic conditions due to anthropogenic climate change.

2.3 Methods

2.3.1 Site selection

For this study we use publicly available suspended sediment concentrations from the U.S. Geological Survey (U.S. Geological Survey, 2022). Although sediment transport occurs both as suspended load and as bedload, directly measuring bedload transport is resource- and labor-intensive (Reid et al., 1980), and would be infeasible

for this large-scale study. Fortunately, the fraction of total load transported as bedload is relatively small except in sand-bedded rivers with very low suspended sediment flux (Turowski et al., 2010). Thus, while suspended sediment and bedload are not equivalent, studying suspended sediment alone provides important insight into the overall patterns of sediment transport efficiency given the large proportion of sediment transported in suspension.

Suspended sediment loads in fluvial systems are also highly sensitive to land use (e.g., Abbott et al., 2018; Gao et al., 2013; Rossi et al., 2009). To reduce the anthropogenic signal in our data, we began with the HCDN-2009 dataset from the GAGES-II project (Falcone, 2011), which identifies U.S. Geological Survey gauge locations suitable for hydroclimatic study across the United States and Puerto Rico. These 743 HCDN-2009 sites have at least two decades of continuous flow records beginning in Water Year 1990, are currently in "reference" condition (that is, not significantly altered by agriculture, dams, irrigation, or other land use in the watershed), have watersheds with no more than 5% impervious surface, and had not been labeled as unsuitable for study by evaluators from state Water Science Centers.

For each HCDN-2009 gauge location with available suspended concentration sediment data, we selected sites with at least 50 discrete field measurements of suspended sediment concentration beginning in Water Year 1990 and spanning at least five unique years. A multi-year record is important to account for any years with anomalous weather patterns, as well as for short-term oscillations in climate, which influence suspended sediment in rivers (Gray et al., 2015).

These high standards for site quality yielded 65 potential USGS gauges, but very few were in the southwestern United States, the driest region in our study area (Fig. 2.1). In order to have a sufficient representation of sites across different hydroclimates, we also drew from gauges outside of the HCDN-2009 dataset, examining sites from the "WestXeric" ecoregion in the GAGES-II database with a hydrologic disturbance index of less than 10 (the maximum in the database being 42), excluding one location with gravel excavation. This process resulted in 20 additional sites from the southwestern U.S.

It is possible that the more lenient standard for hydrologic disturbance index at Xeric West sites introduced bias into our dataset. For example, dams have a large

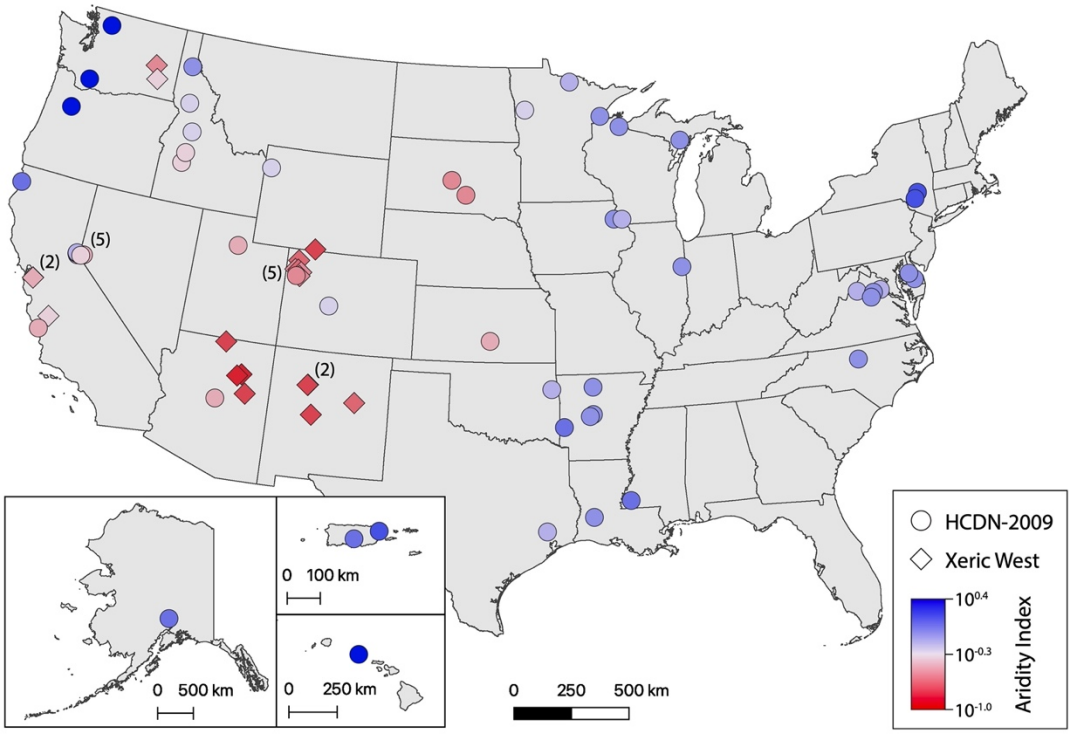

Figure 2.1. Map of the United States with the final set of 71 USGS gauges in this study colored by Aridity Index (Zomer et al., 2022). HCDN-2009 sites (Falcone, 2011) are shown as circles, and sites from the expanded Xeric West dataset are shown as diamonds.

influence on the amount of fine sediment flowing through rivers, and although these structures are absent upstream of the majority of our selected sites, a few Xeric West locations have dams upstream of the USGS gauge station. However, we do not deem this disqualifying in the context of this study; dams trap fine sediment, often leading to *lower* suspended sediment loads and coarsening of bedload downstream (Draut et al., 2011; Galay, 1983; Grant et al., 2013), which would create the opposite effect of what we expect for arid streams in this region. Thus, if anything, inclusion of these dammed sites would likely dampen the signal we observe between climate and suspended sediment behavior.

Furthermore, in terms of possible geographic over- and under-representations, there was a relatively high number of sites in Idaho and Colorado, and five sites within a 300 km^2 quadrilateral near Lake Tahoe. However, we chose not to eliminate any additional sites for the sake of avoiding human bias in our site selection, while still taking note of these small irregularities.

2.3.2 Aridity index as a climate metric

While many parameters can be used to describe a particular climate, arguably the most important aspect is whether that region is dry or humid. With this in mind, we use Aridity Index, or the ratio of mean annual precipitation to potential evapotranspiration, as our principal climatic parameter to assess the influence of climate on sediment transport.

We determined the Aridity Index at each of our gauge locations using a high-resolution raster dataset for the years 1970-2000 (Zomer et al., 2022). This dataset assigns Aridity Index values to 30 arc-second cells (several hundred meters depending on latitude), with lower values representing more arid locations, and higher values more humid. We calculated the mean Aridity Index for all raster cells within each watershed using the *rasterstats* Python package (Perry, 2023). Watershed boundaries for all USGS gauges were provided by the GAGES-II dataset (Falcone, 2011).

2.3.3 Suspended sediment analysis and further site refinement

Continuous stream discharge data, typically recorded every 15 minutes, were obtained for each site over the period of time spanned by suspended sediment concentration data. If discharge measurements began after the earliest suspended sediment measurements, some suspended sediment records were discarded to match the timespan of available discharge data. Each suspended sediment measurement was paired with a corresponding discharge, based on timestamps rounded to the nearest 15-minute interval. If no matching discharge was available within 15 minutes of the suspended sediment measurement, and no alternative record of discharge was available in a separate field measurement dataset, the data point was discarded.

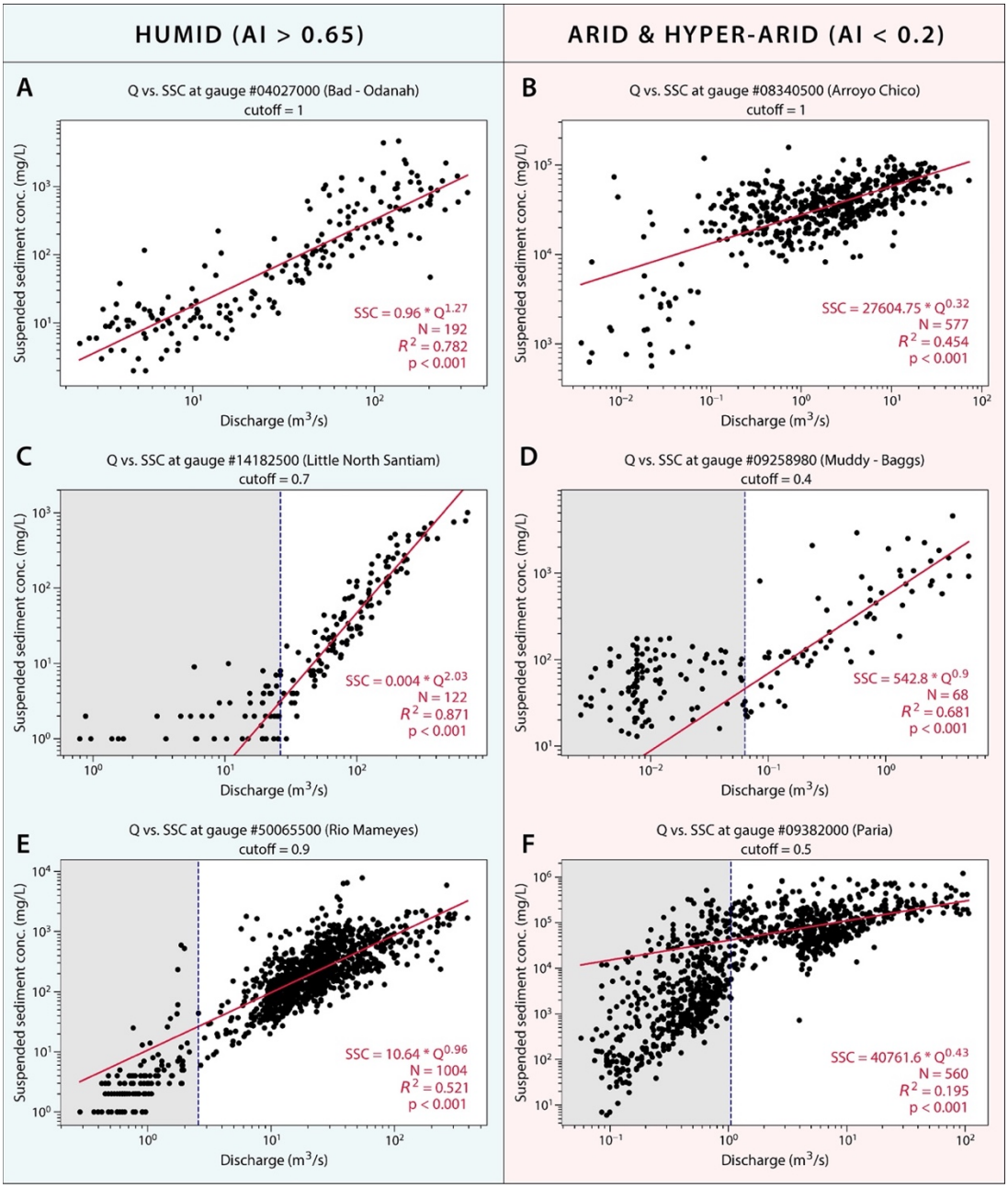

Figure 2.2. Several example power-law fits between discharge and suspended sediment concentration, organized in columns by aridity index (AI). For some sites, no discharge cutoff was applied (A & B), but in most cases, some low-discharge measurements were excluded from rating curve calculations due to data resolution issues and the goal of capturing sediment transport behavior at moderate to high flows (when most transport occurs). Calculated rating curves sometimes underestimated (C & D) or overestimated (E & F) suspended sediment concentrations of excluded points. Corresponding information about the power law regression (red line) is also shown, including the equation, N, R^2, and p-value. "Cutoff" values in plot titles refer to the upper quantile of data points (by discharge) used in the regression.

The relationship between suspended sediment concentration and discharge was usually nonlinear, and for most sites, data behaved linearly in log-log space at moderate and high discharges (Fig. 2.2A, 2.2B). In most cases, we excluded some low-flow data due to data resolution issues; suspended sediment concentration is typically reported as an integer, causing an artificial shallowing of the rating curve slope at low discharges (Fig. 2.2C). In other cases, sediment transport appeared genuinely different at low flow conditions relative to stronger flows (Fig. 2.2D-F); however, given that the majority of sediment transport over time is expected to occur at moderate-to-high discharges (Wolman & Miller, 1960), deemphasizing low-flow conditions is also justifiable from a geomorphic standpoint.

Following the reasoning above, we isolated data above a particular discharge where suspended sediment concentration and discharge began to behave linearly in log-log space, based on a visual fit. For some sites, there was a log-log linear relationship between the two variables even at low discharges, in which case no lower discharge cutoff was applied and all data were used (Fig. 2.2A, 2.2B). A linear regression was applied to the remaining data in log-log space to obtain a best-fit power function relating discharge to suspended sediment concentration in the form

$$SSC = kQ^a, \qquad (1)$$

where SSC is suspended sediment concentration (mg/L) and Q is volumetric discharge (m^3/s). The exponent, *a*, is dimensionless, while the coefficient, *k*, links discharge to concentration and thus has units of $(mg\ L^{-1})(s\ m^{-3})^a$. Suspended sediment measurements of 0 mg/L could not be log-transformed and thus were excluded from

the power law fit; fortunately, these values often occurred at low discharges, which are less significant in this study for the reasons stated above. Given the differences in rating curve behavior at low flow versus moderate to high flow (due to data resolution issues or true trends in sediment transport), some rating curves may have underestimated (Fig. 2.2C, 2.2D) or overestimated sediment concentrations at low flow (Fig. 2.2E, 2.2F). Typically, data resolution issues attributed to integer-based reporting of sediment concentrations were most common in temperate locations (Fig. 2.2C), while rapid rises of suspended sediment concentrations at low flow and subsequent shallowing of the rating curve at higher flow conditions (Fig. 2.2F) was more characteristic of hyper-arid locations in this study. Singular power law fits to these large data sets also ignore variations in suspended sediment rating curves over time due to hysteresis; however, this study aims to examine trends across much longer timescales than individual storm events or particular seasons, so grouping all data together is appropriate. In summary, while power law fits cannot perfectly capture the variety of relationships between suspended sediment and discharge, for the purposes of this large-scale study, these functions should adequately represent sediment transport behavior—particularly at moderate to high flows.

We use the exponent, a, and coefficient, k, in Equation 1 as important quantifiers of sediment transport behavior in this study. Together, these values capture how suspended sediment concentration responds to increasing discharge (a), as well as how much sediment is carried within the flow at any given discharge (k). In order

to avoid drawing erroneous conclusions about exponents and coefficients for the rivers in this study, further data refinement was required.

After applying the discharge cutoff and a power law fit, some sites had no clear relationship between suspended sediment concentration and discharge or few remaining data points (Fig. S2.1). Thus, to preserve data quality and avoid small exponents unrepresentative of true rating curve behavior, sites were discarded if regressions had p-values greater than 0.05 (8 sites) or were based on fewer than 50 measurements (6 sites) (Table S2.1). There was no apparent geographic or climatic pattern in these discarded sites (Fig. S2.2).

The final set of 71 gauge locations spanned a large spectrum of aridity indices and geography (Fig. 2.1). The median number of suspended sediment measurements per site (after regression) was 334, and the median timespan of a given dataset was ~20 years (Table S2.2).

2.4 Results

Rating curve behavior, as described by the coefficient and exponent, varied considerably with aridity. Regression analysis indicates that increases in Aridity Index (AI)—i.e., a wetter climate—are generally associated with decreases in the coefficient ($k = 0.797\ AI^{-4.23}$; $R^2 = 0.47$, $p < 0.001$) and increases in the exponent ($a = 1.28 + 0.368\ ln(AI)$; $R^2 = 0.20$, $p < 0.001$) (Fig. 2.3). These patterns are particularly apparent when plotting the exponent against the coefficient and coloring by the Aridity Index (Fig. 2.4A); while there is some scatter in the data, suspended sediment

rating curves for arid rivers (red) generally have larger coefficients and smaller exponents than for more temperate systems (blue). This figure also shows that overall, coefficients and exponents are inversely correlated; rating curves appear unlikely to have both high coefficients and exponents. This inverse relationship between rating curve parameters has also been observed in prior studies (Asselman, 2000; Syvitski et al., 2000). Of course, this may simply be a consequence of mathematics; assuming there is some limitation on available sediment, a steeper slope in a linear regression will force a smaller intercept. All rating curve coefficients, exponents, and corresponding watershed aridity indices are summarized in Table S2.2.

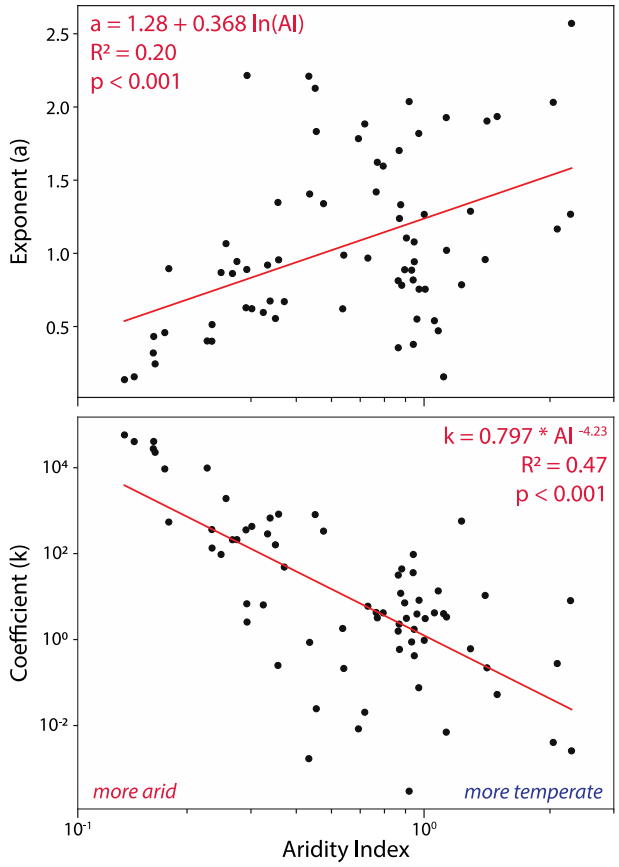

Figure 2.3. Aridity index vs. two rating curve parameters for 71 stream gauges in the United States. Rating curve parameters, *a* and *k*, refer to the exponent and coefficient (respectively) of a power-law fit between discharge (Q; m^3/s) and suspended sediment concentration (SSC; mg/L) in the form $SSC = kQ^a$ (Fig. 2.2). Log axes were used when a particular variable was more normally distributed in log space. Linear regressions in semi-log (above) and log-log (below) space are also shown as red lines, with corresponding equations listed in red text along with an R^2 and p-value for the regression. More arid locations occur to the left of the plots, while more temperate sites tend toward the right.

As another way to visualize these findings, we constructed two representative power-law rating curves for

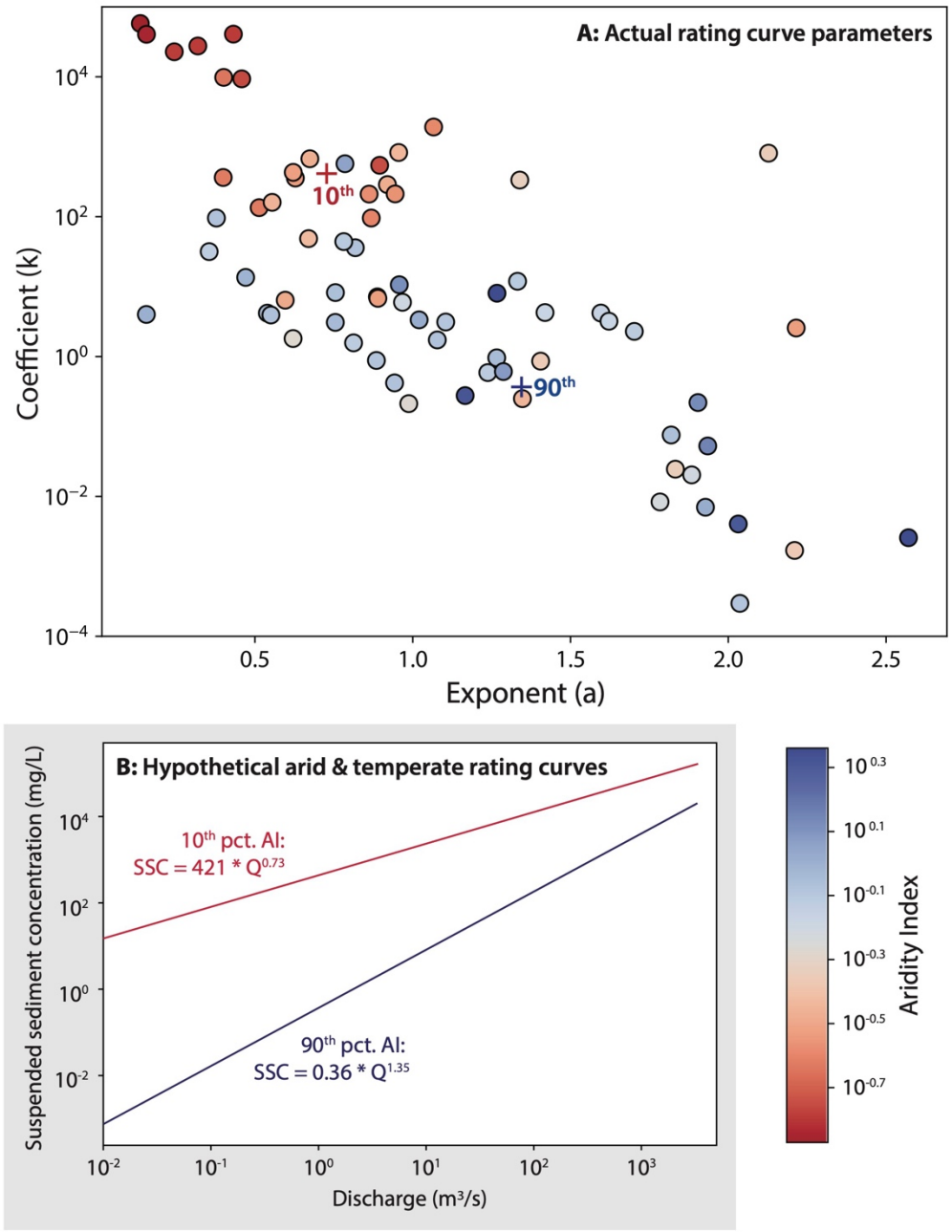

Figure 2.4. Results of suspended sediment rating curve analysis. (A) Coefficients and exponents of power-law rating curves between discharge and suspended sediment concentration, colored by Aridity Index (AI) with more arid sites in red and more temperate sites in blue. The coefficient and exponent pairs for the 10th and 90th percentile AI, estimated using regressions between AI and the two rating curve parameters, are labeled with red and blue crosses, respectively. (B) Representative rating curves between discharge and suspended sediment concentration based on coefficients and exponents estimated at the 10th (arid) and 90th (temperate) percentile Aridity Index (AI), shown as crosses in Panel A. Sediment concentrations are plotted to the highest discharge represented in this dataset, and cut off at 0.01 m^3/s as an arbitrary low value (0 m^3/s cannot be shown on a log scale).

hypothetical arid and temperate streams by inserting the 10th and 90th percentile aridity indices from our site list (0.23 and 1.21, respectively) into the linear regressions between Aridity Index and both rating curve parameters (Fig. 2.3), and plotting suspended sediment concentration over the full range of discharges in our dataset (Fig. 2.4B). In log-log space, the 10th percentile (arid) rating curve is shallower with a higher baseline suspended sediment concentration relative to the 90th percentile (temperate) rating curve. The large difference in the coefficient between the two locations causes the arid stream to have higher suspended sediment concentrations than the temperate stream across all discharges. However, the higher exponent for the representative temperate rating curve causes the suspended sediment concentration to approach that of arid streams as discharge increases. The disparity in suspended sediment concentration between the two rating curves is particularly pronounced at low to moderate discharges, and for the suspended sediment concentration of the temperate stream to exceed that of the arid stream, we must extrapolate the rating curves to higher discharge values than are found in this study.

2.5 Discussion

Our results show that, on average, arid streams have greater suspended sediment concentrations for a given discharge—and thus greater suspended sediment transport efficiency—than streams in more temperate locations (Fig. 2.4B). Furthermore, given the low coefficient and high exponent in their rating curves, rivers in temperate locations transport little suspended sediment at low and moderate flow

conditions, and must reach relatively high flow conditions to transport appreciable volumes of sediment. This highly nonlinear relationship between discharge and suspended sediment concentration is less evident in arid streams, which transport high concentrations of sediment across a wider range of discharges.

2.5.1 Role of river size in rating curve behavior

Before discussing the physical explanation for climate-based contrasts in rating curve behavior, we consider the possibility that the size distribution of rivers in our study skewed our results. In a study of the Rhine River, Asselman (2000) found that with increasing discharge downstream, suspended sediment rating curves shallowed, with the regression coefficient (k) increasing and the exponent (a) decreasing. The author attributed this observation to the fact that the same increase in discharge on a small stream represents a proportionally higher change in flow relative to the mean than in a large river. Hence, smaller rivers would show steeper rating curves simply because of their relatively lower discharge range compared to larger rivers. River discharge may thus be a hidden factor in the broad patterns we see in suspended sediment rating curve behavior across climates.

To explore whether our rating curve trends are influenced by river size, we plotted the rating curve coefficient and exponent against the geometric mean discharge for each site, with discharge values of 0 m^3/s removed from the calculation (Fig. S2.3A). Regression analyses reveal a weak positive relationship between mean

discharge and the exponent, a ($R^2 = 0.14$; $p = 0.002$), and a strong negative relationship between mean discharge and the coefficient, k ($R^2 = 0.54$; $p < 0.001$).

While these regressions show a significant relationship between mean discharge and rating curve behavior, the relationships are the opposite of those from Asselman (2000); increasing discharge in our study correlates with *steeper* rating curves, rather than shallower. Such a relationship was also uncovered by Syvitski et al. (2000) among their study locations. This may in fact be related to climate; rivers in wetter regions tend to be larger, as is clear from the moderate positive relationship between Aridity Index and the geometric mean discharge (Fig. S2.3B). Our analysis reaffirms that climate likely plays a significant role in influencing suspended sediment rating curves in our broad study.

2.5.2 Sediment transport efficiency in relation to sediment yield

Although our work has focused primarily on the distinctive behavior of suspended sediment transport rating curves, the possibility must be addressed that high rates of suspended sediment transport in arid locations (particularly at non-peak flow conditions) are simply a product of high overall sediment loads. As mentioned in the Introduction, multiple studies have examined relationships between annual specific sediment yields and various climatic factors such as precipitation, runoff, temperature, and vegetation cover (e.g., Fournier, 1949; Jansson, 1988; Langbein & Schumm, 1958; Wilson, 1973; Zhang et al., 2022). Perhaps the most well-known of these studies, by Langbein & Schuum (1958), posited that as precipitation increases,

there is a tradeoff between greater runoff, which facilitates erosion, and vegetation density, which reduces it. In this model, sediment yield is maximized in arid and semi-arid climates, which could explain the results of our analysis. However, multiple subsequent studies have cast doubt on these findings, noting that there is no clear relationship between sediment yield and precipitation or runoff, at least on a global scale (Milliman & Farnsworth, 2011; Renwick, 1996; Walling & Webb, 1983; Wilson, 1973). Moreover, multiparameter models of fluvial sediment flux that take into account factors like climate, lithology, slope, and human influence found that climatic factors accounted for only 14% of all variability in fluvial sediment loads, while local geologic and topographic variables were much more important (Syvitski & Milliman, 2007). In summary, past work lends little support to the possibility that rivers in arid locations inherently transport more sediment annually than rivers elsewhere.

While the literature does not strongly suggest a dependence of sediment flux on climate, we can estimate the overall suspended sediment flux at each of our stations to confirm if our data demonstrate such a relationship. To do so, we approximated the annual specific suspended sediment yield, or the total suspended sediment flux per unit watershed area over one year. We first predicted suspended sediment flux over time by multiplying each discharge record (taken every 15 minutes) by the suspended sediment concentration estimated from power law rating curves for each of the 71 gauges. (Notably, standard rating curves without a discharge cutoff were used so as not to severely misrepresent sediment transport at low flow—

see “SSC-Q Plots” in Supplement.) We then integrated the fluxes with respect to time and divided by drainage area to determine the annual specific suspended sediment yield (kg yr^{-1} km^{-2}), which we use as an approximation of the total sediment supply.

A power law regression revealed no significant relationship between aridity and specific suspended sediment yield at our study sites ($R^2 = 0.021$; $p = 0.22$) (Fig. 2.5). Of course, not all proposed models in the literature are power functions, and perhaps a different curve shape would provide a better fit to our data below; a U-shaped curve similar to that of Fournier (1959), for example, may be more appropriate. Regardless of the chosen fit, our analysis demonstrates that the suspended sediment yield at arid locations is not meaningfully greater than that at temperate locations. These results therefore contradict the possibility that fluvial sediment loads are higher in our arid locations than the temperate ones.

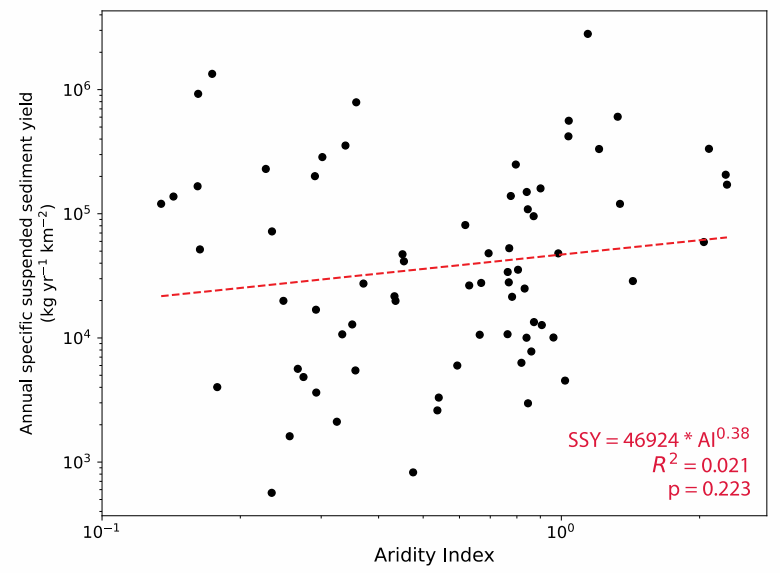

Figure 2.5. Power law regression between Aridity Index and the annual specific suspended sediment yield for the 71 sites in this study. Regression equation, R^2, and p-value are shown in the bottom right.

Moreover, returning to the distinct trends we have observed in sediment rating curves, we see that overall sediment flux also offers limited ability to predict suspended sediment rating curve behavior

for our sites: regression analyses showed no apparent relationship between specific sediment yield and either the rating curve exponent, a (R^2 = 0.001; p = 0.81), or coefficient, k (R^2 = 0.03; p = 0.17) (Fig. 2.6). This suggests that sediment yield is also not particularly relevant when discussing the efficiency of sediment transport.

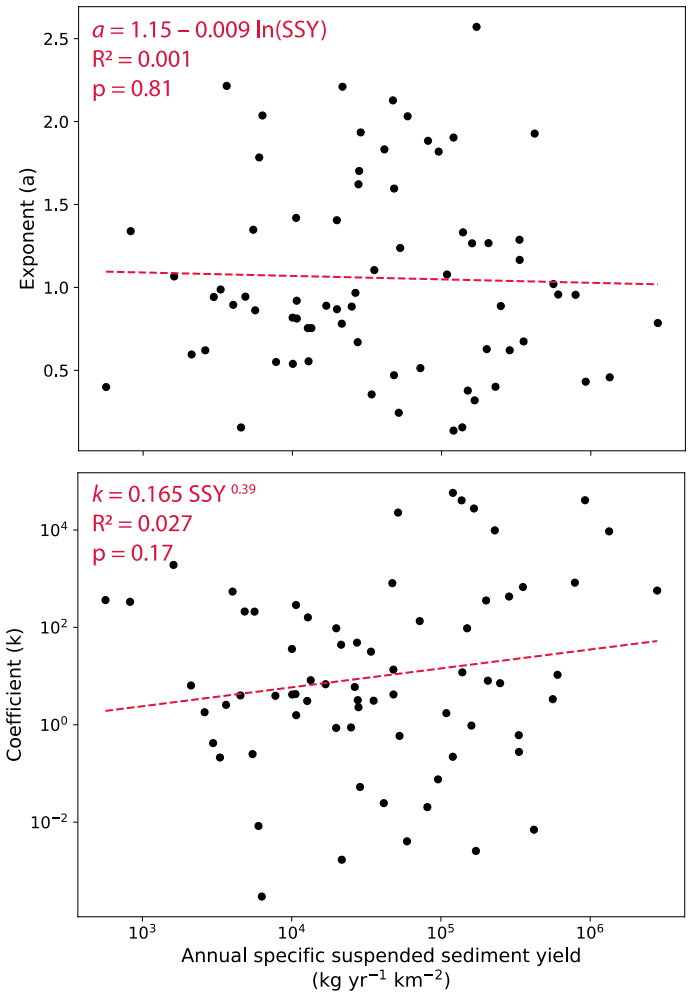

Figure 2.6. Plots of estimated annual specific suspended sediment yield versus power-law rating curve parameters a and k for the 71 USGS gauges used in this study. Linear regressions (in semi-log and log-log space, respectively) do not demonstrate a compelling relationship between sediment yield and rating curve behavior for the sites in this study.

As is evident from our analyses and the established literature, fluvial sediment flux and the supply of sediment to rivers in this study must be examined with more nuance; our work has indicated clear differences in rating curve behavior across climates, but there is no compelling evidence for a significant relationship between the sediment yield and either climate or rating curve behavior. Without any obvious differences in

overall sediment loads across climates, the only explanation for distinct suspended sediment rating curves must be the magnitude and frequency of individual sediment-bearing floods. Variability in a river's "typical" sediment transport event is certainly connected to climate; for example, rivers in arid climates may receive large influxes of sediment following a storm, but significant storm events are more infrequent overall than in temperate locations. This concept is supported by past work suggesting that rivers in arid regions generally have higher mean annual total suspended sediment for a given specific runoff than humid regions (Ludwig & Probst, 1996), and again points to *efficiency* as a key difference in the nature of suspended sediment transport across climates.

There are multiple climate-related variables that affect the magnitude and frequency of suspended sediment transport and could also explain the distinctive behavior of rating curves in this study. We review the most likely possibilities below.

2.5.3 Influence of vegetation cover on sediment supply

The simplest explanation for high fluvial suspended sediment concentrations in arid regions, particularly at low to moderate discharges, is a greater supply of fine sediment to these rivers at those flow conditions in particular. Sediment supply differences could be related to vegetation in the watershed; soil erosion is highly dependent on vegetation density, given that plants provide greater soil cohesion, increase interception and infiltration, and reduce overall runoff (Gyssels et al., 2005; Loch, 2000; Morgan, 2005). Indeed, vegetation removal is often associated with

increased sediment supply to rivers through gradual erosion and shallow landsliding, as well as more frequent sedimentation events due to the lower threshold for significant erosion to take place (Istanbulluoglu et al., 2004; Warrick et al., 2013; Ziemer, 1981). Thus, although the relationship between mean annual precipitation and erosion rates is complicated both in the short and long term (Carretier et al., 2013; Carretier et al., 2018; Walling & Kleo, 1979), overall aridity may influence vegetation density in such a way that sediment supply to rivers is significantly different across climatic regimes. This was, in fact, a key component of the Langbein & Schumm (1958) model, which attributed an observed decrease in sediment yield at high precipitation rates to increasing vegetation density. The lower vegetation density in arid landscapes could allow for significant mobilization of sediment during even relatively modest runoff-generating storms, while much larger, more infrequent storms are required to move sediment in densely vegetated, temperate landscapes.

To investigate the potential role of vegetation in our data, we first estimated vegetation density in each of the 71 study watersheds using the Normalized Difference Vegetation Index (NDVI). We began with a 1-m resolution, 4-band aerial imagery collection acquired during agricultural growing seasons, provided by the USDA National Agriculture Imagery Program (NAIP) (U.S. Department of Agriculture, 2022). Using growing season imagery is preferable as it accurately reflects the presence of vegetation; because NDVI is essentially a measure of vegetation "greenness," estimating an annual mean would greatly underestimate the density of vegetation in deciduous-dominated areas. With this in mind, we used

Google Earth Engine to calculate NDVI from NAIP imagery for the years 2010-2020 using the near-infrared (NIR) and red (R) bands:

$$NDVI = \frac{NIR-R}{NIR+R} \quad (2)$$

Notably, open water (e.g., lakes) should not be considered when evaluating the effects of land vegetation density on soil cohesion in watersheds, so we filtered out cells with NDVI values less than -0.5, representing locations that are almost certainly water. Finally, for each raster cell, we calculated a mean NDVI across all years, and then determined the mean NDVI value for all cells within each watershed using polygons provided by the GAGES-II dataset (Falcone, 2011).

To begin, we find a strong relationship between Aridity Index and NDVI (R^2 = 0.69; $p < 0.001$) (Fig. S2.4). This confirms our assumption that vegetation density should be relatively lower in arid locations, potentially contributing to greater sediment mobilization during storms.

Next, the relationship between vegetation density and sediment transport can be examined by plotting the growing season NDVI against both the coefficient (k) and exponent (a) of the suspended sediment rating curves (Fig. 2.7A). Regression analysis demonstrates a weak positive relationship between mean NDVI and the exponent (R^2 = 0.13; $p = 0.003$) and a moderate to strong negative relationship between mean NDVI and the coefficient (R^2 = 0.40; $p < 0.001$).

The observed relationship between vegetation density and rating curve behavior suggests sediment supply is a potential control on suspended sediment transport efficiency between climates. In general, rivers with denser vegetation in

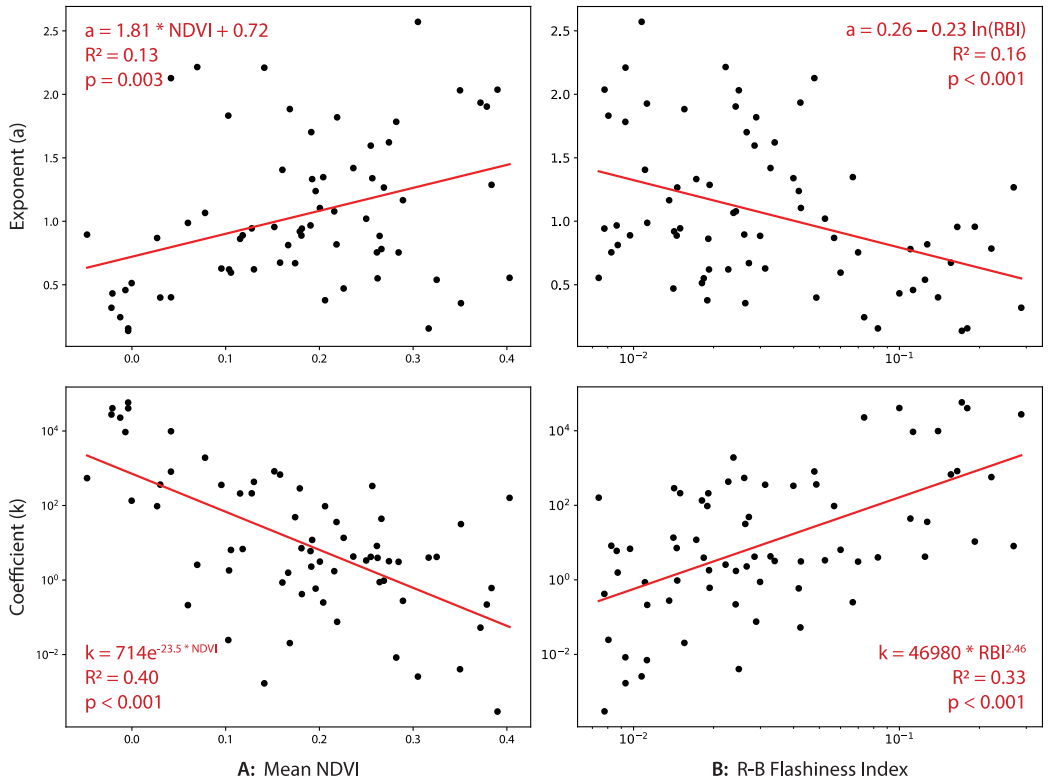

Figure 2.7. Regressions between rating curve power-law parameters (exponent, *a*, and coefficient, *k*) and two possible environmental predictors of sediment transport behavior: (A) Normalized Difference Vegetation Index (NDVI; left) and (B) flow flashiness via the Richards-Baker Flashiness Index (RBI; right) (Baker et al., 2004). Regression equations and corresponding R^2 and p-values are shown in each plot.

their watersheds behave similarly to more temperate (higher Aridity Index) locations, with low rating curve coefficients and high exponents. This may explain the aforementioned behavior of sediment transport in temperate rivers, where suspended sediment concentrations are low during low-flow conditions, but rise rapidly with discharge at higher flow; where there is abundant vegetation, only large and infrequent storms may be able to produce significant hillslope erosion (East et al., 2018). By contrast, in arid regions where vegetation is sparse or patchy, even relatively small storm events mobilize a significant amount of sediment from the

surrounding landscape. This is particularly visible in individual suspended sediment plots from hyper-arid regions, where suspended sediment concentrations are often low or scattered at the lowest flow conditions, but rapidly rise to sustained high concentrations across both moderate and high discharges (e.g., Arroyo Chico and Paria River: Fig. 2.2B & 2.2F; Polacca Wash, Rio Puerco near Bernardo, Oraibi Wash: "SSC-Q Plots" in Supplement).

In summary, our results suggest that differences in vegetation density—and thus erosional thresholds—can explain why high rates of sediment transport occur at relatively lower discharges in arid locations than temperate ones. This is wholly distinct from the effect of vegetation on long-term suspended sediment flux, as there is not a significant relationship between NDVI and the annual specific suspended sediment yield based on a power law fit ($R^2 = 0.002$; $p = 0.70$) (Fig. S2.5). It is more likely that vegetation density influences the magnitude and frequency of sediment supply, thereby influencing overall patterns in suspended sediment transport efficiency across climates.

2.5.4 Flow variability and armoring

Another key climate variable that may influence suspended sediment transport efficiency is variability in precipitation, runoff, and streamflow. While mean annual precipitation is a major influence on overall aridity, the magnitude and frequency of individual precipitation events throughout the year are also quite significant. For instance, regions with moderate but frequent storms year-round will generally be less

arid than locations with only very large, intense storms restricted to a few months. Indeed, across the United States, runoff variability is correlated with Aridity Index, with arid locations experiencing fewer intermediate-frequency runoff events than temperate locations (Rossi et al., 2016).

Differences in precipitation and runoff variability can affect fluvial sediment transport in multiple ways. For one, precipitation variability and vegetation density co-vary, such that regions with strongly seasonal precipitation are typically less vegetated (Hooke, 2000; Lotsch et al., 2003). This can lead to higher sediment yields from the surrounding landscape in the ways we have described above; a less-vegetated watershed will likely have less soil cohesion and reduced infiltration, leading to greater runoff-driven erosion.

However, precipitation variability may also contribute to greater sediment transport efficiency not solely through increased sediment supply, but also through its effect on the sorting of bedload sediment. Flow variability is a major control on whether a riverbed develops "armor"—a coarse, less mobile surface layer above a finer subsurface—which arises due to selective transport of fines under both low-level baseflow and longer flood recessions (Hassan et al., 2006). This could also explain the suspended sediment rating curve behavior we observe in this study, as fine sediment on a loose, unsorted bed surface can quickly be brought into suspension even by relatively low flows, thereby contributing to a relatively high, flatter rating curve (large coefficient, small exponent) (Asselman, 2000). Arid streams, where flow is more infrequent and variable, generally lack significant armor and thus have easily

mobilized beds, leading to high sediment transport rates across all flow strengths. Meanwhile, temperate streams where armor is more developed, have lower suspended sediment transport at low flow conditions and require streamflow to reach some threshold discharge before bedload is mobilized. After this point, suspended sediment concentrations increase quickly, reflected by a steep rating curve (low coefficient, high exponent) (Asselman, 2000). As an example of this climate contrast, Reid & Laronne (1995) compared rates of bedload transport between an ephemeral stream in Israel and a perennial stream in Oregon, claiming that the exceptionally high sediment flux in the ephemeral stream was related to a lack of a coarse armor layer on the riverbed. To the extent that suspended sediment is sourced from the bed of a river, the development of bed armor will strongly influence the mobility of the fine fraction (e.g., Wilcock & Crowe, 2003), and can thus plausibly explain the differences in suspended sediment mobility in arid and temperate settings that we document here.

In lieu of field measurements of surface and subsurface grain size (i.e., armor) at our study sites, we turned to flow variability to test whether bed surface grain size sorting could contribute to the climatic patterns we see in suspended sediment transport, as flow variability is a major control on armor formation (Hassan et al., 2006). We quantified flow variability at each site by calculating the Richards-Baker Flashiness Index (RBI), which compares the sum of incremental changes in discharge (Q, m^3/s) to the total discharge across various timesteps, thus providing a non-dimensional index of how rapidly discharge changes over time (Baker et al., 2004):

$$RBI = \frac{\sum_{i=1}^{n} |Q_i - Q_{i-1}|}{\sum_{i=1}^{n} Q_i} \qquad (3)$$

We used mean hourly discharges, calculated from continuous USGS streamflow data (U.S. Geological Survey, 2022), to determine the Richards-Baker Flashiness Index for each one of our gauge locations, limited to the time span of suspended sediment data used in this study. While Baker et al. (2004) predominantly use mean *daily* discharge to calculate RBI, they note that the chosen interval depends on the application. In this case, hourly averages of discharge are more appropriate because many flash floods in arid locations in our study area occur over the span of hours and minutes, rather than days; mean daily discharge would thus likely dampen the signal of these brief storm events.

Regression analysis indicates that increases in RBI are generally associated with decreases in the exponent ($R^2 = 0.16$; $p < 0.001$) and increases in the coefficient ($R^2 = 0.33$; $p < 0.001$) (Fig. 2.7B). That is, flashier streams parallel the behavior of more arid streams, with lower rating curve exponents and higher coefficients, though interestingly there is not a clear relationship between the Aridity Index and the Richards-Baker Flashiness Index ($R^2 = 0.04$; $p = 0.09$) (Fig. S2.6). In short, the relationship between flashiness and the two rating curve parameters suggests that flow variability could also play a role in determining sediment transport efficiency, potentially through its effect on riverbed armoring.

It is worth noting that riverbed armoring is primarily a bedload process, and we have examined suspended sediment in this study. However, the two processes are closely linked. If a riverbed is unarmored, suspended sediment transport and bedload transport will be strongly correlated, partly because fine sediment can be sourced

from the bed of the channel, and highly armored streams should lack significant suspended sediment concentrations or bedload transport rates at low flow conditions. Furthermore, a large supply of fine sediment from the watershed causes a finer channel bed, and thus high rates of transport in both the suspended load and bedload (Parker & Klingeman, 1982). Finally, the amount of fine sediment in alluvial channels has been shown in some settings to influence movement of the coarse fraction (Dietrich et al., 1989; Iseya & Ikeda, 1987; Parker, 1990; Wilcock & Crowe, 2003), so high suspended sediment concentrations can also facilitate high bedload transport rates in streams. Thus, differences in flow variability between rivers in contrasting climates could contribute to similar differences in armoring, which may explain the distinctive behavior of suspended sediment rating curves.

2.5.5 Relative roles of vegetation and flow variability

Given the similar strength of the relationships between rating curve parameters and the two variables we examine here—vegetation density and flow flashiness—it is not immediately apparent which property best explains the connection between climate and sediment transport efficiency. While the two variables are only weakly correlated ($R^2 = 0.10$; $p = 0.008$) (Fig. S2.7), the complicated relationships between hydrologic, ecologic, and geomorphic processes may make them impossible to disentangle. As noted before, precipitation variability influences vegetation density in a watershed, which in turn controls sediment supply to channels, but that variability also affects riverbed armor formation, which itself can

change the efficiency of sediment transport. Moreover, riverbed armoring is also largely determined by sediment supply (Hassan et al., 2006); a river cannot winnow fine grains from the bed if there is a large input of fine sediment to the channel. Therefore, while riverbed armoring may explain a component of the documented contrasts in fluvial sediment transport efficiency between arid and temperate locations, differences in grain size sorting could also reflect local flow variability or vegetation-driven sediment supply, both of which relate to climate. The complex relationship between aridity, flow variability, armoring, vegetation, and sediment transport is summarized in Figure 2.8.

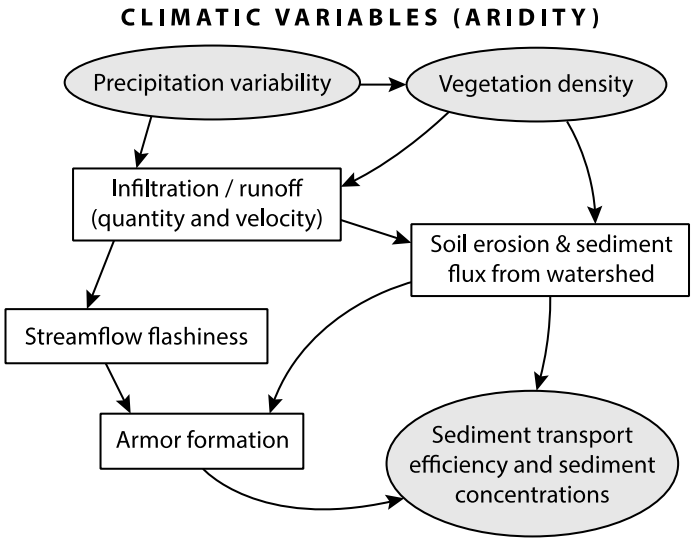

Figure 2.8. Flow chart demonstrating the relationships between two key climatic variables (precipitation and vegetation) and sediment transport efficiency.

Most likely, the compounded effects of both vegetation and flashiness contribute to differences in sediment transport efficiency, rather than any one parameter dominating. Indeed, the Aridity Index is a stronger individual predictor of rating curve parameters than either NDVI or flashiness (Figs. 2.3 & 2.7), implying that sediment transport is determined by multiple factors that all depend on—or contribute to—the overall climate.

While vegetation density and precipitation variability are probably the principal factors controlling suspended sediment transport efficiency, there could be other variables we did not account for. It seems likely, however, that any other climatic variables would be inseparable from either rainfall or vegetation patterns, in the same way that these two variables are interconnected themselves. For example, Syvitski et al. (2000) found covariance between rating curve parameters and factors like mean annual temperature and latitude, variables that should not intuitively influence sediment delivery to rivers. Additional analyses of climate proxies and sediment transport may contribute to a more complete understanding of sediment transport across different climates, but there is most likely no specific variable more responsible for the results of this study than the overall climate itself.

2.6 Conclusions

In this contribution we examine suspended sediment concentrations and continuous flow records from 71 U.S. Geological Survey gauges across North America, finding that increasing aridity coincides with higher coefficients and lower exponents in power-law relationships between discharge and suspended sediment concentration. This rating curve behavior demonstrates that rivers in arid locations generally transport sediment more efficiently than those in temperate regions. Arid streams transport a large volume of suspended sediment across a wide range of discharges, including low to moderate flow conditions, while suspended sediment

transport in temperate streams is minimal at low discharges, but scales quickly as discharge increases.

We attribute the contrast in sediment transport efficiency mainly to differences in vegetation density and precipitation patterns, which in turn affect both sediment supply and streamflow variability. Based on regression analyses, we interpret the relationship between climate and sediment transport behavior as likely due to the combined effect of multiple climatic factors, some of which we may not have considered. Notably, further analyses of specific suspended sediment yield reveal no clear relationship between climate and overall suspended sediment loads, suggesting that the distinct patterns in sediment rating curves are a result of differences in how and when sediment transport occurs across climates.

These results are highly relevant to risk management, particularly with respect to flood hazards and infrastructure damage. Variability in river bed elevation and flood conveyance in the United States is particularly high in arid settings (Slater et al., 2019; Slater & Singer, 2013), leading to major erosion and sediment deposition problems near channels (e.g., Merritt & Wohl, 2003; Wilcox et al., 2016). Our results lend credence to these observations and suggest some mechanistic explanations. Moreover, these hazards are likely to be exacerbated by anthropogenic climate change; presently, new non-perennial and flashier streams are emerging throughout the southern and southwestern U.S. (Overpeck & Udall, 2020; Zipper et al., 2021), and climate change has also led to shifts in vegetation distribution and the frequency of extreme rainfall events and droughts, which have profound consequences for

streamflow, river morphology, and sediment transport (East & Sankey, 2020). It is thus increasingly important to understand inherent properties of rivers, which may shed light on how climate change will affect sediment transport behavior and natural hazard risks.

2.7 Supplementary information

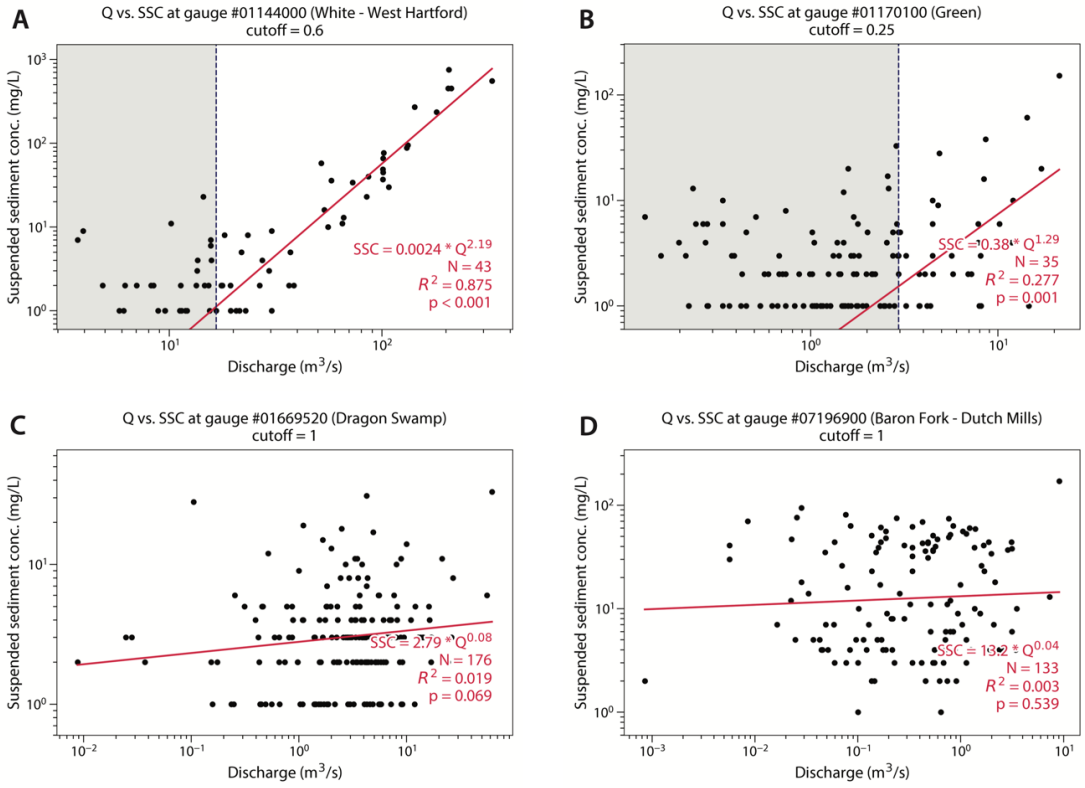

Figure S2.1. Examples of rivers excluded due to low N or high p-values. Some sites had compelling linear relationships but simply lacked sufficient data points following data point exclusion due to discharge cutoff (A), and some locations lacked sediment concentrations sampled at intermediate and high discharges (B). High amounts of scatter producing large p-values was sometimes caused by generally low suspended sediment in the river (C) or simply a high variability in suspended sediment concentrations (D). Inclusion of high-p-value sites in particular would likely skew rating curve results; in these cases, small exponents usually arise due to a poorly defined relationship between suspended sediment concentration and discharge, rather than distinctive shallow rating curve behavior. Also note the clear horizontal banding of points in A-C; suspended sediment concentration is reported as integers only, which often skews rating curve best-fit functions unless a discharge cutoff is applied.

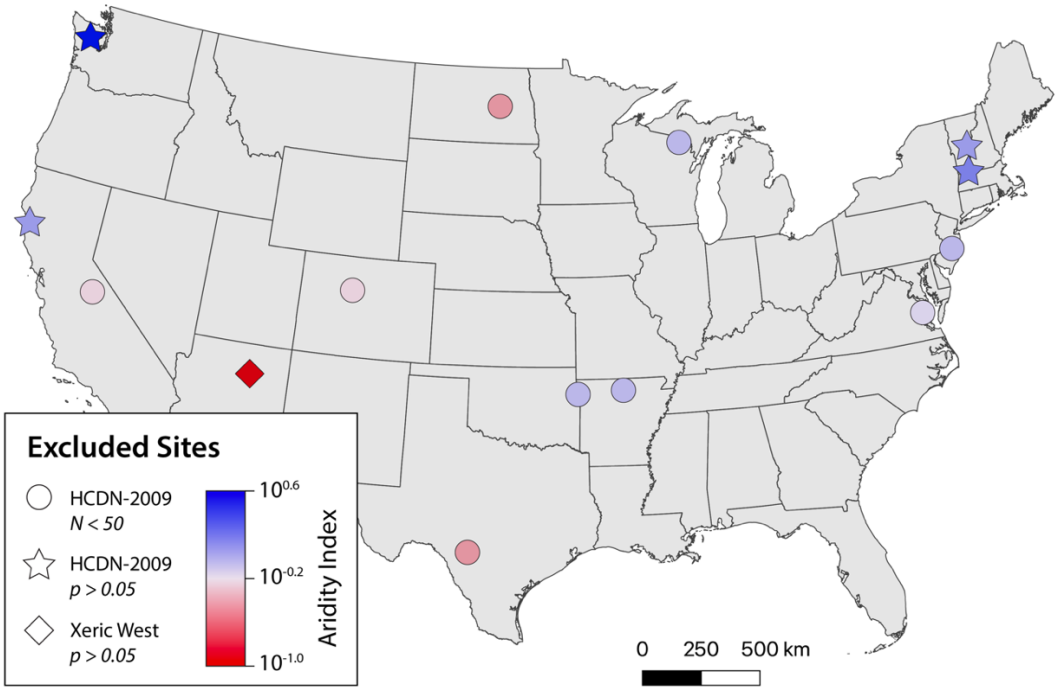

Figure S2.2. Map of excluded sites, colored by Aridity Index (Zomer et al., 2022), with symbols representing the GAGES-II dataset (HCDN-2009 or Xeric West) per Falcone (2011) and reason for exclusion (N or p-value). No sites outside the contiguous United States were excluded. Additional information on all excluded sites is summarized in Table S2.1.

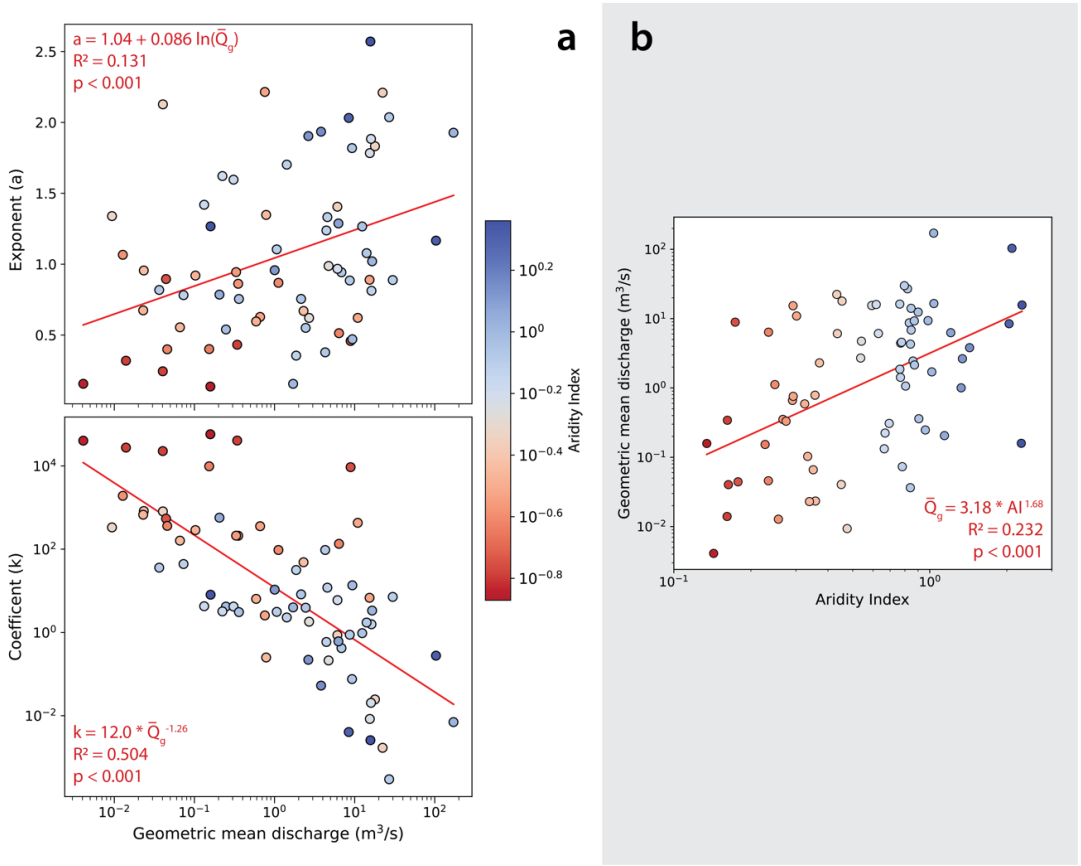

Figure S2.3. Investigation of the role of river discharge in suspended sediment transport for the 71 rivers in this study (Table S2.2). (A) Regressions demonstrate a weak, positive relationship between the geometric mean discharge ($\bar{Q}_g$, m^3/s) and the rating curve exponent (a), and a strong, negative correlation between the geometric mean discharge and the rating curve coefficient (k). (B) Regression analysis reveals a moderate, positive relationship between the Aridity Index and geometric mean discharge.

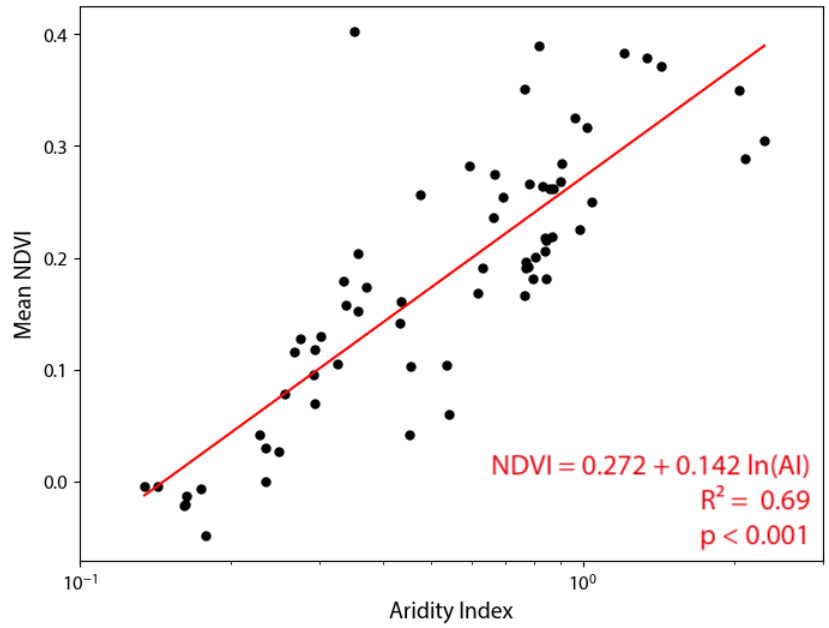

Figure S2.4. Aridity Index versus basin-averaged normalized difference vegetation index (NDVI) for the 71 sites in this study (Table S2.2). A linear regression in semi-log (x-axis) space suggests a moderate to strong correlation between the two variables.

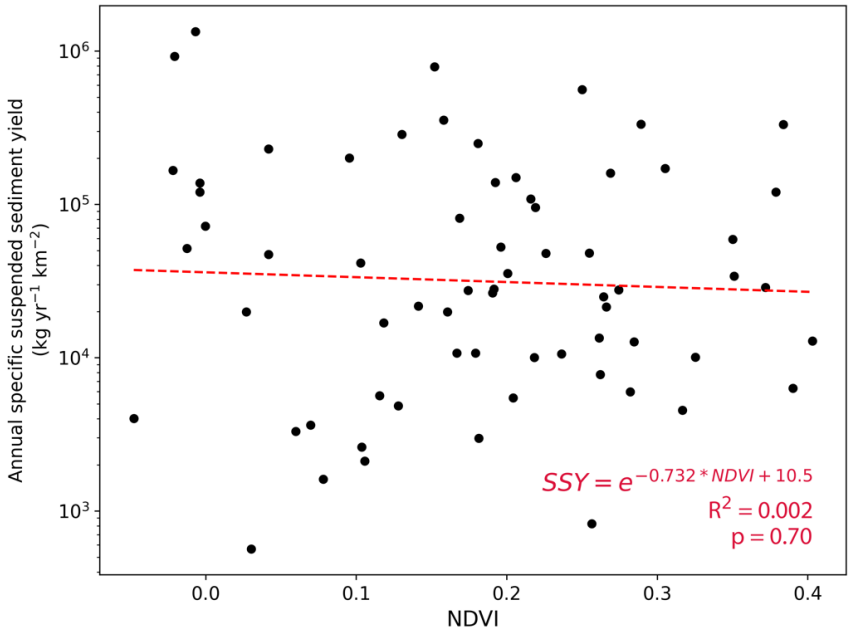

Figure S2.5. Normalized difference vegetation index (NDVI) versus the annual specific suspended sediment yield for the 71 sites in this study (Table S2.2). A linear regression in semi-log space does not indicate a significant correlation between the two variables.

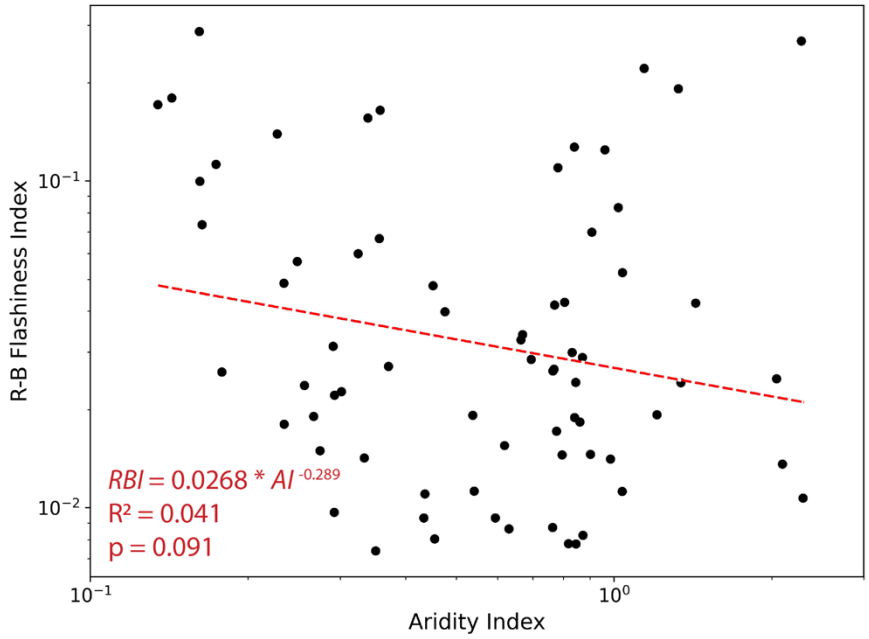

Figure S6. Aridity Index versus Richards-Baker Flashiness Index (Baker et al., 2004) for the 71 sites in this study (Table S2.2). A linear regression in log-log space does not indicate a significant correlation between the two variables.

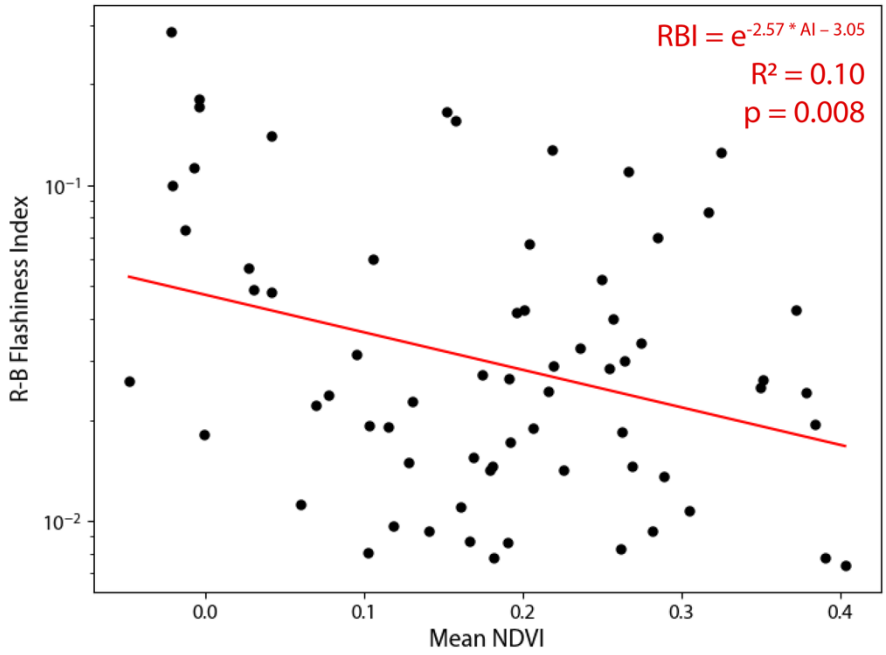

Figure S7. Basin-averaged NDVI vs. Richards-Baker Flashiness Index for the 71 sites in this study (Table S2.2). A linear regression in log-log space suggests a weak negative correlation between the two variables.

Additional supporting information

Tables S2.1 and S2.2 can be found in the Supplementary Files as Table_S2-1.csv and Table_S2-2.csv. Captions are provided below.

Table S2.1. Summary of all sites excluded from rating curve analysis (14). Sites were excluded if $N < 50$ or $p > 0.05$ after a discharge cutoff was applied. "Excl. variable" column indicates whether N or p was responsible for site exclusion. Table also includes information about site location, timespan of data, quantile used for excluding data below a particular discharge ("Cutoff"), rating parameters (k and a), and Aridity Index (AI). p-values were rounded to the fifth decimal place. "Cutoff" number represents the upper quantile of the dataset used; i.e., "0.8" draws from only the upper 80% of all data points when sorted by discharge. See main text for further information.

Table S2.2. Summary of all sites used in final rating curve analysis (71), including pertinent information about site location, timespan of data used, quantile used for excluding data below a particular discharge ("Cutoff"), rating curve coefficient (k) and exponent (a), N, p, Aridity Index (AI), mean Normalized Difference Vegetation Index (NDVI), and specific suspended sediment yield (SSY). p-values were rounded to the fifth decimal place.

Additional Plots: "SSC-Q Plots.zip"

Folder containing calculated rating curves for the 85 USGS gauge locations examined in this study, comprising 71 final sites and 14 excluded sites. Rating curve plots are saved as PNG files with the title "*River Name-USGS ID*-SSC-Q.png", where "River Name" and "USGS ID" correspond to the first two columns of Table S1.1 and Table S1.2 (e.g., "Arroyo Chico-08340500-SSC-Q.png"). If a site had a discharge cutoff applied, the cutoff quantile is also listed at the end of the file name (e.g., "Alum Fork Saline-07362587-SSC-Q_0.5.png"). Images are provided for rating curves both before and after a discharge cutoff was applied; non-cutoff rating curves were exclusively used for calculating the specific sediment yield (see Section 4.1). Each plot between discharge (m^3/s) and suspended sediment concentration (mg/L) also shows the best-fit power-law function to the data, as well as a corresponding equation, N, and the R^2 and p-value for the linear regression in log-log space. Cutoff quantiles are listed in the plot title, and represented by a blue dashed vertical line on the plot; best-fit functions were only based on data to the right of the blue line.

Chapter 3

Linking suspended sediment rating curves to riverbed grain size and armor

William A. L. Chapman & Noah J. Finnegan

3.1 Abstract

River form and function reflect the various natural and anthropogenic processes in a watershed, which all make up a larger sediment transport regime. Frequently studied river attributes such as suspended sediment transport behavior, surface grain size, and grain size sorting all separately provide meaningful information about climate, lithology, and land use change, but the connection between these different river metrics is still not fully understood. In this study, we compare field measurements of bed surface grain size and armor to the power law coefficient and exponent of suspended sediment rating curves for 12 rivers spanning two distinct sediment transport regimes in the United States. Results demonstrate a compelling relationship between rating curve behavior and riverbed organization, with rivers in Idaho and Washington exhibiting larger surface grain sizes, higher armor ratios, smaller power law coefficients, and larger exponents than rivers in Arizona and New Mexico. The extreme differences between our two study regions are likely driven by climatic variables, such as vegetation density and streamflow flashiness, as well as lithologic factors like rock hardness. Additional analysis of sites with different combinations of lithologic and climatic properties supports the hypothesis that our two primary regional datasets are end members with respect to overall sediment transport and riverbed structure, and also reinforces the concept that both climate and

lithology are highly influential in shaping the overall suspended sediment regime. This research provides new perspectives on the use of suspended sediment rating curves to understand the nature of bedload, which may help in stream restoration efforts and hazard mitigation.

3.2 Introduction

The balance of sediment supply and transport capacity is one of the most fundamental concepts in the study of alluvial rivers (Lane, 1954). These two components of the broader sediment transport regime can be broken down into other variables like the grain size distribution and quantity of sediment supplied to a river, as well as the magnitude and frequency of flow events. It is this complex combination of geologic and hydrologic factors that ultimately determines important physical attributes of a river such as annual sediment load, channel morphology, and ecological function. Exploring the relationships between different properties of alluvial rivers can therefore be an effective strategy to understand the broader sediment transport regime.

One of the most widespread tools for understanding sediment transport is the suspended sediment rating curve, a statistical regression of discharge and suspended sediment concentration. Among other things, suspended sediment rating curves have been used to calculate total suspended load in rivers (East et al., 2018; Ellison et al., 2020; Harrington & Harrington, 2013; Horowitz, 2003; Zhang et al., 2012); to quantify changes in sediment transport following anthropogenic or natural

disturbances, such as logging, wildfires, or climate change (Ahn & Steinschneider, 2018; Desilets et al., 2007; Fisher et al., 2021; Warrick & Rubin, 2007); and to identify the source and antecedent conditions of sediment delivery based on hysteresis patterns (Seeger et al., 2004; Smith & Dragovich, 2009). These numerous applications make suspended sediment rating curves a powerful resource in evaluating sediment transport in rivers and the broader landscape.

Riverbed grain size and sorting are two other frequently studied expressions of the sediment transport regime in a given watershed (Dade & Friend, 1998; Sklar et al., 2006). This is because changes in grain size and bed armoring—that is, the development of a coarse surface above a finer subsurface—are directly tied to sediment supply and transport capacity in a river (Dietrich et al., 1989; Parker & Klingeman, 1982). This connection has been reaffirmed by countless studies examining the impacts of dams, vegetation removal, or nearby mining on riverbed grain sizes and armoring (e.g., Chien, 1985; East et al., 2015; Ferguson et al., 2015; Galay, 1983; Ross et al., 2019). Given that bed texture contains information about the sediment transport regime of a river, it seems intuitive that the riverbed should be tied to the suspended sediment rating curve, another expression of sediment transport in a watershed; however, these two metrics are rarely compared directly to one another.

The relationship between suspended sediment rating curves, riverbed structure, and sediment transport regime has been studied indirectly in the past. In a survey of 71 stream gauging stations across the United States, Chapman & Finnegan (2024) found a significant correlation between watershed aridity and suspended

sediment rating curve behavior, and hypothesized that this was partly due to climate-driven differences in the grain size and sorting of riverbed sediment. However, this study lacked measurements of riverbed surface and subsurface grain sizes, so this interpretation was somewhat speculative. Field measurements of riverbed grain size and sorting at some of these study locations would effectively test the authors' hypothesis that climate-based differences in suspended sediment rating curves can accurately be tied to riverbed character.

Defining a clear link between suspended sediment rating curves and riverbed grain size and sorting would also provide a useful predictive tool in fluvial geomorphology research. For example, although bedload and suspended load transport rates in rivers are generally correlated, the relative proportions tend to vary between river systems (Babiński, 2005; Cantalice et al., 2013; Stark et al., 2021; Turowski et al., 2010). Thus, additional knowledge of suspended sediment transport behavior may provide another useful index of overall bed mobility. This is particularly helpful given that measurements of bedload transport rates are remarkably difficult (Garcia et al., 2000; Recking et al., 2012; Reid et al., 1980), while suspended sediment data are frequently collected and widely available online (US Geological Survey, 2024). Furthermore, establishing the relationship between suspended sediment rating curves and riverbed structure would reduce the number of degrees of freedom when attempting to link overall sediment transport regime and specific watershed attributes such as lithology and streamflow variability.

In this study, we combine the results of previous suspended sediment rating curve analyses from Chapman & Finnegan (2024) with direct measurements of riverbed surface and subsurface grain sizes to investigate the relationship between these two commonplace metrics in the field of fluvial geomorphology. Next, as a proof of concept, we explore the potential environmental factors responsible for the observed differences in suspended sediment rating curves and bed structure at our primary study locations, then extend the analysis to additional sediment transport regimes. Through these investigations, this work provides a valuable context for future studies of sediment transport by unifying distinct analytical methods.

3.3 Methods

3.3.1 Site selection and suspended sediment rating curves

To explore how suspended sediment rating curve behavior is associated with the size and sorting of bedload material, we first identified stream gauges across different climatic regimes with sharply contrasting rating curve behavior according to Chapman and Finnegan (2024). We then sampled surface and subsurface grain sizes in the field at each gauge in order to test whether the relationship between discharge and suspended sediment concentration is linked to bed surface grain size and sorting.

The relationship between discharge and suspended sediment concentration is often modeled as a power law relationship (e.g., Horowitz, 2003; Syvitski et al., 2000; Warrick, 2015). Suspended sediment rating curves can thus be represented by the function

$$SSC = kQ^a, \quad (3.1)$$

where *SSC* represents suspended sediment concentration (mg L^{-1}), *Q* is volumetric discharge (m^3 s^{-1}). The power-law exponent, *a*, and coefficient, *k*, define the shape of the curve, and are therefore the primary means of quantifying suspended sediment rating curve behavior. The exponent is dimensionless, and the coefficient has units of (mg L^{-1}) (s m^{-3})^a.

Chapman & Finnegan (2024) calculated *a* and *k* for 71 U.S. Geological Survey stream gauges across the United States, which were chosen using several quality-controlling criteria: all had multidecadal, continuous discharge records, at least 50 suspended sediment measurements spanning several years, and relatively low anthropogenic impact as determined by the GAGES-II project (Falcone, 2011).

We began our site selection with this set of 71 USGS gauges and identified two regions in different climates with particularly contrasting suspended sediment rating curve behavior, as determined by the power law coefficient and exponent calculated by Chapman & Finnegan (2024). These regions were the Northwest (Idaho and Washington) and Southwest United States (Arizona and New Mexico) (Fig. 3.1). Overall, suspended sediment rating curve coefficients are much larger in Arizona and New Mexico rivers compared to sites in Idaho and Washington, while rating curve exponents are smaller. In other words, rating curves for Southwest rivers are shallower, with higher suspended sediment concentrations particularly at lower discharges (Fig. 3.1, inset).

We chose six sites from Chapman & Finnegan (2024) for grain size analysis in the Northwest US, and five in the Southwest US. One additional site, Lochsa River near Lowell, Idaho (USGS gauge 13337000) was added to the Northwest study region, as this site was near other Idaho sites and met the selection criteria cited above. The rating curve coefficient and exponent were also calculated for this site following the methodology of Chapman & Finnegan (2024). This yielded 12 total sites for our analysis (Fig. 3.1).

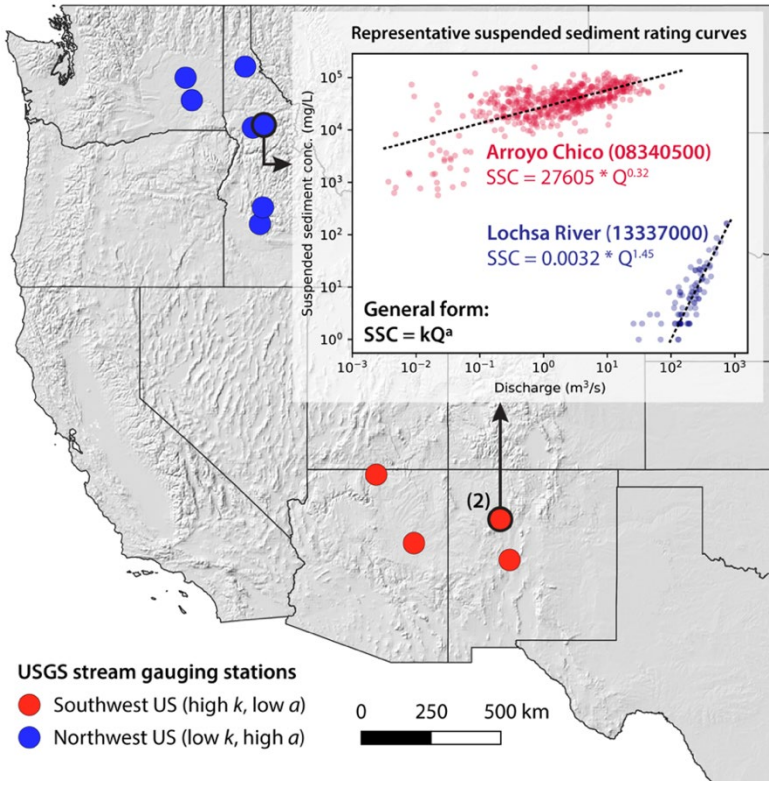

Figure 3.1. Map of the Western United States on a hillshade basemap, with the 12 USGS stream gauge stations examined in this study shown as colored circles. Parenthetical "2" indicates the presence of two nearby sites in New Mexico. Sites are split into two primary regions based on suspended sediment rating curve behavior. Representative rating curves for Arroyo Chico (arid Southwest) and Lochsa River (temperate Northwest) are included in the inset plot to demonstrate differences in sediment transport: Southwest sites typically have higher power law coefficients and lower exponents than Northwest sites.

3.3.2 Field measurements and grain size analysis

For each of the chosen USGS stream gauges, we located the nearest bar where grain size measurements were possible (Fig. S3.1; Fig. S3.2). Most selected bars were

within 2 km of the gauges (and often much closer), but in a few cases, the nearest accessible bar was farther away; for the Palouse River (13351000), we chose a bar ~7 km upstream of the gauge, for the Payette River (13235000), we selected a bar ~3 km upstream, and for the Rio Puerco near Guadalupe (08334000), we sampled ~4 km upstream of the gauge. However, there were no observable differences in hydrology or sediment supply between the bar sites and gauge locations due to tributaries, diversions, or other features.

Given the heterogeneous nature of bars, we selected 3-4 patches along each bar to sample the full range of grain sizes. At each patch, we first took photographs of the bar surface using an iPhone 13 Pro. We then excavated the patch to a depth of approximately one maximum surface grain diameter, thereby removing the armor layer if present (Bunte & Abt, 2001), and took additional photos of the subsurface. In two cases (Paria River, 09382000; and Rio Puerco near Bernardo, 08353000), some patches were internally heterogeneous, so these were split into sub-patches for later averaging. At one site, the South Fork Clearwater River near Stites, Idaho, high-quality photos were not possible due to inclement field conditions. For the remaining 11 sites, this process resulted in 73 photos of surface and subsurface grains for 35 separate patches (Supplementary Files S3.1).

We approximated a manual Wolman pebble count (Wolman, 1954) in surface and subsurface photographs by constructing a grid of at least 100 evenly spaced intersections on each photograph, then measuring the visible minor axis of the grain found at each intersection. Given that most grains lie flat, the minor axis in two-

dimensional space usually corresponds to the grain's intermediate axis; this traditionally is the axis used for estimating grain diameters per the Wolman (1954) method. If a grid intersection lay on a gap between grains, or if the chosen grain was mostly obscured by overlying material, the nearest measurable grain was used instead.

For each patch, we calculated the median diameter of the surface (D_{50}) and subsurface (D_{50s}) grains, as well as an armor ratio (D_{50} / D_{50s}). We then found a representative surface grain size and armor ratio for each of the 12 sites using a mean of all patch values.

Because we could not gather grain size information for the South Fork Clearwater River near Stites (13338500), median surface and subsurface grain diameters for this site were instead taken from King et al. (2004). Separately, surface grain size at the Little Colorado River near Joseph City, AZ (09397300) was too small to resolve in field photographs. However, based on qualitative field observations, the surface was primarily a mix of clay, silt, and fine sand; thus, a representative value of 0.05 mm was chosen for the surface D_{50} at this location.

3.4 Results

Surface grain size measurements and armor ratios varied substantially between sites in the two regions (Table 3.1). Southwest sites in Arizona and New Mexico were relatively fine and unsorted, with bed surfaces primarily comprising medium sand or finer, and armor ratios between 0.2 and 1.5. By contrast, riverbeds in

the Northwest were relatively coarse and armored, with mean surface D_{50} ranging from 9.7 mm to 95 mm, and armor ratios between 4.1 and 31.5. These differences are highlighted in Figure 3.2. Notably, no study locations featured coarse riverbed surfaces but small armor ratios, nor fine riverbed surfaces with large armor ratios.

USGS Gauge #	River	Region (State)	Coefficient (k)	Exponent (a)	# of patches	D_{50} (mm)	D_{50s} (mm)	Armor ratio
08340500	Arroyo Chico	Southwest (NM)	27604.75	0.319	3	0.32	0.27	1.2
08334000	Rio Puerco above Arroyo Chico	Southwest (NM)	9807.69	0.401	3	0.36	0.24	1.5
08353000	Rio Puerco near Bernardo	Southwest (NM)	22789.81	0.244	4	0.35	0.28	1.3
09382000	Paria R.	Southwest (AZ)	40761.60	0.432	3	0.15	0.17	0.7
09397300	Little Colorado R.	Southwest (AZ)	9352.65	0.458	3	0.05*	0.21	0.2*
12413000	Coeur d'Alene R.	Northwest (ID)	0.00030	2.04	3	29.9	8.1	4.6
13185000	Boise R.	Northwest (ID)	0.00170	2.21	3	43.1	1.4	31.5
13235000	Payette R.	Northwest (ID)	0.02455	1.83	3	35.2	1.8	17.5
13337000	Lochsa R.	Northwest (ID)	0.000014	2.43	4	52.2	1.8	30.7
13338500	Clearwater R.	Northwest (ID)	0.00834	1.78	N/A**	95**	23**	4.1**
12464770	Crab Cr.	Northwest (WA)	2.56	2.22	3	9.7	1.7	5.6
13351000	Palouse R.	Northwest (WA)	0.86	1.41	3	28	2.69	14.6

Table 3.1. Grain size measurements, armor ratios, and suspended sediment rating curve parameters for river bars near 12 USGS stream gauging stations in the western United States. Rating curve coefficients (k) and exponents (a) from Chapman & Finnegan (2024) and this study.
* Surface grain size could not be resolved in imagery; estimated as 0.05 mm.
** Grain size information from King et al. (2004).

Grain diameters and armor ratios were broadly consistent within regions. Arizona sites on average featured somewhat smaller armor ratios than New Mexico sites (0.2 and 0.7, compared to 1.2–1.5), but D_{50} only varied on the order of 0.1 mm.

Surface grain sizes and armor ratios of sites in eastern Washington also roughly resembled those of Idaho sites, though on average were less coarse (a mean D_{50} of ~19 mm, compared to ~51 mm in Idaho) and less strongly armored (a mean ratio of 10, as opposed to 18 in Idaho). However, all sites were markedly different from those in the Southwest dataset.

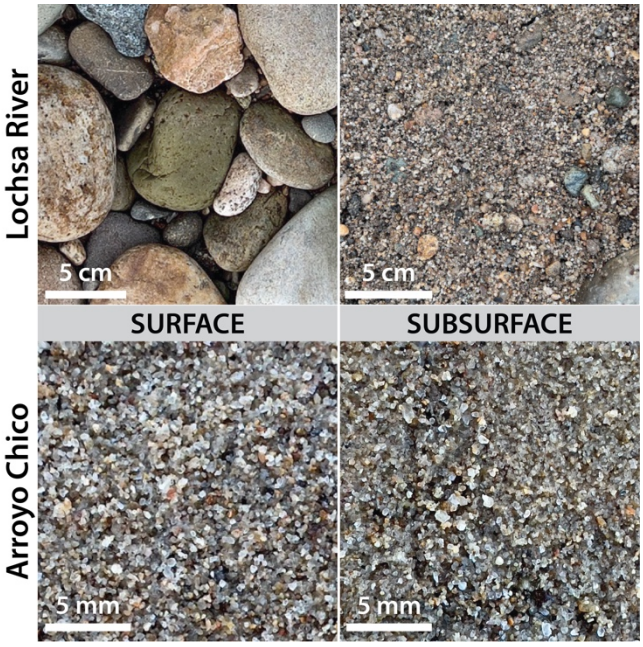

Figure 3.2. Example images of the surface and subsurface of two contrasting riverbeds: Lochsa River (Northwest US) and Arroyo Chico (Southwest US). Northwest sites generally have larger surface grain diameters and armor ratios.

Overall, there may be minor differences in grain size and sorting between sites within a given regional dataset (e.g., Idaho vs. Washington sites in the Northwest dataset), but the relatively small number of sites limits our ability to make meaningful distinctions between sub-regions. Moving forward, we therefore consider only the aggregated regional datasets—which have much more obvious differences—when discussing riverbed characteristics.

Riverbed grain size, sorting, and suspended sediment transport behavior can be viewed together by plotting the power-law exponent against the coefficient, and coloring by surface D_{50} and armor ratio (Fig. 3.3). It is worth noting that although our two regions were selected *because* of their different rating curve behavior, this is

especially apparent in *k-a* parameter space; Northwest sites occupy a completely separate area of the plot than Southwest sites. Moreover, color contrasts between darker Southwest sites in the upper-left of the plot and lighter Northwest sites in lower-right make clear that these two regions do not overlap with respect to median surface grain diameter and armoring. As a whole, this diagram emphasizes the distinct differences between the two regions with respect to both sediment transport behavior and bed composition: Northwest rivers have lower rating curve coefficients, higher exponents, larger bed surface grains, and stronger armoring than Southwest rivers.

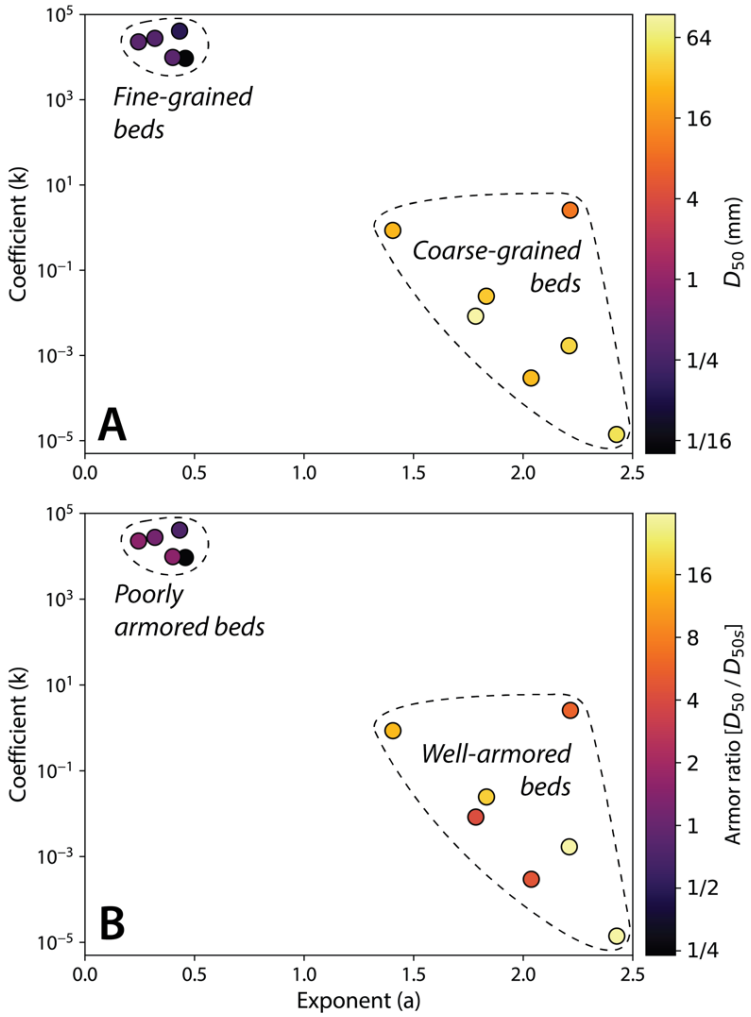

Figure 3.3. Suspended sediment rating curve behavior for 12 study sites, plotted as power-law coefficients and exponents. Sites in the Northwest US (Idaho and Washington) plot in the lower-right, while sites in the Southwest US (Arizona & New Mexico) plot in the upper-left. Each site is colored by the mean surface D_{50} measured at a nearby bar (A), or by the armor ratio (B). Northwest sites have coarser-grained beds and higher armor ratios than Southwest sites.

3.5 Discussion

3.5.1 Linking suspended sediment rating curves and riverbed sediment

The combined results of our rating curve and grain size analyses reveal a strong connection between fluvial suspended sediment transport and the composition of the riverbed. This offers some predictability if only one of these two measurements is known: rivers with fine-grained and unsorted bed are likely to have shallow rating curves with a high coefficient and low exponent; conversely, if a riverbed is coarse and armored, the corresponding suspended sediment rating curve is likely steep, defined by a low coefficient and high exponent.

To understand why these variables are connected, it is important to first consider the physical meaning of the coefficient and exponent in suspended sediment rating curves. A high, shallow rating curve (high coefficient, low exponent) represents high concentrations of suspended sediment are transported across all flow conditions, even at low flow; a steep rating curve (low coefficient, high exponent), on the other hand, implies that very little sediment is transported at low flow conditions, but the amount of suspended sediment transported increases dramatically at higher discharges. Thus, rating curve shape is a reflection of overall suspended sediment mobility in a river. With this in mind, it is logical that suspended sediment rating curves are directly tied to riverbed composition. Fine, unsorted grains on a riverbed can easily be mobilized and brought into suspension at low-flow conditions, while coarse, highly armored beds require relatively higher flows to transport fine bedload material trapped beneath larger, less-mobile surface grains. This interpretation

supports the hypothesis that differences in rating curve shape can be attributed partly to varying grain sizes and strength of riverbed armoring across our study sites.

As noted in the Introduction, suspended sediment rating curves and riverbed grain size and sorting are both manifestations of a broader suspended sediment transport regime. There are numerous climatic and geologic factors that influence sediment supply or transport capacity, affecting both suspended sediment concentration and riverbed grain size distributions. For example, riverbed coarsening has been directly linked to sediment supply to river channels (Dietrich et al., 1989; Parker & Klingeman, 1982), and sediment supply is also a strong predictor of suspended sediment concentration in rivers (VanSickle & Beschta, 1983). Additionally, the variability and intensity of rainfall has been shown to influence suspended sediment concentrations, primarily through its effect on soil erosion (Lana-Renault et al., 2007; Medeiros & De Araújo, 2013), and streamflow variability is a key element of riverbed armor formation alongside sediment supply (Hassan et al., 2006; Vázquez-Tarrío et al., 2020). Thus, while suspended sediment transport behavior in some cases may be a result of how much fine sediment on the riverbed is available to bring into suspension, it may be more helpful to consider suspended sediment rating curves, surface grain sizes, and armor ratios as representative of overall basin characteristics—such as sediment supply and hydrology—that ultimately influence the balance of sediment supply and sediment transport capacity.

3.5.2 Primary determinants of rating curve behavior and riverbed structure

Given the magnitude of differences between our two primary regional datasets, it is worth exploring which specific environmental parameters contribute to the extreme nature of our study locations. In short, why are these rivers in the northwestern and southwestern US so dramatically different from one another with respect to sediment transport? Identifying these underlying factors may help uncover which aspects of a broader transport regime are most influential.

Climate, for one, plays an important role in determining the balance of sediment supply and transport capacity of a given river, and could reasonably explain the differences we see in river behavior between Northwest and Southwest sites. Indeed, Chapman & Finnegan (2024) recorded a significant correlation between suspended sediment rating curves and aridity in US rivers, attributing the relationship partly to differences in riverbed grain size and sorting that result from climate-driven differences in sediment supply and transport capacity. Certainly, several climatic variables, such as mean annual temperature, glacial extent, precipitation variability, and vegetation density, each correlate significantly with the suspended sediment rating curve coefficient and exponent, as do as more general climate indicators like basin aridity (Chapman & Finnegan, 2024; Syvitski & Milliman, 2007). In particular, vegetation density and streamflow variability are probably most relevant to sediment transport regime and bed character. Vegetation greatly influences soil cohesion and infiltration, and by extension, the supply of sediment generated by both surface runoff and landslide events (Gyssels et al., 2005; Vanacker et al., 2007; Warrick, 2015).

Plants also reduce runoff variability, and by extension, streamflow variability, which influences the development of riverbed armor (Hassan et al., 2006). Finally, streamflow variability is also a function of precipitation variability, which affects vegetation density and productivity (Gherardi & Sala, 2015; Lotsch et al., 2003), thus reinforcing the impact of vegetation on sediment supply and transport.

There is indeed a stark contrast in vegetation density and streamflow variability between sites in the Northwest and Southwest datasets. Although eastern Washington is more arid than northwestern Idaho, the Northwest watersheds altogether contain denser vegetation—forests, grasslands, and cultivated land—than study watersheds in the hyperarid Southwest. This may contribute to a reduced supply of fine sediment to Northwest rivers. Furthermore, Southwest desert streams are characteristically flashy and often dry for significant portions of the year, while the streams in our Northwest study area are perennial; moreover, many of the Idaho sites experience significant seasonal snowmelt, which contributes to strong armor development in streams even in semi-arid locations (Hassan et al., 2006; Millares et al., 2014). Taken together, the denser vegetation and low-variability, snowmelt-dominated streamflow in our Northwest dataset likely contribute to much larger surface grains, stronger armoring, and steeper rating curves relative to the Southwest sites. This supports the hypothesis that the correlation between climate and suspended sediment rating curves is related to climate-based differences in riverbed grain size and armoring (Chapman & Finnegan, 2024).

Lithology is another major control on the grain size distribution and quantity of sediment supplied to a river. Rock strength influences both the size distribution of grains supplied to rivers and the sorting of riverbeds, with stronger rocks leading to coarser grain size distributions and larger armor ratios (Mueller & Pitlick, 2005; Roda-Boluda et al., 2018). Watersheds in our Northwest dataset contained relatively hard rocks; in Idaho, granitic and Precambrian metamorphic rocks were abundant, and Washington watersheds featured primarily Columbia River basalts (Johnson & Raines, 1996; Schuster, 2005). Southwest sites in Arizona and New Mexico, on the other hand, featured relatively weak sedimentary rocks, with some volcanics (Green & Jones, 1997; Richard & Kneale, 1998). Given the predominant lithologies in our watersheds, it is unsurprising that Northwest sites have coarser surface grains and a greater degree of riverbed armoring than Southwest sites, which in turn would contribute to steeper rating curves with diminished suspended sediment concentrations at low flow.

The influence of these various climatic and geologic factors likely explain the clear differences in both rating curve behavior and riverbed character between our two primary study regions. We have identified extreme cases that optimize each component variable; for instance, our Northwest sites have high vegetation density, modest streamflow variability, seasonal snowmelt, and hard intrusive rocks, which *all* contribute to a coarser, armored bed and steeper rating curve. This optimization also explains why our sites are located at opposite ends of the *k-a* parameter space

(Chapman & Finnegan, 2024; Fig. 3.3): they may represent end members with respect to riverbed grain sizes, armoring, and the sediment transport regime as a whole.

3.5.3 Relative contributions of climate and lithology to the sediment transport regime

It is likely that many rivers fall somewhere between the two extremes of non-vertically sorted, sand-bedded rivers with shallow suspended sediment rating curves, and armored, coarse-bedded rivers with steep rating curves. This may be the case, for example, for a river located in a region with relatively hard rocks, but with scarce vegetation and highly variable precipitation. However, without expanding beyond our two initial datasets, the relative influences of climate and lithology are unclear.

While a larger dataset and additional fieldwork is required for a more complete understanding of climatic and lithologic influences on sediment transport and bed morphology, past work permits a preliminary investigation into this topic. Here, we add two secondary study areas to our analysis: marine sedimentary rocks of the temperate, forested Oregon Coast Ranges, and hard igneous and metamorphic rocks of the arid southwestern US. These locations differ from our initial dataset in that neither maximizes or minimizes all possible climatic or lithologic influences on grain size, armoring, and rating curve behavior, and therefore might be expected to fall between the end-members established in Figure 3.3.

Across three separate studies of grain size and armoring of Oregon rivers (Jones et al., 2012; O'Connor et al., 2014; Wallick et al., 2011), we identified five

USGS stream gauges monitoring both discharge and sediment concentration that also mostly met the selection criteria outlined in the Methods (hydrologic disturbance was ignored for selection of additional sites) (Table 3.2). Only one site (Nehalem River) had suspended sediment data, grain sizes and armor ratios, and continuous discharge measurements; two sites had suspended sediment measurements and continuous discharge but no grain size information (Siuslaw River and Alsea River); and two sites (South Fork Coquille River and Calapooya River) had grain size information and armor ratios but required use of mean daily discharge (rather than discharge measured at the moment of sediment sampling). Total suspended solids was used in place of suspended sediment concentration for the South Fork Coquille River.

USGS Gauge #	River	Region	Coefficient (k)	Exponent (a)	D_{50} (mm)	D_{50s} (mm)	Armor ratio
09466500	Gila R.	Southwest hard-rock (arid)	85.37	0.80			
10301500	Walker R.	Southwest hard-rock (arid)	30.78	0.71			
11109000	Santa Clara R.	Southwest hard-rock (arid)	55.06	1.38			
14301000	Nehalem R.[1]	Oregon Coast Ranges (temperate)	0.011	1.51	23.6	9.6	2.5
14306500	Alsea R.	Oregon Coast Ranges (temperate)	0.018	1.63			
14307620	Siuslaw R.	Oregon Coast Ranges (temperate)	0.048	1.19			
14320700	Calapooya R.[2]	Oregon Coast Ranges (temperate)	3.32	0.99	28.5	16.8	1.7
14325000	South Fork Coquille R.[3]	Oregon Coast Ranges (temperate)	1.34	1.09	48.8	13.8	3.5

Table 3.2. Additional sites for suspended sediment rating curve and grain size analysis from the Oregon Coast Ranges and arid Southwest. Surface and subsurface D50 measurements and armor ratios are taken from the literature: 1. O'Connor et al. (2014); 2. Wallick et al. (2011); 3. Jones et al. (2012).

For hard-rock watersheds in the Southwest, sites were selected by first identifying USGS stream gauges with basins classified as arid or hyperarid (Zomer et

al., 2022), which served as a proxy for sparse vegetation and high streamflow variability. From these, basins with at least ~50% areal coverage by hard lithologies (primarily igneous and metamorphic rocks) were selected. Among these stream gauges, three sites had sufficient discharge and suspended sediment data: Gila River (AZ), Santa Clara River (CA), and Walker Creek (NV) (Table 3.2). Unfortunately, no grain size or armor measurements were available at these gauging stations.

Suspended sediment rating curve parameters were calculated for sedimentary-dominated Oregon Coast Range rivers and Southwest hard-rock sites following the methodology of Chapman & Finnegan (2024), and plotted alongside available grain size and armor measurements (Fig. 3.4). In *k-a* parameter space, both datasets are located more or less between our original Northwest &

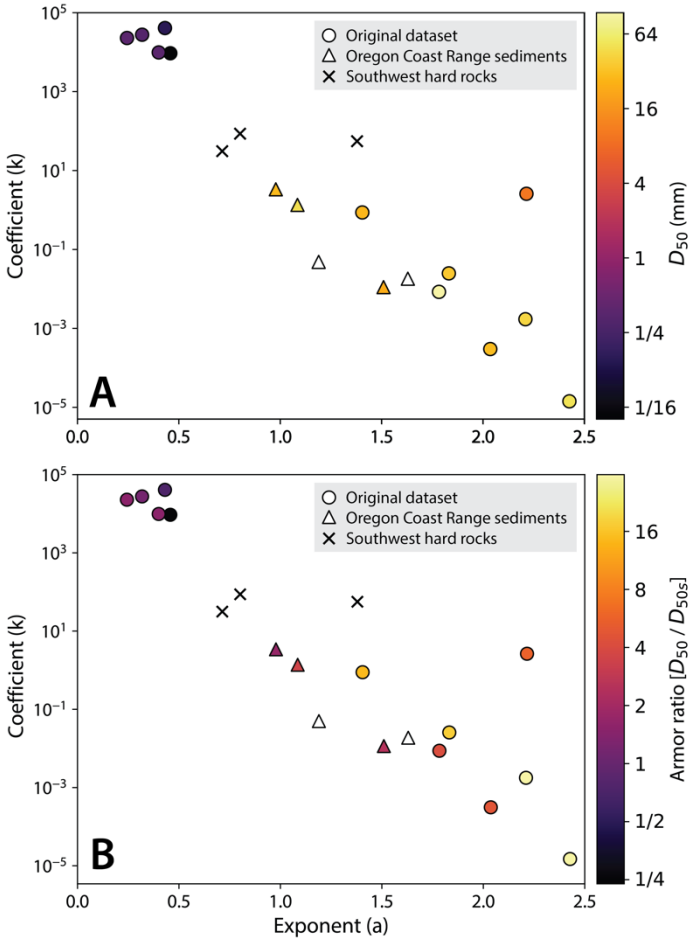

Figure 3.4. Suspended sediment rating curve behavior for the original 12 study sites and eight additional sites from soft-rock basins in temperate Oregon (triangles) and hard-rock basins in the arid Southwestern US (Xs). Sites are colored by the mean surface D_{50} measured at a nearby bar (A), or by the armor ratio (B); if no data are available, no color is assigned.

Southwest sites. The new Southwest hard-rock sites were slightly closer to our original Southwest sites, and Oregon Coast Range sites were slightly closer to our original Northwest sites. Available D_{50} and armor ratios for Oregon sites also fall between regional mean values from our original dataset.

At first glance, climatic variables appear somewhat more influential than rock type, given that sites tend to group more by climate than by rock type in *k-a* space (Fig. 3.4). However, given limitations in data quality and site selection, it is difficult to infer the relative importance of climatic variables and lithology with confidence. Moreover, we can easily imagine scenarios where lithology is the dominant control on rating curve behavior and riverbed morphology; in completely sand-dominated watersheds in densely vegetated, humid locations, rivers should be fine-grained with minimal armor, and suspended sediment rating curves are likely shallow. This is indeed supported by the many sand-bedded rivers in humid climates throughout the world. Nonetheless, the fact that our additional sites have rating curve parameters, D_{50} values, and armor ratios between those of our two primary study regions reaffirms two key hypotheses: 1) the original Northwest and Southwest datasets represent end members in suspended sediment transport behavior and riverbed structure; and 2) both climate and lithology play significant roles in determining the overall sediment transport regime, which is expressed by the shape of suspended sediment rating curves, surface grain size, and sorting of the riverbed.

3.6 Conclusions

Alluvial rivers vary widely across the globe with respect to sediment transport and bed character, ultimately due to differences in sediment supply and transport capacity. In this study, we examine a few common indicators of the sediment transport regime—namely, the power law coefficient and exponent of suspended sediment rating curves, riverbed grain size, and the riverbed armor ratio—to determine the predictive utility of these variables with respect to one another. We selected 12 US Geological Survey stream gauges with contrasting rating curve shapes, and measured surface and subsurface grain sizes at each site. Results indicate strong co-variability between rating curve shape and riverbed structure; rivers in the Northwest US have steep suspended sediment rating curves, coarse-grained surfaces, and large armor ratios, while rivers in the Southwest US have shallow rating curves, fine-grained surfaces, and small armor ratios. This suggests a strong connection between suspended sediment rating curves and the riverbed, meaning that differences in rating curve behavior between rivers may be accompanied by (or partly attributed to) differences in bed morphology.

Additional analysis suggests these two groups of sites represent end-members with respect to rating curve coefficients and exponents, grain size, and armor ratios, largely because of their particular combinations of climatologic and lithologic traits that constitute the sediment transport regime. Other rivers with different sets of watershed attributes may have rating curves and grain size distributions partway between our two primary study regions. Further study is required to determine

whether climatic variables like streamflow variability and vegetation density are more or less significant than lithology in defining the sediment transport regime, but both appear to play non-negligible roles.

Not only does this work identify an important link between common measurements in fluvial geomorphology, but it also has important implications for stream restoration and river ecology. For example, salmonids are highly sensitive to changes in fluvial sediment supply and riverbed grain size, which influence their ability to spawn (Davey & Lapointe, 2007; Hassan et al., 2017; Neupane & Yager, 2013). This research thus reveals the potential to evaluate or track changes in habitat suitability through examinations of suspended sediment rating curves, serving as a useful tool in population recovery efforts.

3.7 Supplementary information

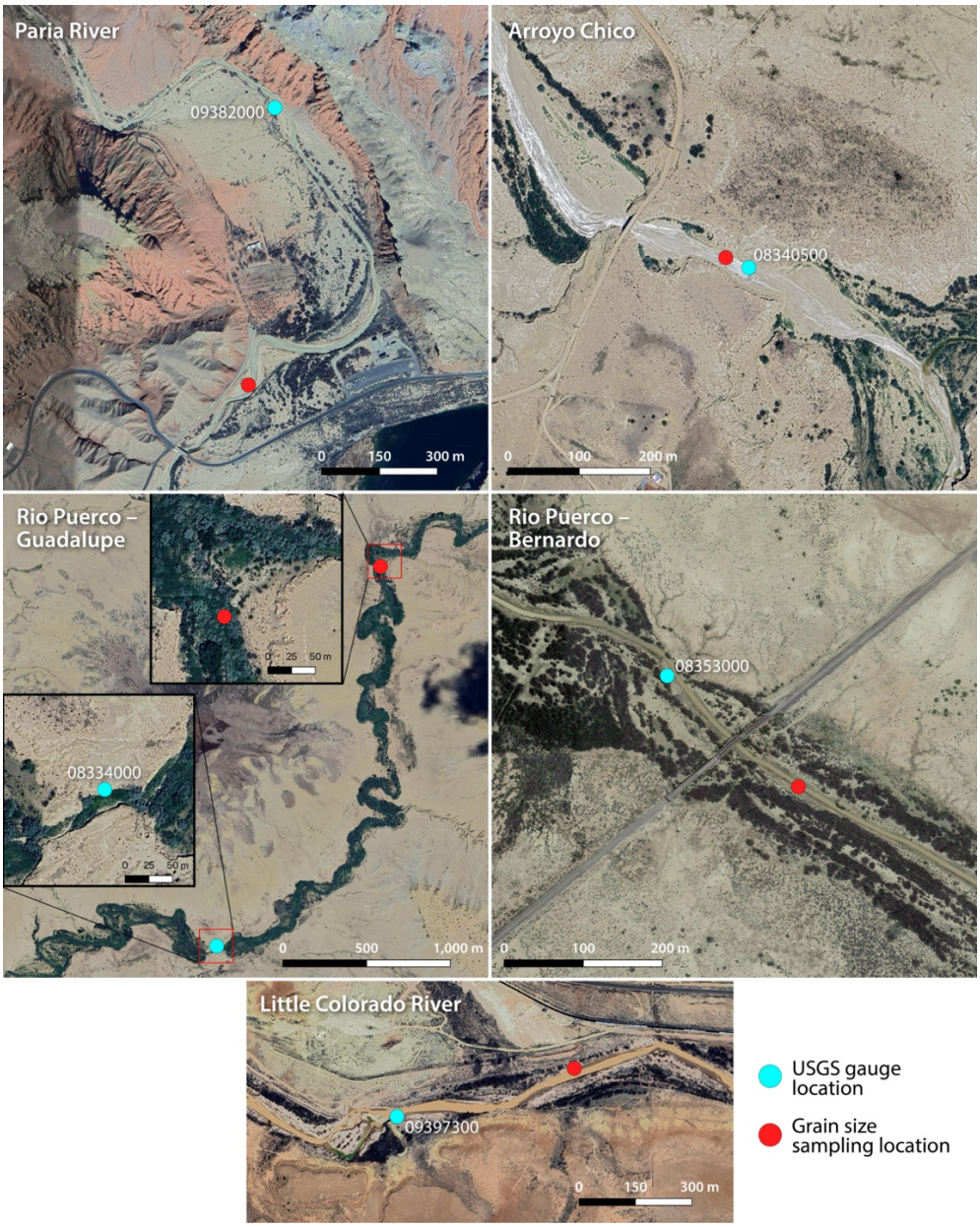

Figure S3.1. Satellite imagery of sites in the Southwest US dataset, with locations of US Geological Survey stream gauging stations shown as blue points, and nearby bar locations chosen for riverbed grain size and armor analysis in red.

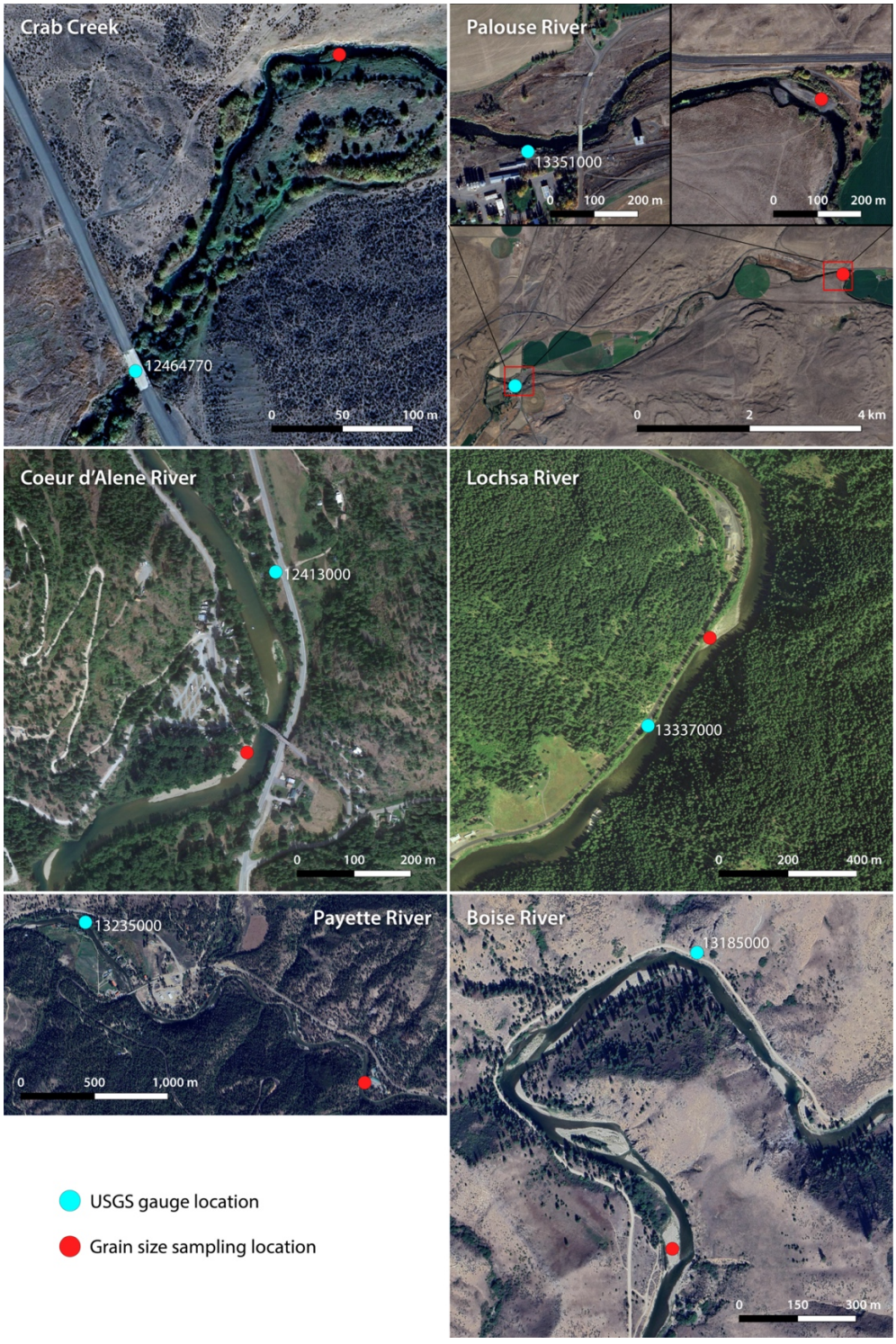

Figure S3.2. Satellite imagery of sites in the Northwest US dataset, with locations of US Geological Survey stream gauging stations shown as blue points, and nearby bar locations chosen for riverbed grain size and armor analysis in red.

Conclusion

Through the three studies discussed above, this work presents examples of how the shifting influences of climate, human land use, and lithology are expressed in the morphology of rivers. By examining fundamental concepts of sediment transport at both the individual grain and continental scales, this research has provided valuable insight into how rivers record information about the natural and anthropogenic processes present in the adjacent hillslopes and the surrounding landscape as a whole.

We began with a case study of the San Lorenzo River, in which various geomorphologic methods were combined to investigate the magnitude and timing of channel incision and floodplain abandonment. This research demonstrated the significant impact of clear-cut logging on river morphology, highlighting the fact that rivers can sometimes respond to shifts in land use in unexpected ways. The following studies expanded the scope considerably by using suspended sediment rating curves to explore the influence of climate on sediment transport efficiency in rivers across the United States, and by examining the relationship between rating curves and riverbed characteristics such as grain size and sorting. These projects established clear connections between the appearance and behavior of a river, climatic variables like vegetation density and streamflow, sediment transport models, and physical river attributes.

Together, these findings provide useful perspectives and tools for future research on fluvial systems. Studying how rivers will respond to both watershed-specific disturbances as well as to large-scale shifts in climate is important for

multiple reasons, including habitat restoration efforts, land use planning, and assessment of flooding and sedimentation risks. A nuanced and thorough understanding of river behavior is therefore essential as we continue to face the challenges posed by expanding human development and climate change.

References

Abbe T.B. & Montgomery, D.R. (2003). Patterns and processes of wood debris accumulation in the Queets river basin, Washington. *Geomorphology*, *51*, 81–107. https://doi.org/10.1016/S0169-555X(02)00326-4

Abbott, S., Julian, J. P., Kamarinas, I., Meitzen, K. M., Fuller, I. C., McColl, S. T., & Dymond, J. R. (2018). State-shifting at the edge of resilience: River suspended sediment responses to land use change and extreme storms. *Geomorphology*, *305*, 49–60. https://doi.org/10.1016/j.geomorph.2017.09.004

Adam, D. P. & West, G. J. (1983). Temperature and precipitation estimates through the Last Glacial Cycle from Clear Lake, California, pollen data. *Science*, *219*, 168–170. https://doi.org/10.1126/science.219.4581.168

Ahn, K.-H., & Steinschneider, S. (2018). Time-varying suspended sediment-discharge rating curves to estimate climate impacts on fluvial sediment transport. *Hydrological Processes*, *32*(1), 102–117. https://doi.org/10.1002/hyp.11402

Anderson, R. S. (1990). Evolution of the northern Santa Cruz Mountains by advection of crust past a San Andreas Fault bend. *Science*, *249*, 397–401. https://doi.org/10.1126/science.249.4967.397

Andréassian V. (2004) Waters and forests: from historical controversy to scientific debate. *Journal of Hydrology*, *291*, 1–27. https://doi.org/10.1016/j.jhydrol.2003.12.015

Asselman, N. E. M. (2000). Fitting and interpretation of sediment rating curves. *Journal of Hydrology*, *234*(3–4), 228–248. https://doi.org/10.1016/S0022-1694(00)00253-5

Babiński, Z. (2005). The relationship between suspended and bed load transport in river channels. In *Sediment Budgets 1* (Vol. 291, pp. 182–188). Foz do Iguaçu, Brazil: IAHS Publications.

Baker, D. B., Richards, R. P., Loftus, T. T., & Kramer, J. W. (2004). A new flashiness index: Characteristics and applications to Midwestern rivers and streams. *Journal of the American Water Resources Association*, *40*(2), 503–522. https://doi.org/10.1111/j.1752-1688.2004.tb01046.x

BalanceGeo. (2015) Pescadero-Butano Creek Watershed Sediment Source and Delivery Analysis, San Mateo County, California: Assessment of Historical Channel, Floodplain, and Estuarine Changes, Sediment Delivery, and Sediment Yield.

Belmont, P., et al. (2011). Large shift in source of fine sediment in the Upper Mississippi River. *Environmental Science & Technology*, *45*, 8804–8810. https://doi.org/dx.doi.org/10.1021/es2019109

Blong, R. J. & Gillespie, R. (1978). Fluvially transported charcoal gives erroneous 14C ages for recent deposits. *Nature*, *271*, 739–741. https://doi.org/10.1038/271739a0

Bronk Ramsey, C. (2009). Bayesian Analysis of Radiocarbon Dates. *Radiocarbon*, *51*, 337–360. https://doi.org/10.1017/S0033822200033865

Bronk Ramsey, C. (2017). Methods for summarizing radiocarbon datasets. *Radiocarbon, 59*, 1809–1833. https://doi.org/10.1017/RDC.2017.108

Bronk Ramsey, C. (2020). OxCal Program, Version 4.4. Oxford Radiocarbon Accelerator Unit: University of Oxford.

Brown, G. W. & Krygier, J. T. (1971). Clear-Cut Logging and Sediment Production in the Oregon Coast Range. *Water Resources Research*, *7*, 1189–1198. https://doi.org/10.1029/WR007i005p01189

Brummer, C. J., Abbe, T. B., Sampson, J. R., & Montgomery, D. R. (2006). Influence of vertical channel change associated with wood accumulations on delineating channel migration zones, Washington, USA. *Geomorphology*, *80*, 295–309. https://doi.org/10.1016/j.geomorph.2006.03.002

Buffington, J. M. & Montgomery, D. R. (1997). A systematic analysis of eight decades of incipient motion studies, with special reference to gravel-bedded rivers. *Water Resources Research*, *33*, 1993–2029. https://doi.org/10.1029/96WR03190

Buffington, J. M. & Montgomery, D. R. (1999). Effects of sediment supply on surface textures of gravel-bed rivers. *Water Resources Research*, *35*, 3523–3530. https://doi.org/10.1029/1999WR900232

Bunte, K., & Abt, S. R. (2001). *Sampling surface and subsurface particle-size distributions in wadable gravel-and cobble-bed streams for analyses in sediment transport, hydraulics, and streambed monitoring* (No. RMRS-GTR-74) (p. RMRS-GTR-74). Ft. Collins, CO: U.S. Department of Agriculture,

Forest Service, Rocky Mountain Research Station. https://doi.org/10.2737/RMRS-GTR-74

Cantalice, J. R. B., Cunha Filho, M., Stosic, B. D., Piscoya, V. C., Guerra, S. M. S., & Singh, V. P. (2013). Relationship between bedload and suspended sediment in the sand-bed Exu River, in the semi-arid region of Brazil. *Hydrological Sciences Journal*, *58*(8), 1789–1802. https://doi.org/10.1080/02626667.2013.839875

Carretier, S., et al. (2018). Review of erosion dynamics along the major N-S climatic gradient in Chile and perspectives. *Geomorphology*, *300*, 45–68.

Carretier, S., Regard, V., Vassallo, R., Aguilar, G., Martinod, J., Riquelme, R., et al. (2013). Slope and climate variability control of erosion in the Andes of central Chile. *Geology*, *41*(2), 195–198. https://doi.org/10.1130/G33735.1

Chapman, W. A. L., & Finnegan, N. J. (2024). The signature of climate in fluvial suspended sediment records. *Journal of Geophysical Research: Earth Surface*, *129*(1), e2023JF007429. https://doi.org/10.1029/2023JF007429

Chien, N. (1985). Changes in river regime after the construction of upstream reservoirs. *Earth Surface Processes and Landforms*, *10*(2), 143–159. https://doi.org/10.1002/esp.3290100207

Church, M., & Slaymaker, O. (1989). Disequilibrium of Holocene sediment yield in glaciated British Columbia. *Nature*, *337*, 452–454. https://doi.org/10.1038/337452a0

Clark, J. C. (1981). Stratigraphy, Paleontology, and Geology of the Central Santa Cruz Mountains, California Coast Ranges. Professional Paper No. 1168. United States Geological Survey: Washington D.C.

Cohen, H., & Laronne, J. B. (2005). High rates of sediment transport by flashfloods in the Southern Judean Desert, Israel. *Hydrological Processes*, *19*(8), 1687–1702. https://doi.org/10.1002/hyp.5630

Collins, B. D., Montgomery, D. R., Fetherston, K. L., & Abbe, T. B. (2012). The floodplain large-wood cycle hypothesis: A mechanism for the physical and biotic structuring of temperate forested alluvial valleys in the North Pacific coastal ecoregion. *Geomorphology*, *139–140*, 460–470. https://doi.org/10.1016/j.geomorph.2011.11.011

Collins, B. D., Montgomery, D. R., Schanz, S. A., & Larsen, I. J. (2016). Rates and mechanisms of bedrock incision and strath terrace formation in a forested catchment, Cascade Range, Washington. *Geological Society of America Bulletin*, *128*, 926–943. https://doi.org/10.1130/B31340.1

Crosby, B. T., Whipple, K. X., Gasparini, N. M., & Wobus, C. W. (2007). Formation of fluvial hanging valleys: Theory and simulation. *Journal of Geophysical Research: Earth Surface*, *112*. https://doi.org/10.1029/2006JF000566

Dade, W. B., & Friend, P. F. (1998). Grain-size, sediment-transport regime, and channel slope in alluvial rivers. *The Journal of Geology*, *106*(6), 661–676. https://doi.org/10.1086/516052

Davey, C., & Lapointe, M. (2007). Sedimentary links and the spatial organization of Atlantic salmon (Salmo salar) spawning habitat in a Canadian Shield river. *Geomorphology*, *83*(1–2), 82–96. https://doi.org/10.1016/j.geomorph.2006.06.011

Desilets, S. L. E., Nijssen, B., Ekwurzel, B., & Ferré, T. P. A. (2007). Post-wildfire changes in suspended sediment rating curves: Sabino Canyon, Arizona. *Hydrological Processes*, *21*(11), 1413–1423. https://doi.org/10.1002/hyp.6352

Dethier, D. P. (2001). Pleistocene incision rates in the western United States calibrated using Lava Creek B tephra. *Geology*, *29*(9), 783–786. https://doi.org/10.1130/0091-7613(2001)029<0783:PIRITW>2.0.CO;2

Dietrich, W. E., Kirchner, J. W., Ikeda, H., & Iseya, F. (1989). Sediment supply and the development of the coarse surface layer in gravel-bedded rivers. *Nature*, *340*(6230), 215–217. https://doi.org/10.1038/340215a0

Dietrich, W. E., Kirchner, J. W., Ikeda, H., & Iseya, F. (1989). Sediment supply and the development of the coarse surface layer in gravel-bedded rivers. *Nature*, *340*(6230), 215–217. https://doi.org/10.1038/340215a0

Downs, P. W., & Piégay, H. (2019). Catchment-scale cumulative impact of human activities on river channels in the late Anthropocene: implications, limitations, prospect. *Geomorphology*, *338*, 88–104. https://doi.org/10.1016/j.geomorph.2019.03.021

Draut, A., Logan, J., & Mastin, M. (2011). Channel evolution on the dammed Elwha River, Washington, USA. *Geomorphology*, *127*, 71–87. https://doi.org/10.1016/j.geomorph.2010.12.008

East, A. E., Stevens, A. W., Ritchie, A. C., Barnard, P. L., Campbell-Swarzenski, P., Collins, B. D., & Conaway, C. H. (2018). A regime shift in sediment export from a coastal watershed during a record wet winter, California: Implications for landscape response to hydroclimatic extremes. *Earth Surface Processes and Landforms*, *43*, 2562–2577. https://doi.org/10.1002/esp.4415

East, A. E., & Sankey, J. B. (2020). Geomorphic and sedimentary effects of modern climate change: Current and anticipated future conditions in the western United States. *Reviews of Geophysics*, *58*(4), e2019RG000692. https://doi.org/10.1029/2019RG000692

East, A. E., Pess, G. R., Bountry, J. A., Magirl, C. S., Ritchie, A. C., Logan, J. B., et al. (2015). Large-scale dam removal on the Elwha River, Washington, USA: River channel and floodplain geomorphic change. *Geomorphology*, *228*, 765–786. https://doi.org/10.1016/j.geomorph.2014.08.028

East, A. E., Stevens, A. W., Ritchie, A. C., Barnard, P. L., Campbell-Swarzenski, P., Collins, B. D., & Conaway, C. H. (2018). A regime shift in sediment export from a coastal watershed during a record wet winter, California: Implications for landscape response to hydroclimatic extremes. *Earth Surface Processes and Landforms*, *43*(12), 2562–2577. https://doi.org/10.1002/esp.4415

East, A. E., Stevens, A. W., Ritchie, A. C., Barnard, P. L., Campbell-Swarzenski, P., Collins, B. D., & Conaway, C. H. (2018). A regime shift in sediment export from a coastal watershed during a record wet winter, California: Implications for landscape response to hydroclimatic extremes. *Earth Surface Processes and Landforms*, *43*(12), 2562–2577. https://doi.org/10.1002/esp.4415

Ellison, C. A., Groten, J. T., Lorenz, D. L., & Koller, K. S. (2020). *Application of dimensionless sediment rating curves to predict suspended-sediment concentraitons, bedload, and annual sediment loads for rivers in Minnesota* (Scientific Investigations Report No. 2016–5146). Reston, VA: U.S. Geological Survey.

Emmett, W. W., & Wolman, M. G. (2001). Effective discharge and gravel-bed rivers. *Earth Surface Processes and Landforms*, *26*, 1369–1380. https://doi.org/10.1002/esp.303

Esri. "World Hillshade" [basemap]. (2020) https://www.arcgis.com/home/item.html?id=1b243539f4514b6ba35e7d995890db1d (Accessed 16 February 2021)

Exner, F. M. (1925). Über die Wechselwirkung zwischen Wasser und geschiebe in Flussen. Sitz. Acad. Wiss. Wien Math. *Naturwiss*, *134*, 165–204.

Falcone, J. A. (2011). *GAGES-II: Geospatial Attributes of Gages for Evaluating Streamflow* (Report). Reston, VA. Retrieved from http://pubs.er.usgs.gov/publication/70046617

Falcone, J. A. (2011). *GAGES-II: Geospatial Attributes of Gages for Evaluating Streamflow* (Report). Reston, VA. Retrieved from http://pubs.er.usgs.gov/publication/70046617

Ferguson, R. I., Church, M., Rennie, C. D., & Venditti, J. G. (2015). Reconstructing a sediment pulse: Modeling the effect of placer mining on Fraser River, Canada. *Journal of Geophysical Research: Earth Surface*, *120*(7), 1436–1454. https://doi.org/10.1002/2015JF003491

Fisher, A., Belmont, P., Murphy, B. P., MacDonald, L., Ferrier, K. L., & Hu, K. (2021). Natural and anthropogenic controls on sediment rating curves in northern California coastal watersheds. *Earth Surface Processes and Landforms*, *46*(8), 1610–1628. https://doi.org/10.1002/esp.5137

Forte, A. M., Yanites, B. J., & Whipple, K. X. (2016). Complexities of landscape evolution during incision through layered stratigraphy with contrasts in rock strength. *Earth Surface Processes and Landforms*, *41*, 1736–1757. https://doi.org/10.1002/esp.3947

Fournier, F. (1949). Les facteurs climatiques de l'érosion du sol. *Bulletin de l'Association de géographes français*, *26*(202), 97–103. https://doi.org/10.3406/bagf.1949.7284

Fuller, T. K., Perg, L. A., Willenbring, J. K., & Lepper, K. (2009). Field evidence for climate-driven changes in sediment supply leading to strath terrace formation. *Geology*, *37*, 467–470. https://doi.org/10.1130/G25487A.1

Galay, V. J. (1983). Causes of river bed degradation. *Water Resources Research*, *19*(5), 1057–1090. https://doi.org/10.1029/WR019i005p01057

Galay, V. J. (1983). Causes of river bed degradation. *Water Resources Research*, *19*(5), 1057–1090. https://doi.org/10.1029/WR019i005p01057

Gao, P., Geissen, V., Ritsema, C. J., Mu, X.-M., & Wang, F. (2013). Impact of climate change and anthropogenic activities on stream flow and sediment discharge in the Wei River basin, China. *Hydrology and Earth System Sciences*, *17*(3), 961–972. https://doi.org/10.5194/hess-17-961-2013

Garcia, C., Laronne, J. B., & Sala, M. (2000). Continuous monitoring of bedload flux in a mountain gravel-bed river. *Geomorphology*, *34*(1–2), 23–31. https://doi.org/10.1016/S0169-555X(99)00128-2

Germanoski, D, & Ritter, D. F. (1988). Tributary response to local base level lowering below a dam. *Regulated Rivers: Research & Management*, *2*, 11–24. https://doi.org/10.1002/rrr.3450020103

Gherardi, L. A., & Sala, O. E. (2015). Enhanced precipitation variability decreases grass- and increases shrub-productivity. *Proceedings of the National Academy of Sciences*, *112*(41), 12735–12740. https://doi.org/10.1073/pnas.1506433112

Gibling, M. R. (2018). River systems and the Anthropocene: A late Pleistocene and Holocene timeline for human influence. *Quaternary*, *1*(3), 21. https://doi.org/10.3390/quat1030021

Gilbert, G. K. (1917). Hydraulic-mining débris in the Sierra Nevada. Professional Paper. United States Geological Survey: Washington D.C.

Grant, G. E., Schmidt, J. C., & Lewis, S. L. (2013). A geological framework for interpreting downstream effects of dams on rivers. In J. E. O'Connor & G. E. Grant (Eds.), *Water Science and Application* (pp. 203–219). Washington, D. C.: American Geophysical Union. https://doi.org/10.1029/007WS13

Gray, A. B., Pasternack, G. B., Watson, E. B., Warrick, J. A., & Goñi, M. A. (2015). The effect of El Niño Southern Oscillation cycles on the decadal scale suspended sediment behavior of a coastal dry-summer subtropical catchment. *Earth Surface Processes and Landforms*, *40*(2), 272–284. https://doi.org/10.1002/esp.3627

Green, G. N., & Jones, G. E. (1997). The digital geologic map of New Mexico in ARC/INFO format. US Geological Survey.

Gudmundsdottir, M. H., Blisniuk, K., Ebert, Y., Levine, N. M., Rood, D. H., Wilson, A., & Hilley, G. E. (2013). Restraining bend tectonics in the Santa Cruz Mountains, California, imaged using 10Be concentrations in river sands. *Geology,* 41, 843–846. https://doi.org/10.1130/G33970.1

Gyssels, G., Poesen, J., Bochet, E., & Li, Y. (2005). Impact of plant roots on the resistance of soils to erosion by water: a review. *Progress in Physical Geography: Earth and Environment*, *29*(2), 189–217. https://doi.org/10.1191/0309133305pp443ra

Gyssels, G., Poesen, J., Bochet, E., & Li, Y. (2005). Impact of plant roots on the resistance of soils to erosion by water: a review. *Progress in Physical*

Geography: Earth and Environment, *29*(2), 189–217. https://doi.org/10.1191/0309133305pp443ra

Hanson, P. R., Mason, J. A., & Goble, R. J. (2006). Fluvial terrace formation along Wyoming's Laramie Range as a response to increased late Pleistocene flood magnitudes. *Geomorphology*, *76*, 12–25. https://doi.org/10.1016/j.geomorph.2005.08.010

Harrington, S. T., & Harrington, J. R. (2013). An assessment of the suspended sediment rating curve approach for load estimation on the Rivers Bandon and Owenabue, Ireland. *Geomorphology*, *185*, 27–38. https://doi.org/10.1016/j.geomorph.2012.12.002

Harvey, M. D., & Watson CC. (1986). Fluvial processes and morphological thresholds in incised channel restoration. *Journal of the American Water Resources Association (JAWRA)*, *22*, 359–368. https://doi.org/10.1111/j.1752-1688.1986.tb01890.x

Hassan, M. A., Egozi, R., & Parker, G. (2006). Experiments on the effect of hydrograph characteristics on vertical grain sorting in gravel bed rivers. *Water Resources Research*, *42*(9). https://doi.org/10.1029/2005WR004707

Hassan, M. A., Egozi, R., & Parker, G. (2006). Experiments on the effect of hydrograph characteristics on vertical grain sorting in gravel bed rivers. *Water Resources Research*, *42*(9). https://doi.org/10.1029/2005WR004707

Hassan, M. A., Ferrer-Boix, C., Cienciala, P., & Chartrand, S. (2017). Sediment Transport and Channel Morphology Implications for Fish Habitat. In A.

Radecki-Pawlik, S. Pagliara, J. Hradecký, & E. Hendrickson (Eds.), *Open Channel Hydraulics, River Hydraulic Structures and Fluvial Geomorphology* (1st ed., pp. 322–348). CRC Press. https://doi.org/10.1201/9781315120584-17

Hooke, R. LeB. (2000). Toward a uniform theory of clastic sediment yield in fluvial systems. *Geological Society of America Bulletin*, *112*(12), 1778–1786. https://doi.org/10.1130/0016-7606(2000)112<1778:TAUTOC>2.0.CO;2

Horowitz, A. J. (2003). An evaluation of sediment rating curves for estimating suspended sediment concentrations for subsequent flux calculations. *Hydrological Processes*, *17*(17), 3387–3409. https://doi.org/10.1002/hyp.1299

Hsieh, M.-L., & Knuepfer, P. L. K. (2001). Middle–late Holocene river terraces in the Erhjen River Basin, southwestern Taiwan—implications of river response to climate change and active tectonic uplift. *Geomorphology*, *38*, 337–372. https://doi.org/10.1016/S0169-555X(00)00105-7

Hunter, J. D. (2007). Matplotlib: A 2D graphics environment. *Computing in Science & Engineering*, *9*(3), 90–95. https://doi.org/10.1109/MCSE.2007.55

Iseya, F., & Ikeda, H. (1987). Pulsations in bedload transport rates induced by a longitudinal sediment sorting: A Flume Study using Sand and Gravel Mixtures. *Geografiska Annaler: Series A, Physical Geography*, *69*(1), 15–27. https://doi.org/10.1080/04353676.1987.11880193

Istanbulluoglu, E., Tarboton, D. G., Pack, R. T., & Luce, C. H. (2004). Modeling of the interactions between forest vegetation, disturbances, and sediment yields.

Journal of Geophysical Research: Earth Surface, *109*(F1). https://doi.org/10.1029/2003JF000041

Jackson, M., & Roering, J. J. (2009). Post-fire geomorphic response in steep, forested landscapes: Oregon Coast Range. *Quaternary Science Reviews*, *28*, 1131–1146. https://doi.org/10.1016/j.quascirev.2008.05.003

James, L. A. (2013). Legacy sediment: Definitions and processes of episodically produced anthropogenic sediment. *Anthropocene*, *2*, 16–26. https://doi.org/10.1016/j.ancene.2013.04.001

Jansson, M. B. (1988). A Global Survey of Sediment Yield. *Geografiska Annaler. Series A, Physical Geography*, *70*(1/2), 81–98. https://doi.org/10.2307/521127

Jeffres, C. A., Opperman, J. J., & Moyle, P. B. (2008). Ephemeral floodplain habitats provide best growth conditions for juvenile Chinook salmon in a California river. *Environmental Biology of Fishes*, *83*, 449–458. https://doi.org/10.1007/s10641-008-9367-1

Johnson, B. R., & Raines, G. L. (1996). *Digital representation of the Idaho State geologic map; a contribution to the Interior Columbia River basin ecosystem management project* (Report No. 95–690). https://doi.org/10.3133/ofr95690

Jones, K. L., O'Connor, J. E., Keith, M. K., Mangano, J. F., & Wallick, J. R. (2012). *Preliminary assessment of channel stability and bed-material transport in the Coquille River basin, southwestern Oregon* (Open-File Report No. 2012–1064) (p. 84). Reston, VA: U.S. Geological Survey.

Katz, J., Moyle, P. B., Quiñones, R. M., Israel, J., & Purdy, S. (2013). Impending extinction of salmon, steelhead, and trout (Salmonidae) in California. *Environmental Biology of Fishes*, *96*, 1169–1186. https://doi.org/10.1007/s10641-012-9974-8

King, J. G., Emmett, W. W., Whiting, P. J., Kenworthy, R. P., & Barry, J. J. (2004). *Sediment transport data and related information for selected coarse-bed streams and rivers in Idaho* (No. RMRS-GTR-131) (p. RMRS-GTR-131). Ft. Collins, CO: U.S. Department of Agriculture, Forest Service, Rocky Mountain Research Station. https://doi.org/10.2737/RMRS-GTR-131

Kondolf, G. M., Piégay, H., & Landon, N. (2002). Channel response to increased and decreased bedload supply from land use change: contrasts between two catchments. *Geomorphology*, *45*, 35–51. https://doi.org/10.1016/S0169-555X(01)00188-X

Lamb, M. P., Dietrich, W. E., & Venditti, J. G. (2008). Is the critical Shields stress for incipient sediment motion dependent on channel-bed slope? *Journal of Geophysical Research*, *113.* https://doi.org/10.1029/2007JF000831

Lana-Renault, N., Regüés, D., Martí-Bono, C., Beguería, S., Latron, J., Nadal, E., et al. (2007). Temporal variability in the relationships between precipitation, discharge and suspended sediment concentration in a small Mediterranean mountain catchment. *Hydrology Research*, *38*(2), 139–150. https://doi.org/10.2166/nh.2007.003

Lane, E. W. (1954). *The importance of fluvial morphology in hydraulic engineering* (Hydraulic Laboratory Report No. 372) (pp. 1–17). Denver, CO: US Department of the Interior, Bureau of Reclamation, Commissioner's Office.

Langbein, W. B., & Schumm, S. A. (1958). Yield of sediment in relation to mean annual precipitation. *Transactions, American Geophysical Union*, *39*(6), 1076–1084. https://doi.org/10.1029/TR039i006p01076

Laronne, J. B., & Reid, I. (1993). Very high rates of bedload sediment transport by ephemeral desert rivers. *Nature*, *366*(6451), 148–150. https://doi.org/10.1038/366148a0

Lenzi, M. A., Mao, L., & Comiti, F. (2003). Interannual variation of suspended sediment load and sediment yield in an alpine catchment. *Hydrological Sciences Journal*, *48*(6), 899–915. https://doi.org/10.1623/hysj.48.6.899.51425

Liébault, F., & Piégay, H. (2002). Causes of 20th century channel narrowing in mountain and piedmont rivers of southeastern France. *Earth Surface Processes and Landforms*, *27*, 425–444. https://doi.org/10.1002/esp.328

Liébault, F., Jantzi, H., Klotz, S., Laronne, J. B., & Recking, A. (2016). Bedload monitoring under conditions of ultra-high suspended sediment concentrations. *Journal of Hydrology*, *540*, 947–958. https://doi.org/10.1016/j.jhydrol.2016.07.014

Limaye, A. B. S., & Lamb, M. P. (2016). Numerical model predictions of autogenic fluvial terraces and comparison to climate change expectations. *Journal of*

Geophysical Research: Earth Surface, *121*, 512–544. https://doi.org/10.1002/2014JF003392

Loch, R. J. (2000). Effects of vegetation cover on runoff and erosion under simulated rain and overland flow on a rehabilitated site on the Meandu Mine, Tarong, Queensland. *Soil Research*, *38*(2), 299. https://doi.org/10.1071/SR99030

Lorimer, C. G., Porter, D. J., Madej, M. A., Stuart, J. D., Veirs, S. D., Norman, S. P., et al. (2009). Presettlement and modern disturbance regimes in coast redwood forests: Implications for the conservation of old-growth stands. *Forest Ecology and Management*, *258*(7), 1038–1054. https://doi.org/10.1016/j.foreco.2009.07.008

Lotsch, A., Friedl, M. A., Anderson, B. T., & Tucker, C. J. (2003). Coupled vegetation-precipitation variability observed from satellite and climate records. *Geophysical Research Letters*, *30*(14). https://doi.org/10.1029/2003GL017506

Lotsch, A., Friedl, M. A., Anderson, B. T., & Tucker, C. J. (2003). Coupled vegetation-precipitation variability observed from satellite and climate records. *Geophysical Research Letters*, *30*(14). https://doi.org/10.1029/2003GL017506

Lowell P. G. (1990). A review of redwood harvesting: Another look. *California Department of Forestry and Fire Protection*, 30.

Ludwig, W., & Probst, J.-L. (1996). A global modelling of the climatic, morphological, and lithological control of river sediment discharges to the

oceans. In D. E. Walling & B. W. Webb (Eds.), *Erosion and Sediment Yield: Global and Regional Perspectives* (pp. 21–28). Wallingford: IAHS.

Lyons, J. K., & Beschta, R. L. (1983). Land use, floods, and channel changes: Upper Middle Fork Willamette River, Oregon (1936–1980). *Water Resources Research*, *19*, 463–471. https://doi.org/10.1029/WR019i002p00463

Madej, M. A., & Ozaki, V. (1996). Channel response to sediment wave propagation and movement, Redwood Creek, California, USA. Earth Surface Processes and Landforms 21: 911–927. https://doi.org/10.1002/(SICI)1096-9837(199610)21:10<911::AID-ESP621>3.0.CO;2-1

Marshall, J. A., Roering, J. J., Bartlein, P. J., Gavin, D. G., Granger, D. E., Rempel, A. W., Praskievicz, S. J., Hales, T. C. (2015). Frost for the trees: Did climate increase erosion in unglaciated landscapes during the late Pleistocene? *Science Advances*, *1*, e1500715. https://doi.org/10.1126/sciadv.1500715

Medeiros, P. H. A., & De Araújo, J. C. (2013). Temporal variability of rainfall in a semiarid environment in Brazil and its effect on sediment transport processes. *Journal of Soils and Sediments*. https://doi.org/10.1007/s11368-013-0809-9

Merritt, D. M., & Wohl, E. E. (2003). Downstream hydraulic geometry and channel adjustment during a flood along an ephemeral, arid-region drainage. *Geomorphology*, *52*(3–4), 165–180. https://doi.org/10.1016/S0169-555X(02)00241-6

Millares, A., Polo, M. J., Moñino, A., Herrero, J., & Losada, M. A. (2014). Bedload dynamics and associated snowmelt influence in mountainous and semiarid

alluvial rivers. *Geomorphology*, *206*, 330–342. https://doi.org/10.1016/j.geomorph.2013.09.038

Milliman, J. D., & Farnsworth, K. L. (2011). Runoff, erosion, and delivery to the coastal ocean. In *River Discharge to the Coastal Ocean: A Global Synthesis* (pp. 13–69). Cambridge: Cambridge University Press. https://doi.org/10.1017/CBO9780511781247.003

Misset, C., Recking, A., Navratil, O., Legout, C., Poirel, A., Cazilhac, M., et al. (2019). Quantifying bed-related suspended load in gravel bed rivers through an analysis of the bedload-suspended load relationship. *Earth Surface Processes and Landforms*, *44*(9), 1722–1733. https://doi.org/10.1002/esp.4606

Montgomery, D. R., Abbe T. B., Buffington, J. M., Peterson, N. P., Schmidt, K. M., & Stock, J. D. (1996). Distribution of bedrock and alluvial channels in forested mountain drainage basins. *Nature*, *381*, 587–589. https://doi.org/10.1038/381587a0

Montgomery, D. R., Massong, T. M., & Hawley, S. C. S. (2003). Influence of debris flows and log jams on the location of pools and alluvial channel reaches, Oregon Coast Range. *Geological Society of America Bulletin*, *115*, 78–88. https://doi.org/10.1130/0016-7606(2003)115<0078:IODFAL>2.0.CO;2

Moore, R. D., & Wondzell, S. M. (2005). Physical hydrology and the effects of forest harvesting in the Pacific Northwest: A review. *Journal of the American Water Resources Association (JAWRA)*: *41*(4): 763-784. https://doi.org/10.1111/j.1752-1688.2005.tb03770.x

Morgan, R. P. C. (2005). *Soil Erosion and Conservation* (3rd ed.). Malden, MA: Blackwell Publishing.

Mueller, E. R., Pitlick, J., & Nelson, J. M. (2005). Variation in the reference Shields stress for bed load transport in gravel-bed streams and rivers. *Water Resources Research*, *41*. https://doi.org/10.1029/2004WR003692

Mueller, E. R., & Pitlick, J. (2005). Morphologically based model of bed load transport capacity in a headwater stream. *Journal of Geophysical Research: Earth Surface*, *110*(F2). https://doi.org/10.1029/2003JF000117

Musselman, Z. A. (2011). The localized role of base level lowering on channel adjustment of tributary streams in the Trinity River basin downstream of Livingston Dam, Texas, USA. *Geomorphology*, *128*, 42–56. https://doi.org/10.1016/j.geomorph.2010.12.021

Napolitano, M. B. (1998). *Persistence of Historical Logging Impacts on Channel Form in Mainstem North Fork Caspar Creek, in Proceedings, Conference on Coastal Watersheds: The Caspar Creek Story.* General Technical Report PSW-GTR-168. Pacific Southwest Research Station, Forest Service, US Department of Agriculture: 97–101. https://doi.org/10.2737/PSW-GTR-168

Nasr, B. M., La Selle, S., Chapman, W. A. L., & Finnegan, N. J. (2021). Vibracore CT scans from the San Lorenzo River. U.S. Geological Survey data release. https://doi.org/10.5066/P9ZT7ZOX

Neary, D. G., Ryan, K. C., & DeBano, L. F. (2005). Wildland fire in ecosystems: effects of fire on soils and water (No. RMRS-GTR-42-V4) (p. RMRS-GTR-

42-V4). Ft. Collins, CO: U.S. Department of Agriculture, Forest Service, Rocky Mountain Research Station. https://doi.org/10.2737/RMRS-GTR-42-V4

Neupane, S., & Yager, E. M. (2013). Numerical simulation of the impact of sediment supply and streamflow variations on channel grain sizes and Chinook salmon habitat in mountain drainage networks. *Earth Surface Processes and Landforms*, *38*(15), 1822–1837. https://doi.org/10.1002/esp.3426

Noble, E. L. (1965). *Sediment reduction through watershed rehabilitation* (Miscellaneous Publication No. 970) (pp. 114–123). Washington, D.C.: US Department of Agriculture.

O'Connor, J. E., Mangano, J. F., Anderson, S. W., Wallick, J. R., Jones, K. L., & Keith, M. K. (2014). Geologic and physiographic controls on bed-material yield, transport, and channel morphology for alluvial and bedrock rivers, western Oregon. *Geological Society of America Bulletin*, *126*(3–4), 377–397. https://doi.org/10.1130/B30831.1

Overpeck, J. T., & Udall, B. (2020). Climate change and the aridification of North America. *Proceedings of the National Academy of Sciences*, *117*(22), 11856–11858. https://doi.org/10.1073/pnas.2006323117

Parker, G., Wilcock, P. R., Paola, C., Dietrich, W. E., & Pitlick, J. (2007). Physical basis for quasi-universal relations describing bankfull hydraulic geometry of single-thread gravel bed rivers. *Journal of Geophysical Research*, *112*. https://doi.org/10.1029/2006JF000549

Parker, G. (1978). Self-formed straight rivers with equilibrium banks and mobile bed. Part 2. The gravel river. *Journal of Fluid Mechanics*, *89*, 127–146. https://doi.org/10.1017/S0022112078002505

Parker, G. (1990). Surface-based bedload transport relation for gravel rivers. *Journal of Hydraulic Research*, *28*(4), 417–436. https://doi.org/10.1080/00221689009499058

Parker, G., & Klingeman, P. C. (1982). On why gravel bed streams are paved. *Water Resources Research*, *18*(5), 1409–1423. https://doi.org/10.1029/WR018i005p01409

Parker, G., & Klingeman, P. C. (1982). On why gravel bed streams are paved. *Water Resources Research*, *18*(5), 1409–1423. https://doi.org/10.1029/WR018i005p01409

Pazzaglia, F. J. (2013). 9.22: Fluvial Terraces. In Shroder, JF (Ed.), Treatise on Geomorphology, Volume 9: Fluvial Geomorphology. Academic Press: San Diego, CA; 379–412. https://doi.org/10.1016/B978-0-12-374739-6.00248-7

Perry, M. T. (2023). *rasterstats*: Summary statistics of geospatial raster datasets based on vector geometries (Version 0.18.0) [Python]. Available at https://github.com/perrygeo/python-rasterstats.git.

Personius, S. F., Kelsey, H. M., & Grabau, P. C. (1993). Evidence for regional stream aggradation in the Central Oregon Coast Range during the Pleistocene-Holocene transition. *Quaternary Research*, *40*, 297–308. https://doi.org/10.1006/qres.1993.1083

Pfeiffer, A. M., Finnegan, N. J., & Willenbring, J. K. (2017). Sediment supply controls equilibrium channel geometry in gravel rivers. *Proceedings of the National Academy of Sciences*, *114*, 3346–3351. https://doi.org/10.1073/pnas.1612907114

Pfeiffer, A. M., Collins, B. D., Anderson, S. W., Montgomery, D. R., & Istanbulluoglu, E. (2019). River bed elevation variability reflects sediment supply, rather than peak flows, in the uplands of Washington State. *Water Resources Research*, *55*, 6795–6810. https://doi.org/10.1029/2019WR025394

Pierce, J. L., Meyer, G. A., & Rittenour, T. (2011). The relation of Holocene fluvial terraces to changes in climate and sediment supply, South Fork Payette River, Idaho. *Quaternary Science Reviews*, *30*, 628–645. https://doi.org/10.1016/j.quascirev.2010.11.013

Pierce, J. L., Meyer, G. A., & Timothy Jull, A. J. (2004). Fire-induced erosion and millennial-scale climate change in northern ponderosa pine forests. *Nature*, *432*, 87–90. https://doi.org/10.1038/nature03058

Puigdefábregas, J. (2005). The role of vegetation patterns in structuring runoff and sediment fluxes in drylands. *Earth Surface Processes and Landforms*, *30*(2), 133–147. https://doi.org/10.1002/esp.1181

Quantum Spatial. (2020) San Mateo RCD – Santa Cruz LiDAR Project.

Quinn, T. P., & Peterson, N. P. (1996). The influence of habitat complexity and fish size on over-winter survival and growth of individually marked juvenile coho salmon (*Oncorhynchus kisutch*) in Big Beef Creek, Washington. *Canadian*

Journal of Fisheries and Aquatic Sciences, *53*, 1555–1564. https://doi.org/10.1139/f96-092

Recking A. (2013) Simple method for calculating reach-averaged bed-load transport. Journal of Hydraulic Engineering 139: 70–75. https://doi.org/10.1061/(ASCE)HY.1943-7900.0000653

Recking, A., Liébault, F., Peteuil, C., & Jolimet, T. (2012). Testing bedload transport equations with consideration of time scales. Earth Surface Processes and Landforms, 37(7), 774–789. https://doi.org/10.1002/esp.3213

Reid, L. M., & Lewis, J. (2009). Rates, timing, and mechanisms of rainfall interception loss in a coastal redwood forest. *Journal of Hydrology*, *375*, 459–470. https://doi.org/10.1016/j.jhydrol.2009.06.048

Reid, I., & Laronne, J. B. (1995). Bed load sediment transport in an ephemeral stream and a comparison with seasonal and perennial counterparts. *Water Resources Research*, *31*(3), 773–781. https://doi.org/10.1029/94WR02233

Reid, I., Layman, J. T., & Frostick, L. E. (1980). The continuous measurement of bedload discharge. *Journal of Hydraulic Research*, *18*(3), 243–249. https://doi.org/10.1080/00221688009499550

Reid, I., Layman, J. T., & Frostick, L. E. (1980). The continuous measurement of bedload discharge. *Journal of Hydraulic Research*, *18*(3), 243–249. https://doi.org/10.1080/00221688009499550

Reimer, P. J., et al. (2020) The IntCal20 Northern Hemisphere Radiocarbon Age Calibration Curve (0–55 cal kBP). *Radiocarbon*, *62*, 725–757. https://doi.org/10.1017/RDC.2020.41

Renwick, W. H. (1996). Continent-scale reservoir sedimentation patterns in the United States. In *Erosion & Sediment Yield: Global and Regional Perspectives* (Vol. 236, pp. 513–522). International Association of Hydrological Sciences (IAHS).

Richard, S. M., & Kneale, S. M. (1998). Geologic Map of Arizona. Retrieved from http://hdl.handle.net/10150/630076

Rinaldi M. (2003). Recent channel adjustments in alluvial rivers of Tuscany, central Italy. Earth Surface Processes and Landforms 28(6): 587–608. https://doi.org/10.1002/esp.464

Rinaldi M., Simon A. (1998). Bed-level adjustments in the Arno River, central Italy. Geomorphology 22(1): 57–71. https://doi.org/10.1016/S0169-555X(97)00054-8

Roberts, R. G., & Church, M. (1986). The sediment budget in severely disturbed watersheds, Queen Charlotte Ranges, British Columbia. *Canadian Journal of Forest Research*, *16*(5), 1092–1106. https://doi.org/10.1139/x86-189

Roda-Boluda, D. C., D'Arcy, M., McDonald, J., & Whittaker, A. C. (2018). Lithological controls on hillslope sediment supply: insights from landslide activity and grain size distributions. *Earth Surface Processes and Landforms*, *43*(5), 956–977. https://doi.org/10.1002/esp.4281

Rood, R. C. (1975). The historical geography and environmental impact of the lumber industry of the Santa Cruz Mountains. University of California, Santa Cruz.

Rosgen, D. L. (1997). A geomorphological approach to restoration of incised rivers. Proceedings of the Conference on Management of Landscapes Disturbed by Channel Incision, 1, 12–29.

Ross, J. A., Infante, D. M., Martin, D. J., & Rey, M. (2019). Effects of Riparian Timber Harvest on Southeast Alaska Stream Habitat after 30–40 Years: Insights for Management. *North American Journal of Fisheries Management*, *39*(2), 328–342. https://doi.org/10.1002/nafm.10270

Rossi, A., Massei, N., Laignel, B., Sebag, D., & Copard, Y. (2009). The response of the Mississippi River to climate fluctuations and reservoir construction as indicated by wavelet analysis of streamflow and suspended-sediment load, 1950–1975. *Journal of Hydrology*, *377*(3–4), 237–244. https://doi.org/10.1016/j.jhydrol.2009.08.032

Rossi, M. W., Whipple, K. X., & Vivoni, E. R. (2016). Precipitation and evapotranspiration controls on daily runoff variability in the contiguous United States and Puerto Rico. *Journal of Geophysical Research: Earth Surface*, *121*(1), 128–145. https://doi.org/10.1002/2015JF003446

Safeeq, M., Grant, G. E., Lewis, S. L., & Hayes, S. K. (2020). Disentangling effects of forest harvest on long-term hydrologic and sediment dynamics, western Cascades, Oregon. *Journal of Hydrology*, *580*, 124259. https://doi.org/10.1016/j.jhydrol.2019.124259

Sankey, J. B., Kreitler, J., Hawbaker, T. J., McVay, J. L., Miller, M. E., Mueller, E. R., et al. (2017). Climate, wildfire, and erosion ensemble foretells more sediment in western USA watersheds. *Geophysical Research Letters*, *44*(17), 8884–8892. https://doi.org/10.1002/2017GL073979

Schanz, S.A., Montgomery, D.R., & Collins, B.D. (2019). Anthropogenic strath terrace formation caused by reduced sediment retention. Proceedings of the National Academy of Sciences 116: 8734–8739. https://doi.org/10.1073/pnas.1814627116

Schildgen, T., Dethier, D. P., Bierman, P., & Caffee, M. (2002). 26Al and 10Be dating of late pleistocene and holocene fill terraces: a record of fluvial deposition and incision, Colorado front range. *Earth Surface Processes and Landforms*, *27*, 773–787. https://doi.org/10.1002/esp.352

Schuster, J. E. (2005). Geologic Map of Washington State. Olympia: Washington State Department of Natural Resources, Division of Geology and Earth Resources.

Seeger, M., Errea, M.-P., Beguería, S., Arnáez, J., Martí, C., & García-Ruiz, J. M. (2004). Catchment soil moisture and rainfall characteristics as determinant factors for discharge/suspended sediment hysteretic loops in a small headwater catchment in the Spanish pyrenees. *Journal of Hydrology*, *288*(3–4), 299–311. https://doi.org/10.1016/j.jhydrol.2003.10.012

Shakesby, R. A., & Doerr, S. H. (2006). Wildfire as a hydrological and geomorphological agent. *Earth-Science Reviews*, *74*, 269–307. https://doi.org/10.1016/j.earscirev.2005.10.006

Simon, A., & Rinaldi, M. (2006). Disturbance, stream incision, and channel evolution: The roles of excess transport capacity and boundary materials in controlling channel response. *Geomorphology*, *79*(3–4), 361–383. https://doi.org/10.1016/j.geomorph.2006.06.037

Sklar, L. S., Dietrich, W. E., Foufoula-Georgiou, E., Lashermes, B., & Bellugi, D. (2006). Do gravel bed river size distributions record channel network structure? *Water Resources Research*, *42*(6). https://doi.org/10.1029/2006WR005035

Slater, L. J., & Singer, M. B. (2013). Imprint of climate and climate change in alluvial riverbeds: Continental United States, 1950-2011. *Geology*, *41*(5), 595–598. https://doi.org/10.1130/G34070.1

Slater, L. J., Khouakhi, A., & Wilby, R. L. (2019). River channel conveyance capacity adjusts to modes of climate variability. *Scientific Reports*, *9*(12619). https://doi.org/10.1038/s41598-019-48782-1

Smith, H. G., & Dragovich, D. (2009). Interpreting sediment delivery processes using suspended sediment-discharge hysteresis patterns from nested upland catchments, south-eastern Australia. *Hydrological Processes*, *23*(17), 2415–2426. https://doi.org/10.1002/hyp.7357

Stanley, R. G., & McCaffrey, R. (1983). Extent and offset history of the Ben Lomond fault, Santa Cruz County, California. In Andersen, DW & Rymer MJ (Eds.), *Tectonics and Sedimentation along Faults of the San Andreas System*. Society of Economic Paleontology and Mineralogy, Pacific Section; 79–90.

Stark, K., Cadol, D., Varyu, D., & Laronne, J. B. (2021). Direct, continuous measurements of ultra-high sediment fluxes in a sandy gravel-bed ephemeral river. *Geomorphology*, *382*. https://doi.org/10.1016/j.geomorph.2021.107682

Stark, K., Cadol, D., Varyu, D., & Laronne, J. B. (2021). Direct, continuous measurements of ultra-high sediment fluxes in a sandy gravel-bed ephemeral river. *Geomorphology*, *382*. https://doi.org/10.1016/j.geomorph.2021.107682

Stecca G, Zolezzi G, Hicks DM, Surian N. (2019) Reduced braiding of rivers in human-modified landscapes: Converging trajectories and diversity of causes. *Earth-Science Reviews*, *188*, 291–311. https://doi.org/10.1016/j.earscirev.2018.10.016

Swanson, F. J., & Dyrness, C. T. (1975). Impact of clear-cutting and road construction on soil erosion by landslides in the western Cascade Range, Oregon. *Geology*, *3*(7): 393–396. https://doi.org/10.1130/0091-7613(1975)3<393:IOCARC>2.0.CO;2

Swanson, F. J. (1981). Fire and geomorphic processes, in Mooney HA, et al. (eds.), Fire Regime and Ecosystem Properties. General Technical Report WO v.26. USDA, Forest Service. United States Government Planning Office, Washington, DC: 401-421.

Syvitski, J. P. M., & Milliman, J. D. (2007). Geology, geography, and humans battle for dominance over the delivery of fluvial sediment to the coastal ocean. *The Journal of Geology*, *115*(1), 1–19. https://doi.org/10.1086/509246

Syvitski, J. P. M., & Milliman, J. D. (2007). Geology, geography, and humans battle for dominance over the delivery of fluvial sediment to the coastal ocean. *The Journal of Geology*, *115*(1), 1–19. https://doi.org/10.1086/509246

Syvitski, J. P., Morehead, M. D., Bahr, D. B., & Mulder, T. (2000). Estimating fluvial sediment transport: The rating parameters. *Water Resources Research*, *36*(9), 2747–2760. https://doi.org/10.1029/2000WR900133

Syvitski, J. P., Morehead, M. D., Bahr, D. B., & Mulder, T. (2000). Estimating fluvial sediment transport: The rating parameters. *Water Resources Research*, *36*(9), 2747–2760. https://doi.org/10.1029/2000WR900133

Townsend, K. F., Nelson, M. S., Rittenour, T. M., & Pederson, J. L. (2019). Anatomy and evolution of a dynamic arroyo system, Kanab Creek, southern Utah, USA. *GSA Bulletin*, *131*, 2094–2109. https://doi.org/10.1130/B35195.1

Turowski, J. M., Rickenmann, D., & Dadson, S. J. (2010). The partitioning of the total sediment load of a river into suspended load and bedload: a review of empirical data. *Sedimentology*, *57*(4), 1126–1146. https://doi.org/10.1111/j.1365-3091.2009.01140.x

Turowski, J. M., Rickenmann, D., & Dadson, S. J. (2010). The partitioning of the total sediment load of a river into suspended load and bedload: a review of

empirical data. *Sedimentology*, *57*(4), 1126–1146. https://doi.org/10.1111/j.1365-3091.2009.01140.x

U.S. Department of Agriculture. (2022). NAIP: National Agriculture Imagery Program [GIS dataset]. USDA Farm Production and Conservation – Business Center, Geospatial Enterprise Operations. Retrieved from https://developers.google.com/earth-engine/datasets/catalog/USDA_NAIP_DOQQ

U.S. Geological Survey (2022). USGS Current Water Data for the Nation. Retrieved March 16, 2022, from https://waterdata.usgs.gov/nwis/rt

U.S. Geological Survey. (2020) USGS 11160500 San Lorenzo River at Big Trees, CA. USGS Current Conditions for the Nation [online]. Available from: https://nwis.waterdata.usgs.gov/usa/nwis/qwdata/?site_no=11160500, https://dx.doi.org/10.5066/F7P55KJN

US Geological Survey. (2024). National Water Information System (USGS Water Data for the Nation). Retrieved March 16, 2022, from https://waterdata.usgs.gov/nwis

Vanacker, V., Von Blanckenburg, F., Govers, G., Molina, A., Poesen, J., Deckers, J., & Kubik, P. (2007). Restoring dense vegetation can slow mountain erosion to near natural benchmark levels. *Geology*, *35*(4), 303. https://doi.org/10.1130/G23109A.1

VanSickle, J., & Beschta, R. L. (1983). Supply-based models of suspended sediment transport in streams. *Water Resources Research*, *19*(3), 768–778. https://doi.org/10.1029/WR019i003p00768

Vázquez-Tarrío, D., Piégay, H., & Menéndez-Duarte, R. (2020). Textural signatures of sediment supply in gravel-bed rivers: Revisiting the armour ratio. *Earth-Science Reviews*, *207*, 103211. https://doi.org/10.1016/j.earscirev.2020.103211

Virtanen, P., Gommers, R., Oliphant, T. E., Haberland, M., Reddy, T., Cournapeau, D., et al. (2020). SciPy 1.0: fundamental algorithms for scientific computing in Python. *Nature Methods*, *17*(3), 261–272. https://doi.org/10.1038/s41592-019-0686-2

Wallick, J. R., O'Connor, J. E., Anderson, S., Keith, M., Cannon, C., & Risley, J. C. (2011). *Channel change and bed-material transport in the Umpqua River basin, Oregon* (Scientific Investigations Report No. 2011–5041) (p. 112). Reston, VA: U.S. Geological Survey.

Walling, D. E. (1977). Assessing the accuracy of suspended sediment rating curves for a small basin. *Water Resources Research*, *13*, 531–538. https://doi.org/10.1029/WR013i003p00531

Walling, D. E., & Kleo, A. H. (1979). Sediment yields of rivers in areas of low precipitation: a global view. In *The Hydrology of Areas of Low Precipitation* (pp. 479–493). Wallingford, Oxfordshire, UK: IAHS Publications.

Walling, D. E., & Webb, B. W. (1983). Patterns of sediment yield. In K. J. Gregory (Ed.), *Background to Palaeohydrology* (pp. 69–100). Chinchester: John Wiley & Sons.

Walter, R. C., & Merritts, D. J. (2008). Natural streams and the legacy of water-powered mills. *Science*, *319*, 299–304. https://doi.org/10.1126/science.1151716

Warrick, J. A. (2015). Trend analyses with river sediment rating curves. *Hydrological Processes*, *29*(6), 936–949. https://doi.org/10.1002/hyp.10198

Warrick, J. A., & Rubin, D. M. (2007). Suspended-sediment rating curve response to urbanization and wildfire, Santa Ana River, California. *Journal of Geophysical Research: Earth Surface*, *112*(F2). https://doi.org/10.1029/2006JF000662

Warrick, J. A., Madej, M. A., Goñi, M. A., & Wheatcroft, R. A. (2013). Trends in the suspended-sediment yields of coastal rivers of northern California, 1955–2010. *Journal of Hydrology*, *489*, 108–123. https://doi.org/10.1016/j.jhydrol.2013.02.041

Weitkamp, L. A., Wainwright, T. C., Bryant, G. J., Milner, G. B., Teel, D. J., Kope, R. G., & Waples, R. S. (1995). Status review of coho salmon from Washington, Oregon, and California. Technical Memorandum NMFS-NWFSC-24. National Oceanic and Atmospheric Administration. Seattle, Washington, USA.

Wickert, A. D., & Schildgen, T. F. (2019). Long-profile evolution of transport-limited gravel-bed rivers. *Earth Surface Dynamics*, *7*, 17–43. https://doi.org/10.5194/esurf-7-17-2019

Wilcock, P. R., & Crowe, J. C. (2003). Surface-based transport model for mixed-size sediment. *Journal of Hydraulic Engineering*, *129*(2), 120–128. https://doi.org/10.1061/(ASCE)0733-9429(2003)129:2(120)

Wilcox, A. C., Escauriaza, C., Agredano, R., Mignot, E., Zuazo, V., Otárola, S., et al. (2016). An integrated analysis of the March 2015 Atacama floods. *Geophysical Research Letters*, *43*(15), 8035–8043. https://doi.org/10.1002/2016GL069751

Wilson, L. (1973). Variations in mean annual sediment yield as a function of mean annual precipitation. *American Journal of Science*, *273*, 335–349. https://doi.org/10.2475/ajs.273.4.335

Wobus, C. W., Crosby, B. T., & Whipple, K. X. (2006) Hanging valleys in fluvial systems: Controls on occurrence and implications for landscape evolution. *Journal of Geophysical Research: Earth Surface*, *111*. https://doi.org/10.1029/2005JF000406

Wolman, M. G., & Miller, J. P. (1960). Magnitude and Frequency of Forces in Geomorphic Processes. *The Journal of Geology*, *68*, 54–74. https://doi.org/10.1086/626637

Wolman, M. G. (1954). A method of sampling coarse river-bed material. *Eos, Transactions American Geophysical Union*, *35*(6), 951–956. https://doi.org/10.1029/TR035i006p00951

Wolman, M. G., & Miller, J. P. (1960). Magnitude and frequency of forces in geomorphic processes. *The Journal of Geology*, *68*(1), 54–74. https://doi.org/10.1086/626637

Wyżga, B., Zawiejska, J., & Radecki-Pawlik, A. (2016). Impact of channel incision on the hydraulics of flood flows: Examples from Polish Carpathian rivers. *Geomorphology*, *272*, 10–20. https://doi.org/10.1016/j.geomorph.2015.05.017

Yanites, B. J., Tucker, G. E., Mueller, K. J., & Chen, Y.-G. (2010). How rivers react to large earthquakes: Evidence from central Taiwan. *Geology*, *38*, 639–642. https://doi.org/10.1130/G30883.1

Zhang, F., Zeng, C., Wang, G., Wang, L., & Shi, X. (2022). Runoff and sediment yield in relation to precipitation, temperature and glaciers on the Tibetan Plateau. International Soil and *Water Conservation Research*, *10*(2), 197–207. https://doi.org/10.1016/j.iswcr.2021.09.004

Zhang, W., Wei, X., Jinhai, Z., Yuliang, Z., & Zhang, Y. (2012). Estimating suspended sediment loads in the Pearl River Delta region using sediment rating curves. *Continental Shelf Research*, *38*, 35–46. https://doi.org/10.1016/j.csr.2012.02.017

Ziemer, R. R. (1981). The role of vegetation in the stability of forested slopes. *Proceedings of the International Union of Forestry Research Organizations, XVII World Congress: Kyoto, Japan*, *1*, 297–308.

Zipper, S. C., Hammond, J. C., Shanafield, M., Zimmer, M., Datry, T., Jones, C. N., et al. (2021). Pervasive changes in stream intermittency across the United States. *Environmental Research Letters*, *16*(084033), 1–17. https://doi.org/10.1088/1748-9326/ac14ec

Zomer, R. J., Xu, J., & Trabucco, A. (2022). Version 3 of the Global Aridity Index and Potential Evapotranspiration Database. *Scientific Data*, *9*(409), 1–15. https://doi.org/10.1038/s41597-022-01493-1

Zomer, R. J., Xu, J., & Trabucco, A. (2022). Version 3 of the Global Aridity Index and Potential Evapotranspiration Database. *Scientific Data*, *9*(409), 1–15. https://doi.org/10.1038/s41597-022-01493-1